A modelling study of the permafrost carbon feedback to climate change: feedback strength, timing, and carbon cycle consequences

by

Andrew Hugh MacDougall
BSc, St. Francis Xavier University, 2008
MSc, Simon Fraser University, 2010

A Dissertation Submitted in Partial Fulfillment of the
Requirements for the Degree of

DOCTOR OF PHILOSOPHY

in the School of Earth and Ocean Sciences

A modelling study of the permafrost carbon feedback to climate change: feedback strength, timing, and carbon cycle consequences

by

Andrew Hugh MacDougall
BSc, St. Francis Xavier University, 2008
MSc, Simon Fraser University, 2010

Supervisory Committee

---

Dr. Andrew J. Weaver, Supervisor
(School of Earth and Ocean Sciences)

---

Dr. Colin Goldblatt, Departmental Member
(School of Earth and Ocean Sciences)

---

Dr. Vivek K. Arora, Departmental Member
(Canadian Centre for Climate Modelling and Analysis)

---

Dr. David Atkinson, Outside Member
(Department of Geography)

**Supervisory Committee**

---

Dr. Andrew J. Weaver, Supervisor
(School of Earth and Ocean Sciences)

---

Dr. Colin Goldblatt, Departmental Member
(School of Earth and Ocean Sciences)

---

Dr. Vivek K. Arora, Departmental Member
(Canadian Centre for Climate Modelling and Analysis)

---

Dr. David Atkinson, Outside Member
(Department of Geography)

## ABSTRACT

The recent quantification of the reservoir of carbon held in permafrost soils has rekindled the concern that the terrestrial biosphere will transition from a carbon sink to a carbon source during the 21st century. This dissertation is a compilation of four modelling studies that investigate the permafrost carbon feedback, its consequences for the projected future behaviour of the carbon cycle, and the origins of the proportionally between cumulative $CO_2$ emissions and near surface temperature change. The dissertation is centred around five questions: 1) what is the strength and timing of the permafrost carbon feedback to climate change? 2) If anthropogenic $CO_2$ emissions cease, will atmospheric $CO_2$ concentration continue to increase? 3) Can climate warming be reversed using artificial atmospheric carbon-dioxide removal? 4) What are the underlying physical mechanisms that explain the existence in Earth system models of the proportionality between cumulative $CO_2$ emissions and mean global near surface temperature change? And 5) can strong terrestrial carbon cycle feedbacks, such as the permafrost carbon feedback, disrupt this proportionality?

By investigating the these questions using the University of Victoria Earth System Climate Model (UVic ESCM) and analytical mathematics the following conclusions are drawn:

1) The permafrost carbon feedback to climate change is simulated to have a strength of 0.25 °C (0.1 to 0.75)°C by the year 2100 CE independent of emission pathway followed in the 21st century. This range is contingent on the size of the permafrost carbon pool and the simulated model climate sensitivity.

2) If $CO_2$ emissions were to suddenly cease, the UVic ESCM suggests that whether or not $CO_2$ would continue to build up in the atmosphere is contingent on climate sensitivity and the concentration of non-$CO_2$ greenhouse gasses in the atmosphere. For a given model climate sensitivity there is a threshold value of radiative forcing from non-$CO_2$ greenhouse gasses above which $CO_2$ will continue to build up in the atmosphere for centuries after cessation of anthropogenic $CO_2$ emissions. For a UVic ESCM the threshold value for the Representative Concentration Pathway (RCP) derived emission scenarios is approximately $0.6\,\mathrm{W\,m^{-2}}$ of non-$CO_2$ greenhouse gas radiative forcing. The consequences of being above this threshold value are mild, with the model projecting a further 11-22 ppmv rise in atmosphere $CO_2$ concentration after emissions cease.

3) If technologies were developed and deployed to remove carbon from the atmosphere simulations with the UVic ESCM suggest that a Holocene-like climate could be restored by the end of the present millennium (except under a high climate sensitivity and high emission scenario). However, more carbon must be removed from the atmosphere than was originally emitted to it.

4) The proportionality between cumulative $CO_2$ emissions and global mean temperature change seen in most Earth system model simulations appears to arises from two factors: I) the stability of the airborne fraction of emitted carbon provided by the ocean uptake of carbon begin nearly a function of $CO_2$ emission rate; and II) the diminishing heat uptake by the oceans compensating for the reduced radiative forcing per unit mass $CO_2$ at high atmospheric $CO_2$ concentrations.

5) Strong terrestrial carbon cycle feedbacks can disrupt the proportionality between cumulative $CO_2$ emissions and global mean temperature change. However, within the range of emission rates project for the RCPs the permafrost carbon feedback is not strong enough to disrupt the relationship.

Overall, the addition of the permafrost carbon pool to the UVic ESCM alters model behaviour in ways that if representative of the natural world will make sta-

bilizing climate or reversing climate change more difficult than has previously been foreseen.

# Contents

**Supervisory Committee** **ii**

**Abstract** **iii**

**Table of Contents** **vi**

**List of Tables** **ix**

**List of Figures** **xi**

**Acknowledgements** **xviii**

**Dedication** **xx**

**1 Introduction** **1**

1.1 Background . . . . . 2

1.2 Key Questions . . . . . 4

1.3 Thesis Outline . . . . . 4

**2 Significant contribution to climate warming from the permafrost carbon feedback** **6**

2.1 Introduction . . . . . 6

2.2 Methods . . . . . 7

2.2.1 UVic ESCM . . . . . 7

2.2.2 Experiment Design . . . . . 8

2.3 Results and Discussion . . . . . 8

2.4 Conclusions . . . . . 15

**3 If anthropogenic $CO_2$ emissions cease, will atmospheric $CO_2$ concentration continue to increase?** **16**

3.1 Introduction . . . . . 16
3.2 Methods . . . . . 20
3.2.1 Model description . . . . . 20
3.2.2 Allowing for balance . . . . . 21
3.2.3 Finding balance . . . . . 22
3.2.4 Experiments . . . . . 22
3.3 Results . . . . . 23
3.3.1 Select results . . . . . 23
3.3.2 Balance experiments . . . . . 27
3.3.3 Unbalanced experiments . . . . . 33
3.3.4 Breakdown of assumptions . . . . . 37
3.4 Discussion . . . . . 38
3.4.1 Why is balancing atmospheric $CO_2$ possible? . . . . . 38
3.4.2 Model dependance . . . . . 42
3.4.3 Timescale of balance . . . . . 42
3.4.4 Policy implications . . . . . 43
3.4.5 Forcing and feedback uncertainties . . . . . 43
3.5 Conclusions . . . . . 44

**4 Reversing climate warming by artificial atmospheric carbon-dioxide removal: can a Holocene-like climate be restored? 45**
4.1 Introduction . . . . . 45
4.2 Methods . . . . . 47
4.2.1 Future scenarios . . . . . 47
4.2.2 The UVic ESCM . . . . . 49
4.3 Results . . . . . 50
4.4 Discussion . . . . . 54
4.4.1 A Holocene-like climate . . . . . 54
4.4.2 The effectiveness of removing carbon . . . . . 54
4.5 Conclusions . . . . . 55

**5 The origin and limits of the near proportionality between climate warming and cumulative $CO_2$ emissions 57**
5.1 Introduction . . . . . 57
5.2 Modelling methods and experiment design . . . . . 59

5.2.1 Model description . . . . . 59
5.2.2 Experiment design . . . . . 60
5.3 Analytical analysis . . . . . 60
5.3.1 An exponential increase in emissions . . . . . 66
5.3.2 The TCRE window . . . . . 68
5.4 Model results . . . . . 74
5.4.1 Constant rate experiment . . . . . 74
5.4.2 Permafrost carbon and the RCPs . . . . . 76
5.5 Discussion . . . . . 79
5.6 Conclusions . . . . . 80

**6 Conclusions and future directions** **81**
6.1 Conclusions . . . . . 81
6.2 Future directions . . . . . 83

**A Additional Information** **85**
A.1 Supplementary material for: Significant contribution to climate warming from the permafrost carbon feedback . . . . . 85
A.1.1 UVic ESCM soil carbon component . . . . . 85
A.1.2 UVic ESCM permafrost dynamics component . . . . . 86
A.1.3 Diagnosed emissions pathways . . . . . 89
A.1.4 The permafrost carbon pool . . . . . 91
A.1.5 Permafrost carbon and the carbon cycle . . . . . 94
A.1.6 Absolute temperature change . . . . . 99
A.1.7 Industrial shutdown experiment . . . . . 99
A.1.8 Comparison to previous efforts . . . . . 102
A.2 Extended modelling methods description . . . . . 103
A.2.1 Introduction . . . . . 103
A.2.2 Physical climate components . . . . . 105
A.2.3 Carbon Cycle . . . . . 107
A.2.4 Acquisition of the UVic ESCM . . . . . 110

**Bibliography** **111**

# List of Tables

Table 2.1 Additional global average warming from the inclusion of the permafrost carbon pool into the UVic ESCM, at year 2100 CE (column 2) and 2300 CE (column 3). . . . . 9
Table 2.2 Additional atmospheric $CO_2$ from the inclusion of the permafrost carbon pool into the UVic ESCM, at year 2100 CE (column 2) and 2300 CE (column 3). . . . . 11

Table 3.1 Peak $CO_2$ concentrations for a given quantity of cumulative anthropogenic carbon emissions, year of peak, and change in concentration relative to 20 years after shutdown. . . . . 34
Table 3.2 Cumulative emissions from soils from year of cessation of anthropogenic carbon emissions to year of peak atmospheric $CO_2$. Also shown is the partition of this carbon to the atmosphere, land plants, and the oceans. . . . . 35
Table 3.3 Fractional uptake by the atmosphere, land plants, and the oceans of carbon emitted by soils between cessation of anthropogenic carbon emissions and peak atmospheric $CO_2$ concentration. . . . 36

Table 4.1 Cumulative fossil fuel carbon emissions and cumulative carbon drawdown for each of the MCPs. Results are for model runs with a climate sensitivity of 3.2 °C . . . . . 53

Table 5.1 Parameters used in this manuscript, their units and the typical values of the parameters used in calculations. . . . . 61

Table 5.2 $\phi$ values and correlation coefficients for the semi-infinite half space parameterization fitted to eleven climate models that participated in CMIP5. The models were selected for having full ocean general circulation models and for having stored the planetary heat imbalance as a model output. The model experiment examined is the instant quadrupling of $CO_2$ experiment. . . . . 62

Table 5.3 Compatible emission for each RCP taking the permafrost carbon feedback to climate change into account. Values are cumulative carbon emissions between 2012 and 2100 CE. AR5 range taken from IPCC (2013). All values are in Pg of carbon. Ranges in final column were computed by varying the climate sensitivity of the UVic ESCM between 2.0 and 4.5°C for a doubling of atmospheric $CO_2$. . . . . 78

Table A.1 Relative reduction in permafrost area in the UVic ESCM and for models assessed in IPCC AR5 for year 2100 (relative to pre-industrial). . . . . 88

Table A.2 Simulated soil carbon in permafrost affected soils north of 45° N for the decade 1990-1999. . . . . 92

# List of Figures

Figure 2.1 Global average surface air temperature (SAT) anomaly with respect to baseline runs with no carbon sequestered in permafrost soil layers. Coloured areas are the likely SAT anomaly ranges for each diagnosed emissions pathway (DEP). The median for each DEP is superimposed as a black line. Note that the upper bounds for the two low emission pathway (DEP 2.6 and 4.5) have the greatest SAT anomaly (but not the greatest total warming). 10

Figure 2.2 Changes in the size of each Earth system carbon pool in response to the addition of permafrost carbon to the UVic ESCM. That is, the difference in the size of each carbon pool between simulations with and without permafrost carbon. All values are relative to the initial size of the frozen permafrost carbon pool (and a summation of all of the pools adds up to 100% for each year). Soil layers that thaw but are subsequently returned to a permafrost state continue to be administered by the active soil carbon pool, leading to the apparent high rate of transfer of carbon to the active soil carbon pool in the 20th century. . . . . 13

Figure 2.3 Evolution of atmospheric $CO_2$ concentration in response to a cessation of anthropogenic $CO_2$ and sulphate emissions in the year 2013. Dotted line represents the response for a climate sensitivity (to a doubling of $CO_2$) of 2.0°C, the dashed line a climate sensitivity of 3.0°C and the solid line a climate sensitivity of 4.5°C. . . . . 14

Figure 3.1 $CO_2$ emissions with time (left column) and $CO_2$ concentration with time for three selected cumulative emissions integration points. Atmospheric $CO_2$ concentrations with time after cessation of anthropogenic $CO_2$ emissions given for non-$CO_2$ greenhouse gas forcings at pre-industrial ($0.0\,W\,m^{-2}$), balancing and $2.0\ W\,m^{-2}$ magnitudes. . . . . 25

Figure 3.2 Net fluxes between, and changes in mass, of each of the major carbon pools. a) Averaged over a decade before cessation of fossil $CO_2$ emissions. b) Averaged over a decade 50 years after cessation of fossil $CO_2$ emissions. Fluxes are from the transient experiment following DEP 8.5, with anthropogenic $CO_2$ emissions ceasing in the year 2050. The surface ocean is taken at the top 250 m of the water column. . . . . 26

Figure 3.3 Non-$CO_2$ radiative forcing required to maintain a constant level of $CO_2$ in the atmosphere after cessation of emissions for a given quantity of cumulative anthropogenic carbon emissions. a.) Carbon emitted as a pulse over the course of one year. b.) Carbon emitted at 1% of cumulative emissions per year for 100 years. c.) Carbon emitted following a given Diagnosed Emissions Pathway (DEP). The green line shows the historical cumulative anthropogenic carbon emissions – non-$CO_2$ radiative forcing curve. The current radiative forcing from non-$CO_2$ greenhouse gasses is above the level needed to maintain balance after cessation of emissions. . . . . 28

Figure 3.4 Difference in soil respiration between model simulation at balancing and pre-industrial magnitudes of non-$CO_2$ greenhouse gas forcing, for selected cumulative emission integration points. Maps are for the fifth decade after cessation of emissions. Notice that in each case most of the additional soil respiration caused by additional non-$CO_2$ greenhouse gas forcing originates from former permafrost soils. For cumulative emissions of 1920 Pg C increasing the magnitude of non-$CO_2$ greenhouse gas forcing reduces the rate of soil respiration in the tropics. This reduction in soil respiration is coincident with a reduction of net primary productivity in these regions. As soil carbon turn-over rates are high in the tropics a reduction in litter-fall will quickly lead to a reduction in soil respiration (once litter-fall and soil respiration are in equilibrium). . . . . 29

Figure 3.5 Difference in Net Primary Production (NPP) between the ramp up experiment and a.) transient emissions experiment following DEP 8.5 for cumulative anthropogenic carbon emissions of 1920 Pg C (Transient emission - Ramp up). b.) Same as **a.** except following DEP 6.0. Note that positive NPP anomalies are concentrated in central Eurasia, the Sahel, and the subtropics of Africa and South America. . . . . 31

Figure 3.6 Estimated radiative forcing from non-$CO_2$ greenhouse gasses for trace-gas concentration prescribed for each of the four Representative Concentration Pathways (RCPs) (Moss et al., 2010). Note that even the most optimistic estimate for future non-$CO_2$ greenhouse gas forcing is consistent with approximately balancing ocean uptake of carbon with emissions from the terrestrial biosphere in the present simulations. . . . . 32

Figure 3.7 Rate of ocean uptake of carbon and terrestrial emissions of carbon for a simulation where the rates cannot be balanced. Opposite sign conventions are used for the two carbon fluxes to accommodate comparison of the magnitude of each. Notice that terrestrial emissions are already larger than ocean uptake when emissions cease. This example is from the transient emissions experiment for 3840 Pg of cumulative anthropogenic carbon emissions with a non-$CO_2$ radiative forcing of 3.0 $W\,m^{-2}$ after cessation of carbon emissions. . . . . 37

Figure 3.8 Change in Surface Air Temperature (SAT) verses release of carbon from the permafrost carbon pool to the active soil carbon pool, as simulated by the UVic ESCM for year 2300 following four emissions pathways (MacDougall et al., 2012). Note that between temperature increases of between 1 to 5°C the release of carbon from its sequestered state is nearly linear. . . . . 41

Figure 4.1 Forcing for each of the Mirrored Concentration Pathways (MCPs). Note that all of the MCPs except MCP 2.6 reach peak $CO_2$ concentration after the year 2100 CE. . . . . 48

Figure 4.2 Earth-system metrics as simulated by the UVic ESCM under each of the four MCPs. Dotted lines are simulations with a climate sensitivity of 2.0 °C, solid lines are simulations with a climate sensitivity of 3.2 °C, and dashed lines are simulations with a climate sensitivity of 4.5 °C. Metrics in panels a.–f. and h. where generated using the frozen ground version of the UVic ESCM, panel g. is from the dynamic ice-sheet version of the model, and panel i. is a metric combining output from both version of the model. Note that the combined sea-level rise includes only contributions from thermosteric rise and Greenland, and does not include contributions from Antarctica, small glaciers and ice-caps, or ground-water mining. . . . . 52

Figure 5.1 First derivative of TCRE ($\Lambda$) computed for values in table 5.1. Note that the derivative reaches zero at 677 Pg C. . . . . 65

Figure 5.2 Temperature verses cumulative carbon emissions curves (a. and c.) and TCRE curves (b. and d.) for various analytical approximations of the climate system. $r$ is the rate of carbon emissions and $\alpha$ is the airborne fraction of carbon. . . . . 67
Figure 5.3 Airborne fraction of carbon for each of the constant rate experiments carried out with the UVic ESCM. Note that airborne fraction of carbon rises faster as a function of cumulative $CO_2$ emissions for simulation with permafrost carbon and for simulation with a higher climate sensitivity to a doubling of $CO_2$. . . 69
Figure 5.4 Ocean-borne fraction of carbon for each of the constant rate experiments carried out with the UVic ESCM. Note that ocean-borne fraction of carbon is approximately a function of carbon emission rate . . . . . 70
Figure 5.5 Land-borne fraction of carbon for each of the constant rate experiments carried out with the UVic ESCM. Note that land-borne fraction of carbon becomes more rate dependent and steeply declining in simulations with permafrost carbon and simulations at a higher climate sensitivity. . . . . 71
Figure 5.6 Range of values for which TCRE is approximately constant as functions of variations in parameter values. The solid black line is the point where terms in equation 5.17 exactly cancel one another out. The shaded region indicates the region where TCRE is approximately constant. Note that the horizontal axis for the ocean heat uptake parameter (c.) is logarithmic. . . . . 73
Figure 5.7 Temperature verses cumulative carbon emissions curves for constant rate experiment simulations carried out with the UVic ESCM. Note that TCRE becomes non-constant and path dependent for simulations with strong terrestrial carbon cycle feedbacks. The vertical line seen at the right of the panels represents the residual warming that occurs after emissions cease. Notably the peak temperature anomaly seen after emissions cease remains independent of $CO_2$ emissions rate, even in cases with large transient differences in temperature. . . . . 75

Figure 5.8 Temperature verses cumulative carbon emissions curves for simulations of the Representative Concentration Pathways (RCPs) carried out with the UVic ESCM. . . . . 77
Figure 5.9 Diagnosed emissions pathways for each RCP for the UVic ESCM with (solid lines) and without (dotted lines) permafrost carbon. Note that there is a different scale for the vertical axis in each panel. Also note that the addition of the permafrost carbon feedback necessitates lower allowable peak emissions and a faster elimination of net carbon emissions for compatibility with each RCP. . . . . 78

Figure A.1 Extent of permafrost under four future emissions pathway. Median values for each range are shown as a black line. . . . . 87
Figure A.2 Emissions pathways diagnosed from representative concentration pathways 2.6, 4.5, 6.0 and 8.5. a. Anthropogenic carbon emissions rate. b. Cumulative anthropogenic carbon emissions. Note that DEP 2.6 requires negative carbon emissions. Historical emissions are from Boden et al. (2011). The periodic variations seen in panel a. are a consequence of the variation in external radiative forcing from the solar cycle. . . . . 90
Figure A.3 Carbon density in the top 1.5 m of soil for International Satellite Land Surface Climatology Project, Initiative II (ISLSCP-II) carbon density data (Scholes and de Colstoun, 2012), interpolated to the grid of the UVic ESCM (Data), and the simulated carbon density in the UVic ESCM in the top 1.5 m of soil (Simulated). 93
Figure A.4 Global and permafrost region carbon density depth profiles for UVic ESCM. Profiles given for decades 1990–1999 and 2290-2299 for each DEP. . . . . 94
Figure A.5 Absolute $CO_2$ concentration for each all DEP simulations with permafrost carbon. Median values for each range are shown as a black line. . . . . 95
Figure A.6 Anomaly in $CO_2$ concentration with respect to baseline runs with no permafrost carbon, for each DEP. Median values for each range are shown as a black line. . . . . 96

Figure A.7 Changes in the size of each Earth system carbon pool in response to the addition of permafrost carbon to the UVic ESCM. That is, the difference in the size of each carbon pool between simulations with and without permafrost carbon. All values are relative to the initial size of the frozen permafrost carbon pool (and a summation of all of the pools adds up to 100% for each year). . . . . 97

Figure A.8 Carbon emissions (or uptake) from terrestrial carbon pools. Negative values indicate a carbon sink with respect to the atmosphere, positive values a source of carbon to the atmosphere. The periodic variations in emissions rate are a consequence of the variation in external radiative forcing from the solar cycle. . 98

Figure A.9 Absolute Surface Air Temperature (SAT) anomaly for each all DEP simulations with permafrost carbon. Median values for each range are shown as a black line. . . . . 99

Figure A.10 Response of the carbon-cycle to a shutdown of industrial activity under varying climate sensitivities. Dotted lines indicate a climate sensitivity of 2.0°C, dashed lines a climate sensitivity of 3.0°C and solid lines a climate sensitivity of 4.5°C. a.–f. Rate of change of oceanic and terrestrial carbon pools. The terrestrial and oceanic carbon pools are displayed using opposite sign conventions to accommodate comparison of the magnitude of the rates of change. For the ocean positive is into the ocean and for the terrestrial biosphere positive is towards the atmosphere. The sudden increase in the rate of carbon release from the terrestrial carbon pool when anthropogenic emissions are shutdown is caused by the termination of $CO_2$ fertilization of land vegetation. g.,h. Atmospheric $CO_2$ concentrations in response to shutdown of industrial activity. The periodic variations emission rate from terrestrial carbon pool are a consequence of the variation in external radiative forcing from the solar cycle. . . . . 101

Figure A.11 Schematic diagram of the University of Victoria Earth System Climate Model. Fluxes of energy, water, and carbon are show with arrows. . . . . 104

# ACKNOWLEDGEMENTS

I am especially grateful to my supervisor Dr Andrew Weaver who has always promptly found time to advise me when I have needed guidance or comments, despite being the busiest person I have ever met. Importantly Andrew W. encouraged me to pursue new questions as they emerged from experiments, which has very much shaped this thesis. Andrew W.'s advice and guidance during my first not-very-successful encounters with the media were invaluable and appreciated.

I am indebted to Professor Pierre Friedlingstein for his advice and guidance during my visit to the University of Exeter. Dr Colin Goldblatt read and criticized three of the papers that comprise this thesis for which I am very grateful. Colin's advice on my career path and teaching are also greatly appreciated. I am thankful for mathematical help provided by Dr Adam Monahan.

My thesis committee members Dr Andrew Weaver, Dr Colin Goldblatt, Dr David Atkinson, and Dr Vivek Arora provided extremely helpful advise shaping the scope of this thesis. I am especially grateful to my committee for allowing me to change the scope of this thesis as my research evolved. I am thankful to Dr H.D. Matthews, M. Hain, and five anonymous reviewers who helped clarify the paper based chapters. I am very grateful to my external examiner Dr. Kevin Schaefer whose review of this dissertation improved its overall clarity.

The staff of the climate lab made this work possible. I am indebted to Michael Eby for his advice on how to use and modify the UVic model, for his feedback and guidance on my project, especially for the work contained in Chapter 3. I thank Ed Wiebe for keeping the computer system working smoothly and for his general technological wizardry. I thank Wanda Lewis for her skilful management UVic bureaucracy. I am grateful to the other students in the climate lab who have provided ideas, endless discussion, and good times.

I am grateful to Natural Science and Engineering Research Council of Canada (NSERC) which has provided funding to me throughout my PhD through an *Alexander Graham Bell Canadian Graduate Scholarship D2* and subsequently through the *CREATE Training Program in Interdisciplinary Climate Science at the University of Victoria*. I am also grateful for the *Michael Smith Foreign Study Supplement* provided through NSERC. I thank the University of Victoria for all forms of funding and support provided.

This thesis is the capstone of a 23 year education. I thank the educators who

went out of their way to help and inspire me along this journey. Especially: Dr Gwenn Flowers, Dr Hugo Beltrami, Dr Antonio Weingartshofer, Colette Rennie, Evelyn Cooke, and June Noble.

My greatest debt is to my parents, Hugh and Rosemary who have never ceased to support and encourage me throughout my long education.

# DEDICATION

To those who fought on my behalf and those who taught me to read.

# Chapter 1

# Introduction

In the quarter-millennium since the invention of the coal fuelled steam engine, burning of fossil fuels and land-use changes have resulted in the emission of ∼550 Pg of carbon to the atmosphere (IPCC, 2013). The action of the oceans and the terrestrial biosphere has removed ∼55% of this carbon from the atmosphere (IPCC, 2013) greatly mitigating the climate warming resulting from human activities. Whether or not these natural processes will continue to operate to remove carbon from the atmosphere into the future is of great scientific interest and social concern. The ocean will continue to absorb carbon from the atmosphere until $CO_2$ in surface water is in chemical equilibrium with other species of dissolved inorganic carbon and the partial pressure of $CO_2$ in ocean surface water is equilibrium with the atmospheric $CO_2$. However, the future behaviour of the terrestrial biosphere is uncertain (Friedlingstein et al., 2006). It may continue to take up carbon from the atmosphere or transform from a carbon sink to a carbon source releasing the carbon it once held and exacerbating climate change. The upward reevaluation of the estimated quantity of carbon held in permafrost soils (Tarnocai et al., 2009) has lead to fears that the latter is the case and that a sink to source transition is now inevitable (Schuur and Abbott, 2011). Given these concerns there is a need to incorporate the permafrost carbon pool into Earth-system models, to evaluate the strength and timing of the permafrost carbon feedback, and to assess the effect of the feedback on our understanding of the global carbon cycle.

## 1.1 Background

$CO_2$ emitted to the atmosphere by the burning of fossil fuels and land-use changes is partitioned between the atmosphere, the ocean, and the terrestrial biosphere via an assemblage of natural processes (Ciais et al., 2013). The quantity of carbon that remains in the atmosphere and that is taken up by the oceans is well constrained by empirical measurements (Ciais et al., 2013). However, no method exists to directly infer the fraction of carbon that is taken up by the terrestrial biosphere at the global scale (Ciais et al., 2013). Therefore this quantity is usually taken as the residual of total emission, ocean uptake, and the airborne fraction of carbon. Several mechanisms contribute to the uptake of carbon into the terrestrial biosphere including: the $CO_2$ fertilization effect, abandonment of former agricultural and forestry lands, and climate change induced advance of tree-lines (Ciais et al., 2013). Partitioning between these different mechanisms at the global scale remains a major challenge and introduces considerable uncertainty into projections of how terrestrial uptake of carbon will change in the future.

The first models of the terrestrial carbon cycle were incorporated into Earth-system models prior to the Third Assessment Report of the Intergovernmental Panel on Climate Change (IPCC TAR) (e.g. Cox et al., 2000). These models typically incorporate representations of photosynthesis, autotrophic respiration, a soil carbon pool, and heterotrophic respiration (e.g. Friedlingstein et al., 2006). More complex terrestrial carbon cycle models include multiple plant function types representing different classes of plants (for example grasses, broadleaf trees, shrubs, ext.), and contain multiple soil carbon pools representing organic matter of varying susceptibility to decay (Ciais et al., 2013). Earth system models simulate a wide range of terrestrial carbon uptake under simulated future climates (Arora et al., 2013, Friedlingstein et al., 2006). Some Earth system models have simulated a continued uptake of carbon by the terrestrial biosphere until 2100, while at least one model projected a sink to source transition in the mid 21$^{st}$ century driven by the collapse of the Amazon rainforest (Friedlingstein et al., 2006, Cox et al., 2000). The latter scenario is now considered unlikely, however within Earth system model simulations a consensus exists that the fraction of emitted fossil fuel carbon taken up by the terrestrial biosphere will decline as climate change proceeds (Ciais et al., 2013, Arora et al., 2013, Cox et al., 2013).

Simulations of the global carbon cycle have revealed several emergent features which are relevant for climate policy. Climate warming from $CO_2$ emissions is simu-

lated to be path independent. That is, warming (to the first order) is a function of the total quantity of cumulative carbon emissions not the specific history of when and at what rate the carbon was emitted to the atmosphere (e.g. Zickfeld et al., 2012). If $CO_2$ emissions were to totally cease, climate warming would also nearly cease as the uptake of carbon by the oceans reduces the atmospheric concentration of $CO_2$ counteracting the unrealized warming from the planetary radiative imbalance (e.g. Matthews and Weaver, 2010). For cumulative carbon emission up to approximately 2000 Pg C transient warming of climate is proportional to cumulative carbon emissions (Matthews et al., 2009, Gregory et al., 2009). This feature of the carbon cycle allows a metric of climate change to be defined designated the Transient Climate Response to [cumulative $CO_2$] Emissions (TCRE) (Gregory et al., 2009, Ciais et al., 2013). The metric directly relates the cause of climate change ($CO_2$ emissions) to the most used index of climate change (near surface air temperature change) and is therefore useful for policy discussions and communication of climate change to the general public (e.g. IPCC, 2013).

Until the end of the previous decade it was believed that the permafrost region held an insignificant fraction of the global soil carbon reservoir. For example the permafrost carbon pool was estimated by Jobbágy and Jackson (2000) to hold 192 Pg C out of an estimated global total of ∼2400 Pg C. Such early estimates where based on a very small number of soil samples which only sampled the active soil layer (the region of soil that thaws in the summer in the permafrost zone) (Tarnocai et al., 2009). These estimates overlooked several key processes that can incorporate organic matter from surface soil into the perennially frozen region of soil (permafrost soil). Principle among these processes is cryoturbation a freeze-thaw generated mechanical mixing process that causes subduction of organic carbon rich soils from the surface into permafrost soils (e.g. Schuur et al., 2008). Tarnocai et al. (2009) took advantage of newly assembled databases of soil carbon depth profiles from the permafrost region to re-estimate the quantity of carbon in permafrost soils. This assessment estimated that permafrost soil contain 1672 Pg C of which 1024 Pg C is in the top 3 m of soil, 241 Pg C is in deep river delta deposits, and 407 Pg C is in deep Siberian yedoma deposits (a type of aeolian derived soils that were rapidly deposited during glacial climates). The existence of this large previously poorly quantified reservoir of terrestrial carbon calls into question the model derived understanding of how the terrestrial biosphere will respond to anthropogenic climate change.

## 1.2 Key Questions

This dissertation is a compilation of papers centred on a series of questions about how the carbon cycle will behave in the future in response to continued anthropogenic emissions of $CO_2$ and other greenhouse gasses to the atmosphere. The tool that is used to investigate these questions is a version University of Victoria Earth System Climate Model (UVic ESCM) modified to take into account the permafrost carbon pool. The five key questions that I have sought to investigate in this work are:

1. What is the strength and timing of the permafrost carbon feedback to climate change?

2. If anthropogenic $CO_2$ emissions cease, will atmospheric $CO_2$ concentration continue to increase?

3. Can climate warming be reversed using artificial atmospheric carbon-dioxide removal?

4. What are the underlying physical mechanisms that explain the existence in Earth system models of the proportionality between cumulative $CO_2$ emissions and mean global near surface temperature change?

5. Can strong terrestrial carbon cycle feedbacks, such as the permafrost carbon feedback, disrupt this proportionality?

## 1.3 Thesis Outline

The remainder of this thesis is organized as follows:

**Chapter 2** describes modifications to the UVic ESCM to incorporate the permafrost carbon pool. The chapter also describes simulations that examine the strength and timing of the permafrost carbon feedback.

**Chapter 3** reports on model experiments that seek to find the non-$CO_2$ greenhouse gas forcing necessary to balance uptake of carbon by the ocean and release of carbon from the terrestrial biosphere following a total cessation of anthropogenic $CO_2$ emissions.

**Chapter 4** examines novel future scenarios that prescribe a gradual return to pre-industrial radiative forcing. Carbon emissions compatible with each of these scenarios are diagnosed to estimate total required negative emissions.

**Chapter 5** analysis the underlying mechanisms that produce the proportionality between cumulative $CO_2$ emissions and near surface temperature change. This analysis draws on analytical mathematical methods and model experiments where $CO_2$ is emitted at a constant rate.

**Chapter 6** summarizes the key conclusions of this thesis and suggest avenues for further study.

**Appendix A.1** is the supplementary materials for **Chapter 2** and **Appendix A.2** is an extended model description of the UVic ESCM.

# Chapter 2

# Significant contribution to climate warming from the permafrost carbon feedback

This chapter is based on the contents of the paper:
MacDougall, A. H., C. A. Avis, and A. J. Weaver, 2012: Significant existing commitment to warming from the permafrost carbon feedback. *Nat. Geosci.*, **5**, 719–721, DOI:10.1038/NGEO1573.

## 2.1 Introduction

Permafrost soils contain an estimated 1700 Pg of carbon, almost twice the current atmospheric carbon pool (Tarnocai et al., 2009). As permafrost soils thaw due to climate warming, respiration of organic matter within these soils will transfer carbon to the atmosphere, potentially leading to a positive feedback (Schuur et al., 2008). Previous uncoupled and one-dimensional efforts to model this feedback have simulated a release from permafrost soils of between 7 to 17 Pg C (Zhuang et al., 2006) and 68 to 138 Pg C (Schaefer et al., 2011) by 2100. Here we use a coupled global climate model to quantify the magnitude of the permafrost carbon feedback. The additional surface warming created by the feedback is independent of the emissions pathway followed in the 21st century and is estimated to be between 0.15 to 1.70 °C by 2300. The upper bound for the strength of the feedback is reached under the less intensive emissions pathways. This counterintuitive characteristic is a consequence of the higher radiative

efficiency of a unit of $CO_2$ at lower background atmospheric $CO_2$ concentrations. The model simulates a release of between 68 to 508 Pg C from permafrost soils by 2100. These results suggest that the climate system may already be committed to significant warming from the permafrost carbon feedback.

## 2.2 Methods

### 2.2.1 UVic ESCM

The University of Victoria Earth System Climate Model (UVic ESCM) is a coupled model of intermediate complexity (Weaver et al., 2001), which includes a fully coupled representations of oceanic (Schmittner et al., 2008) and terrestrial carbon cycles (Matthews et al., 2004). Here a version of the model incorporating soil freeze thaw processes (Avis et al., 2011) is augmented to include a representation of sequestered carbon in permafrost soils. The method of transferring sequestered permafrost carbon to the active soil carbon pool presented by (Schaefer et al., 2011) is followed, wherein the active carbon pool is administered by the existing soil carbon model component, and a threshold depth (equal to the deepest historical active layer thickness) separates the active soil and permafrost carbon pools. When the thaw depth of soil exceeds this threshold, the carbon from the newly thawed layers is transferred to the active soil carbon pool and the threshold depth is increased. Permafrost carbon is assumed to have a globally uniform density and extends only down to a depth of 3.35 m. The UVic ESCM soil carbon component has been modified such that soil respiration does not occur in soil layers with a temperature below 0°C. Soil respiration is calculated independently in each soil layer and carbon from litter-fall is distributed (as a decreasing fraction with depth) into layers with a temperature above a threshold of 1°C. The model is spun-up under estimated radiative forcing for the year 850 CE and a transient run performed until the year 1900 CE to ensure the threshold depth represents the historical maximum boundary between the active layer and permafrost soils. After 1900 CE permafrost carbon is turned on in the model. The climate sensitivity of the UVic ESCM is varied by altering the outgoing top-of-the-atmosphere longwave radiation as a function of mean global temperature, following Zickfeld et al. (2008).

### 2.2.2 Experiment Design

To estimate a likely range for the strength of the permafrost carbon feedback, a suite of sensitivity tests are conducted that explore the estimated range of permafrost carbon density (15.75–26.25 $\mathrm{kg\,m^{-3}}$) (Schaefer et al., 2011) and the likely range of the climate sensitivity to a doubling of $CO_2$ (2–4.5 °C) (Hegerl et al., 2007). The simulated carbon in soils initially underlain by permafrost north of 45°N, contained in both frozen soil layers and the active layer, is 1026 Pg C averaged over the decade 1990–1999 for our medium estimate of permafrost carbon density. This simulated carbon pool is close to a recent estimate of 1024 Pg C in the top 3 m of the soils of the permafrost region (this estimate includes both carbon held in permafrost and non-permafrost soils within the northern permafrost region) Tarnocai et al. (2009).

As a first step, carbon emissions are diagnosed from simulations of the UVic ESCM driven by specified Representative Concentration Pathways (RCPs) (Moss et al., 2010). The resulting Diagnosed Emissions Pathways (DEPs), designated by numbers corresponding to the RCP that each DEP is derived from (RCPs 2.6, 4.5, 6.0, and 8.5 — Appendix A.1 Fig. A.2), are then used to force the UVic ESCM. Emissions pathways are necessary to allow $CO_2$ to freely evolve in the atmosphere in response to the permafrost carbon feedback. The model is integrated under each DEP for combinations of the end-points and mid-points of permafrost carbon density and climate sensitivity, in addition to baseline runs for each climate sensitivity with permafrost carbon density set to zero.

## 2.3 Results and Discussion

Figure 2.1 shows the additional global average warming from the permafrost carbon feedback (relative to baseline runs with no permafrost carbon) for each of the DEPs. The additional warming by the end of the 21st century is remarkably consistent between the DEPs; 0.23 (0.09 to 0.73)°C for DEP 2.6, 0.26 (0.11 to 0.75)°C for DEP 4.5, 0.24 (0.10 to 0.69)°C for DEP 6.0, and 0.27 (0.11 to 0.69)°C for DEP 8.5. By the end of the 23rd century, the additional warming from the PCF has diverged between the DEPs, with the highest upper bounds for the lowest two emission pathways; 0.37 (0.13 to 1.62)°C for DEP 2.6, 0.59 (0.22 to 1.69)°C for DEP 4.5, 0.73 (0.28 to 1.31)°C for DEP 6.0, and 0.39 (0.23 to 0.63)°C for DEP 8.5 (Table 2.1). Under the low emissions pathways reductions in carbon emissions limit the amount of carbon liberated

Table 2.1: Additional global average warming from the inclusion of the permafrost carbon pool into the UVic ESCM, at year 2100 CE (column 2) and 2300 CE (column 3).

| Emissions Pathway | Warming 2100 (°C) | Warming 2300 (°C) |
|---|---|---|
| DEP 2.6 | 0.23 (0.09 to 0.73) | 0.37 (0.13 to 1.62) |
| DEP 4.5 | 0.26 (0.11 to 0.75) | 0.59 (0.22 to 1.69) |
| DEP 6.0 | 0.24 (0.10 to 0.69) | 0.73 (0.28 to 1.31) |
| DEP 8.5 | 0.27 (0.11 to 0.69) | 0.39 (0.23 to 0.63) |

from the permafrost. But the carbon that is transferred to the atmosphere has a higher radiative efficiency than the same unit of carbon released under a high emissions pathway, leading to a strong permafrost carbon feedback under low emissions pathways.

By the end of the 21st century the net effect of the permafrost carbon feedback on the atmosphere is an additional $CO_2$ concentration (relative to baseline runs with no permafrost carbon) of: 39 (17 to 99) ppmv for DEP 2.6, 58 (26 to 132) ppmv for DEP 4.5, 67 (32 to 148) ppmv for DEP 6.0, and 101 (53 to 213) ppmv for DEP 8.5. Collectively, soil layers that were formerly permafrost continue to release $CO_2$ to the atmosphere throughout the 22nd and 23rd centuries despite greater than 90% reductions in anthropogenic carbon emissions (from peak values) or, in the case of DEP 2.6, negative anthropogenic emissions (this DEP presumes the development of technology to remove $CO_2$ from the atmosphere). By the end of the 23rd century the net effect of the permafrost carbon feedback on the atmosphere is an additional $CO_2$ concentration of: 44 (18 to 146) ppmv for DEP 2.6, 104 (49 to 299) ppmv for DEP 4.5, 185 (82 to 338) ppmv for DEP 6.0, and 279 (196 to 374) ppmv for DEP 8.5 (see also Appendix A.1 Fig. A.6 and Table 2.2).

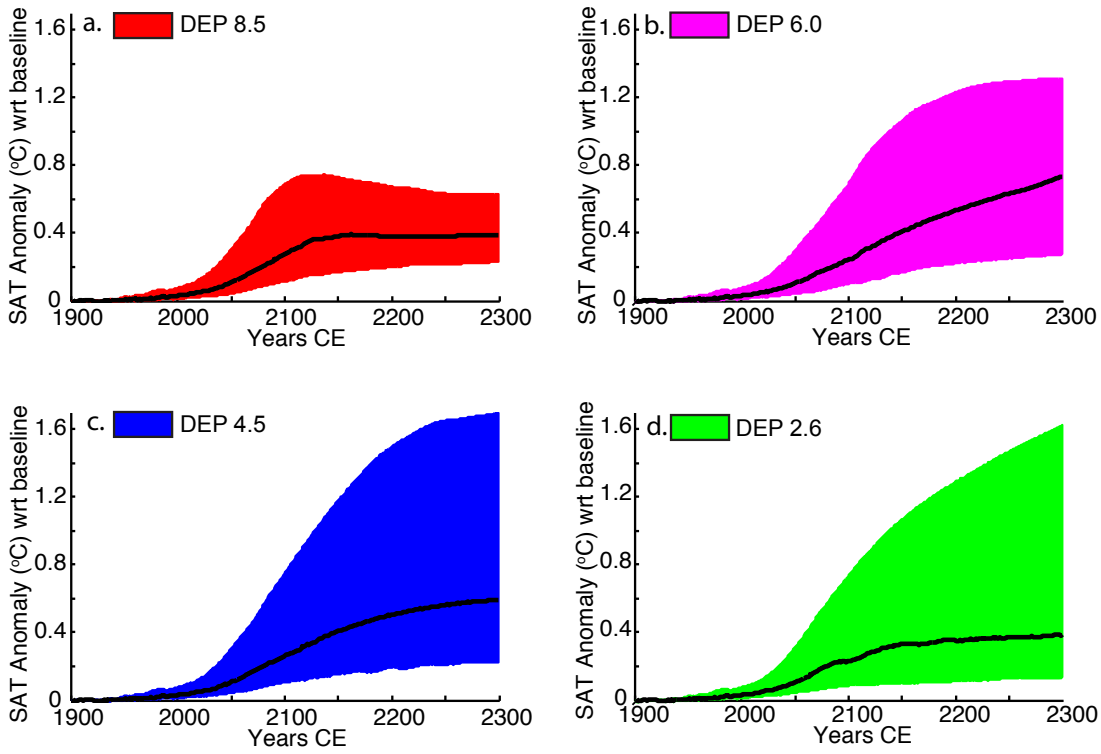


Figure 2.1: Global average surface air temperature (SAT) anomaly with respect to baseline runs with no carbon sequestered in permafrost soil layers. Coloured areas are the likely SAT anomaly ranges for each diagnosed emissions pathway (DEP). The median for each DEP is superimposed as a black line. Note that the upper bounds for the two low emission pathway (DEP 2.6 and 4.5) have the greatest SAT anomaly (but not the greatest total warming).

Table 2.2: Additional atmospheric $CO_2$ from the inclusion of the permafrost carbon pool into the UVic ESCM, at year 2100 CE (column 2) and 2300 CE (column 3).

| Emissions Pathway | Additional $CO_2$ 2100 (ppmv) | Additional $CO_2$ 2300 (ppmv) |
|---|---|---|
| DEP 2.6 | 39 (17 to 99) | 44 (18 to 146) |
| DEP 4.5 | 58 (26 to 132) | 104 (49 to 299) |
| DEP 6.0 | 67 (32 to 148) | 185 (82 to 338) |
| DEP 8.5 | 101 (53 to 213) | 279 (196 to 374) |

Figure 2.2 displays the effect of the permafrost carbon feedback on each of the Earth's carbon pools for DEPs 4.5 and 8.5 under varying climate sensitivities (for DEPs 2.6 and 6.0 see Appendix A.1 Fig. A.7). It is clear that the climate sensitivity has a dramatic effect on the fraction of the permafrost carbon that is transferred to the atmosphere, ranging for DEP 4.5 from 21% under a climate sensitivity of 2.0°C to 69% under a climate sensitivity of 4.5°C. The permafrost carbon density has only a small influence on the relative effect of permafrost carbon on the other carbon pools (not shown). Permafrost carbon is initially transferred to the active soil carbon pool as permafrost thaws. The active soil carbon pool grows until the mid 21st century then declines as soil respiration transfers carbon out of soil faster than it is being transferred in by thawing permafrost. In some model runs the active soil carbon pool becomes smaller than in the baseline run; this is a secondary carbon-cycle feedback driven by additional warming from the permafrost carbon feedback. From the atmosphere, carbon is transferred to land vegetation and the ocean carbon pool. The effect of the permafrost carbon feedback on land vegetation is in all cases small. The ocean acts as a medium term sink for permafrost carbon, absorbing 11% to 25% of the carbon by the end of the 23rd century under DEP 4.5. The permafrost carbon feedback transforms the terrestrial land surface from a sink for carbon to a source of carbon to the atmosphere. This transition occurs in 2053 (2013 to 2078) for DEP 2.6, 2068 (2026 to 2104) for DEP 4.5, 2091 (2029 to 2131) for DEP 6.0, and 2065 (2014 to 2100) for DEP 8.5 (Appendix A.1 Fig. A.8). In the absence of the permafrost carbon feedback, such a transition occurs within the UVic ESCM simulations between 2079–2198, contingent on climate sensitivity and emissions pathway.

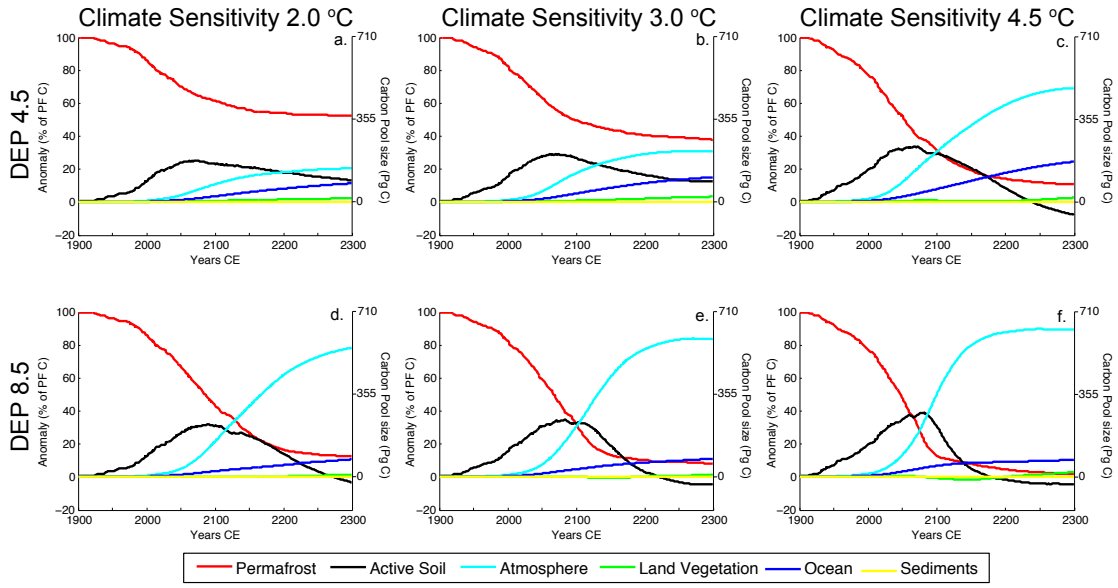


Figure 2.2: Changes in the size of each Earth system carbon pool in response to the addition of permafrost carbon to the UVic ESCM. That is, the difference in the size of each carbon pool between simulations with and without permafrost carbon. All values are relative to the initial size of the frozen permafrost carbon pool (and a summation of all of the pools adds up to 100% for each year). Soil layers that thaw but are subsequently returned to a permafrost state continue to be administered by the active soil carbon pool, leading to the apparent high rate of transfer of carbon to the active soil carbon pool in the 20th century.

With the simulated cessation of anthropogenic $CO_2$ emissions the $CO_2$ fertilization of plants also ceases, leaving only the oceans as a fast sink for carbon in the UVic ESCM. The strength of this sink is partially determined by the quantity of $CO_2$ that has been added to the atmosphere. If the rate at which $CO_2$ is being released from the terrestrial land surface exceeds the rate at which the oceans can take up $CO_2$, then $CO_2$ will continue to build up in the atmosphere, further warming the surface and driving a self-sustaining carbon-cycle feedback. In experiments where DEP 8.5 is followed up to a given date when emissions are instantaneously reduced to zero, all simulations with climate sensitivities above 3.0 °C produce a self-sustaining permafrost carbon feedback even if emissions are reduced to zero in 2013 (Fig. 2.3, Appendix A.1 Fig. A.10).

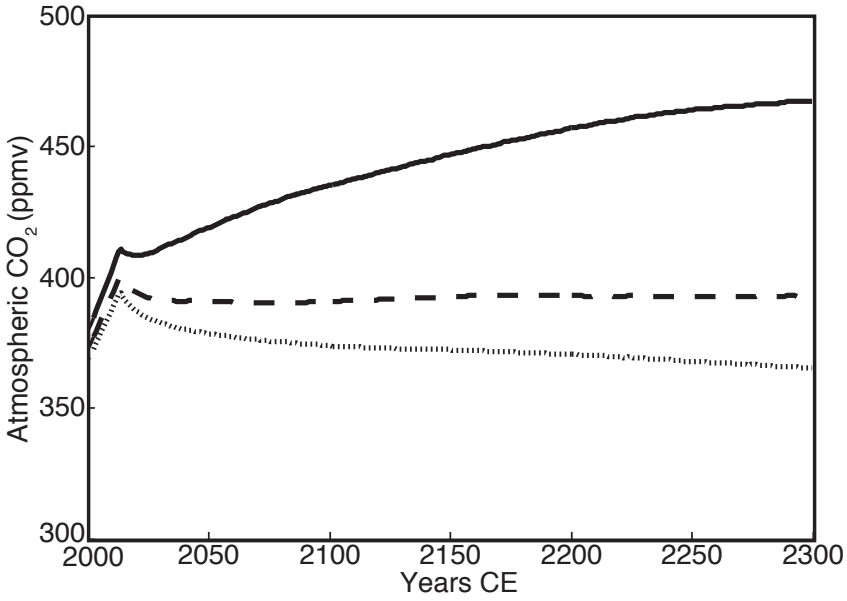


Figure 2.3: Evolution of atmospheric $CO_2$ concentration in response to a cessation of anthropogenic $CO_2$ and sulphate emissions in the year 2013. Dotted line represents the response for a climate sensitivity (to a doubling of $CO_2$) of 2.0°C, the dashed line a climate sensitivity of 3.0°C and the solid line a climate sensitivity of 4.5°C.

The UVic ESCM simulates a release from all soils of 174 (68 to 508) Pg C by 2100 as a consequence of the inclusion of the permafrost carbon feedback. This release of carbon is larger than that previously estimated using uncoupled ecosystem and one-dimensional models (Zhuang et al., 2006, Schaefer et al., 2011, Koven et al., 2011, Schneider von Deimling et al., 2012). Each of these models simulate a different

assemblage of soil-physical processes, have varying sized initial permafrost carbon pools, and are forced with differing emissions pathways. In addition, the cited models are unable to fully account for the subsequent feedback that the release of carbon has on further climate warming. All of these factors conceivably contribute to the inter-model range in estimated release of carbon from permafrost soils. (see Appendix A.1 section A.1.8 for a more detailed intercomparison of the cited model studies).

The method used here to estimate of the strength of the PCF is in a number of ways conservative. As a coarse resolution climate model, the UVic ESCM is only able to simulate permafrost thaw due to active layer thickening and talik formation. The other two processes that may accelerate permafrost thawing (thermal erosion, and thermokarst development (Schuur et al., 2008)) and the effects of fire are not simulated. The UVic ESCM soil component does not presently simulate methanogenesis, therefore all emissions from permafrost are assumed to be in the form of $CO_2$. The UVic ESCM also has an Arctic amplification that is at the low end of range simulated by other climate models. As a consequence it produces an estimate of permafrost degradation that is in the low to middle part of the inter-model range (Avis et al., 2011). I have chosen not to prescribe permafrost carbon below 3.35 m depth to accommodate a globally consistent prognostic simulation of permafrost. I have further assumed that the highly recalcitrant fraction of the permafrost carbon will never decay and have not accounted for the heat given off by heterotrophic respiration in soils (Luke and Cox, 2011). A potentially important negative feedback, enhanced plant growth from nutrients released from decaying organic mater, is also not taken into account in the UVic ESCM.

## 2.4 Conclusions

The UVic ESCM simulates a stronger permafrost carbon feedback than previous uncoupled modelling efforts to quantify this feedback (Zhuang et al., 2006, Schaefer et al., 2011, Koven et al., 2011, Schneider von Deimling et al., 2012). However, considering the processes not taken into account by the model I caution that upward reevaluation of the strength of the permafrost carbon feedback is plausible. Nevertheless the strength and committed nature of the permafrost carbon feedback simulated here suggests that it is important to initiate and sustain monitoring of carbon fluxes from permafrost soils and changes in the permafrost itself. Such data will be invaluable for validating and improving model results such as those presented here.

# Chapter 3

# If anthropogenic $CO_2$ emissions cease, will atmospheric $CO_2$ concentration continue to increase?

This chapter is based on the contents of the paper:
MacDougall, A. H., M. Eby, and A. J. Weaver, 2013: If anthropogenic $CO_2$ emissions cease, will atmospheric $CO_2$ concentration continue to increase? *J. Climate*, **26**, 9563–9576, DOI:10.1175/JCL-D-12-00751.1

## 3.1 Introduction

In the present climate approximately half of the carbon emitted to the atmosphere is taken up by the oceans and the terrestrial biosphere, greatly mitigating the effect of anthropogenic carbon emissions on climate (Denman et al., 2007). Whether these negative carbon-cycle feedbacks will continue to operate into the future (e.g. Friedlingstein et al., 2006) or after cessation of anthropogenic $CO_2$ emissions (e.g. Gillett et al., 2011) is a subject of recent scientific interest. There are five processes within the global carbon cycle that act on centennial or shorter timescales that are important for conceptualizing the mass balance of the atmospheric carbon pool. These are: 1) enhanced soil respiration, 2) $CO_2$ fertilization, 3) ecosystem changes, 4) uptake of carbon by the surface ocean, and 5) transport of carbon into the deep ocean.

Enhanced soil respiration occurs when an increase in soil temperature induces heterotrophic organisms to consume soil carbon at a faster rate, and continues until

the rate of plant litter-fall into the soil matches the soil respiration rate (e.g. Jenkinson et al., 1991). Enhanced soil respiration is initiated as soon as soils come into thermal equilibrium with an increased surface temperature (Luo and Zhou, 2006). In temperate and tropical climates this typically occurs within a year of the change in surface temperature, but in polar climates can be significantly delayed by latent heat effects in permafrost soils (Schuur et al., 2008).

Adding $CO_2$ to the atmosphere will promote plant growth via $CO_2$ fertilization (Denman et al., 2007), unless other nutrient limitations or environmental conditions are preventing increased growth. This effect begins as soon as atmospheric $CO_2$ concentration increases and ceases once plant growth comes into equilibrium with the new $CO_2$ concentration (Denman et al., 2007). Woody plants, such as trees and shrubs, are expected to take up carbon into their wood biomass for up to two centuries after atmospheric $CO_2$ has ceased increasing. At high atmospheric $CO_2$ concentrations (ca. 800–1000 ppmv) $CO_2$ fertilization saturates since $CO_2$ concentration is no longer rate-limiting for photosynthesis in C3 plant species (Falkowski et al., 2000).

Changes in climate can induce ecosystem changes as plant species migrate to climates that meet their physiological needs (e.g. Baldocchi and Valentini, 2004). Transition from one ecosystem to another can be sudden, as in the case of the rainforest to grassland transition seen in some climate models (e.g. Malhi et al., 2009). In many manifestations, however, ecological transition occurs slowly due to the decennial timescale for tree growth (Baldocchi and Valentini, 2004). Ecosystem changes can be either a positive or negative carbon cycle feedback depending on whether afforestation or deforestation is being induced. In tropical regions, increases in temperature are expected to inhibit plant growth by increasing water stress and by exceeding plant physiological limits. At high latitudes warming is expected in enhance plant growth by increasing the length of the growing season. Anthropogenic land use changes also induce positive or negative carbon cycle feedback through deforestation, agricultural practices and abandonment of formerly cultivated lands (Denman et al., 2007).

The ocean takes up and releases $CO_2$ as a function of the gradient in the partial pressure of $CO_2$ between the surface of the ocean and the atmosphere (Denman et al., 2007). If atmospheric $CO_2$ concentration is increased from non-oceanic sources (e.g. fossil fuel emissions or deforestation), the partial pressure difference between the surface ocean and the atmosphere increases. This creates a stronger partial pressure gradient and increases the rate of ocean uptake of $CO_2$ (Friedlingstein et al., 2006). The strength of this feedback is constrained by the temperature dependance of the

solubility of $CO_2$ in water and by the carbonate chemistry of the ocean (e.g. Greenblatt and Sarmiento, 2004). Like most other gasses, the solubility of $CO_2$ in water decreases with an increase in water temperature, such that the partial pressure of $CO_2$ in water is higher at a higher temperature for the same aqueous concentration of $CO_2$ (e.g. Greenblatt and Sarmiento, 2004). The carbonate buffering system of the ocean allows the oceans to hold far more carbon than would be possible in distilled water (Falkowski et al., 2000). When $CO_2$ dissolves in the ocean it quickly comes into equilibrium with other species of dissolved inorganic carbon:

$$CO_2 + CO_3^{2-} + H_2O \longleftrightarrow 2\,HCO_3^{-}. \tag{3.1}$$

The surface ocean has a limited supply of the $CO_3^{2-}$ anions so that as more inorganic carbon is added to the ocean a higher fraction of the carbon will be held as $CO_{2\,(aq)}$, until such time that the ocean can dissolve more $CO_3^{2-}$ from sediments (Le Qéré and Metzl, 2004). Therefore, as climate warms, due to increasing atmospheric $CO_2$, the relative fraction of the fossil carbon that the surface ocean is able to take up carbon is reduced (Denman et al., 2007).

Carbon is exported from the surface ocean to the ocean interior though subduction of cold dense ($CO_2$ enriched) water at deep-water formation sites (in the North Atlantic and Southern Ocean) and via the biological pump (e.g. Sigman et al., 2010). The biological pump is the transport of organic carbon into the deep ocean from its production at the surface. In the ocean interior this organic material is oxidized to $CO_2$ (Greenblatt and Sarmiento, 2004). Changes in meridional overturning circulation and biological activity in the surface ocean affect this sink of carbon into the deep ocean (Denman et al., 2007).

In most models of the global carbon cycle, the carbon cycle feedbacks together have a stabilizing effect on climate. Higher $CO_2$ concentration induces warming and enhanced soil respiration but also increases plant growth and ocean uptake of carbon. In models, the ocean and land vegetation generally absorb more carbon than soils are emitting (Friedlingstein et al., 2006).

Anthropogenically produced greenhouse gasses besides $CO_2$ contribute to climate change (Forster et al., 2007). The most important of these well-mixed species are $CH_4$, $N_2O$, and Halocarbons which respectively contributed radiative forcings of $0.48\,W\,m^{-2}$, $0.16\,W\,m^{-2}$, and $0.34\,W\,m^{-2}$ in 2005. The atmospheric life times of $CH_4$ and $N_2O$ are 12 and 114 years respectively. The Halocarbons have lifetimes

ranging between decades and thousands of years (Forster et al., 2007). Non-$CO_2$ greenhouses gasses interact with carbon cycle dynamics in that they contribute to the warming of the climate without inducing $CO_2$ fertilization or strengthening the gradient in $CO_2$ partial pressure between the atmosphere and the ocean (Huntingford et al., 2011). That is, these gasses do not induce two of the powerful negative feedbacks to climate change while contributing to the enhanced soil respiration, reduction in the solubility of $CO_2$ in the ocean, as well as to temperature induced ecosystem changes. In this chapter non-$CO_2$ greenhouse gas forcings are reported as anomalies from pre-industrial non-$CO_2$ greenhouse gas forcing.

Sulphate aerosols reflect shortwave radiation back into space producing a negative radiative forcing with respect to the planetary surface (Murphy et al., 2009). Throughout most of the industrial age the net effect of the sulphate aerosols has roughly canceled out the positive radiative forcing from non-$CO_2$ greenhouse gasses (Forster et al., 2007, Murphy et al., 2009). The atmospheric lifetime of sulphate aerosols is on the order of days to weeks (Lohmann and Feichter, 2005). Therefore, a constant source of these aerosols is needed to maintain their presence in the atmosphere. The largest source of sulphate aerosols to the atmosphere is fossil fuel burning (Forster et al., 2007). It is expected that if anthropogenic burning of fossil fuels were to suddenly cease then aerosols would rain out of the atmosphere shortly thereafter removing the negative radiative forcing they presently produce. The experiments detailed below contemplate the effects on the global carbon cycle of the complete cessation of anthropogenic carbon emissions on centennial timescales. We assume that the effects of sulphate aerosols dissipate within weeks of such an event, and therefore assume that the radiative forcing from sulphate aerosols is zero after cessation of carbon emissions. However, not all aerosol forcing is associated with fossil fuel emissions so it is not implausible that significant aerosol emissions from biomass burning and anthropogenic sources could continue after fossil fuel emissions cease.

Experiments using Earth system climate models have suggested that if anthropogenic carbon emission were to cease that natural carbon sinks would continue to operate, slowly scrubbing $CO_2$ out of the atmosphere (Matthews and Weaver, 2010, Gillett et al., 2011, Matthews and Zickfeld, 2012). The inclusion of a permafrost carbon component into the University of Victoria Earth System Climate Model (UVic ESCM) has strengthened the soil respiration feedback, which modifies the response of the model to the immediate cessation of anthropogenic emissions (MacDougall et al., 2012). When forced with a constrained and prescribed climate sensitivity of 3.0°C, at-

mospheric $CO_2$ remains almost constant for centuries after cessation of anthropogenic carbon emissions, no-matter when carbon emissions cease in the 21st century (MacDougall et al., 2012). The model result that under specified conditions $CO_2$ remains constant in the atmosphere after cessation of anthropogenic $CO_2$ emissions suggests that there is a magnitude of non-$CO_2$ greenhouse gas forcing that induces a balance between modelled carbon sources and sinks. If non-$CO_2$ greenhouse gas forcing is maintained above this threshold, $CO_2$ will continue to build up in the atmosphere following a cessation of anthropogenic $CO_2$ emissions. Here we develop a method to find this carbon-cycle balance point, explore the consequences of exceeding this threshold, and discuss the circumstances of why this balance may be attainable in the natural world.

## 3.2 Methods

### 3.2.1 Model description

The UVic ESCM is a coupled climate model of intermediate complexity (Weaver et al., 2001) with fully coupled oceanic (Schmittner et al., 2008) and terrestrial carbon cycle components (Matthews et al., 2004, Meissner et al., 2003). For this study the permafrost carbon version of the UVic ESCM is used. The frozen ground component of this model is described in Avis et al. (2011) and Avis (2012). The parameterization of the permafrost carbon pool is described in MacDougall et al. (2012).

The oceanic carbon cycle component of the UVic ESCM is composed of an Ocean Carbon-Cycle Model Intercomparison Project type inorganic carbon cycle model. Ocean biology is simulated using a nutrient-phytoplankton-zooplankton-detritus ecosystem model (Schmittner et al., 2008). An oxic-only model of sediment respiration is used to simulate ocean sedimentary processes (Archer, 1996). Terrestrial vegetation is simulated using the TRIFFID dynamic vegetation model coupled to a simplified version of the Hadley Centre Met Office surface exchange scheme (Meissner et al., 2003). The subsurface scheme has been modified to a 14 layer representation, extending down to a depth of 250 m, with exponentially increasing layer thicknesses (Avis et al., 2011). The modified subsurface scheme allows for freeze-thaw processes and has spatially varying thermal and hydraulic properties. These properties are interpolated to the model grid from soil mineral properties and organic content from the International Satellite Land Surface Climatology project soil database (Scholes

and de Colstoun, 2012).The soil contains two carbon pools: an active carbon pool and a permafrost carbon pool. The active carbon pool is generated by the balance of heterotrophic soil respiration and plant litter-fall from the TRIFFID vegetation model. The permafrost carbon pool exists only in soil layers that have been permanently frozen since model spin-up. The permafrost carbon is assigned a globally uniform carbon density. If a permafrost layer thaws it (and the carbon within it) are irreversibly transferred to the control of the active soil carbon component. Thereafter the carbon within the layer will begin to decay (MacDougall et al., 2012). An extended description of the UVic ESCM is found in Appendix A.2.

In order to allow atmospheric $CO_2$ to freely evolve, the UVic ESCM is forced with carbon emissions. Certain experiments detailed below are forced using emission pathways diagnosed from Representative Concentration Pathways (RCPs). These Diagnosed Emissions Pathways (DEPs) were derived by forcing the UVic ESCM with each RCP and diagnosing fossil fuel emissions as a residual of the global carbon cycle (see Appendix A.1 for a detailed description and validation). The UVic ESCM's inherent climate sensitivity of 3.2°C is used in all experiments.

### 3.2.2 Allowing for balance

In the Canadian Earth System Model (CanESM) and previous versions of the UVic ESCM the immediate response to a complete cessation of anthropogenic carbon emissions is a fast drop in atmospheric $CO_2$ concentration that lasts for approximately 20 years (Matthews and Zickfeld, 2012, Gillett et al., 2011). After the system has had time to adjust to the sudden cessation of anthropogenic emissions, atmospheric $CO_2$ goes into a slow exponential decline in these simulations. The ocean uptake and $CO_2$ emissions from the terrestrial biosphere cannot be balanced during these first 20 years with a plausible non-$CO_2$ greenhouse gas forcing (during this period in most experiments the terrestrial biosphere is transitioning from a sink to a source of carbon). However, after the system adjusts to the sudden change in forcing it may be possible to induce a balance. For the remainder of this discussion we will focus on this period beyond the first 20 years after cessation of anthropogenic emissions. The 20 year period is likely a consequence of the abrupt cessation of anthropogenic emissions. A gradual elimination of emissions would presumable lead to a more continuous transition to a post-fossil fuel global carbon cycle.

### 3.2.3 Finding balance

Here we infer that for a given quantity of cumulative carbon emissions there is a magnitude of non-$CO_2$ greenhouse gas forcing that will induce a balance between terrestrial carbon emissions and ocean uptake of carbon for the period starting 20 years after the cessation of anthropogenic carbon emissions. To find this magnitude of non-$CO_2$ greenhouse gasses an iterative root finding method is used:

1. After cessation of anthropogenic $CO_2$ emissions the UVic ESCM is run for 100 years forced under a constant aggregated non-$CO_2$ greenhouse gas forcing ($R_{\text{agg}}$).

2. The Earth system is allowed to adjust after cessation of $CO_2$ emissions for 20 years

3. If $CO_2$ accumulates in the atmosphere after the 20 year adjustment period the experiment is repeated with a reduced $R_{\text{agg}}$.

4. If instead $CO_2$ decreases in the atmosphere after the 20 year adjustment period the experiment is repeated with an increased $R_{\text{agg}}$.

5. This loop is continued until atmospheric $CO_2$ is balanced to within 2.0 ppmv over the last 80 years of the simulation.

If a balance cannot be found then one or more of the assumptions that have been made must be false. See section 3.4.1 for a discussion of the conditions under which this method can work.

### 3.2.4 Experiments

Three balance experiments were conducted by varying the rate of anthropogenic carbon emissions. In all experiments the iterative method was used to find the carbon balance point for cumulative anthropogenic emissions of 80, 160, 320, 640, 980, and 1920 Pg of carbon (Pg C). In the pulse experiment, carbon was emitted to the atmosphere over the course of one year. There were no sulphate aerosols or volcanic events in this experiment and agricultural areas were held constant at their pre-industrial extent. In the ramp-up experiment, carbon was increased at a rate of 1% of total emissions a year for 100 years. During the 100 year ramp-up agricultural areas were

held constant at a pre-industrial extent, there were no sulphate aerosols, no volcanic events, and non-$CO_2$ greenhouse gas forcing was held at zero.

In the transient emissions experiment emissions pathways were followed until the required amount of carbon had been released to the atmosphere. During the transient period the prescribed non-$CO_2$ greenhouse gas, sulphate emissions, volcanic events, land-use changes, and solar output variation were followed for each DEP. When cumulative anthropogenic carbon emissions reached the desired total carbon, sulphate emissions were instantaneously reduced to zero. After cessation of carbon emissions agricultural areas were held constant, and volcanic events and the solar output were fixed to their long-term means. The DEPs 8.5, 6.0, and 4.5 were followed, although most of the cumulative emission integration points occur before the DEPs diverge (DEP 2.6 is set aside due to the negative anthropogenic emissions required under that pathway).

Additional experiments were conducted for magnitudes of non-$CO_2$ greenhouse gasses not expected to balance uptake of carbon by the ocean and emission of carbon from the terrestrial biosphere. These experiments were intended to demonstrate the effect of not reaching or exceeding the balance point for realistic non-$CO_2$ greenhouse gas forcing. These experiments were identical to the transient emissions experiment until cessation of carbon emissions. After cessation, non-$CO_2$ greenhouse gas forcing was held at a constant non-balancing value, agricultural areas were held constant, and volcanic events and the solar output were fixed to their long-term means. The values chosen were 0.0 $\mathrm{W\,m^{-2}}$, 0.95 $\mathrm{W\,m^{-2}}$ and 2.0 $\mathrm{W\,m^{-2}}$ respectively. These values are the pre-industrial non-$CO_2$ greenhouse gas forcing, the present-day non-$CO_2$ greenhouse gas forcing, and the maximum non-$CO_2$ greenhouse gas forcing projected under RCP 8.5. All values are relative to pre-industrial non-$CO_2$ greenhouse gas forcing. These experiments are designated as the unbalanced experiments.

## 3.3 Results

### 3.3.1 Select results

Selected results for the transient and unbalanced experiments are shown in Figure 3.1. The figure displays atmospheric $CO_2$ concentrations and anthropogenic emissions with time for the pre-industrial (0.0 $\mathrm{W\,m^{-2}}$), balancing, and 2.0 $\mathrm{W\,m^{-2}}$ non-$CO_2$ radiative forcings. The figure demonstrates the three possible atmospheric $CO_2$ tra-

jectories after cessation of anthropogenic $CO_2$ emissions: atmospheric $CO_2$ decreases, atmospheric $CO_2$ remains nearly constant, or atmospheric $CO_2$ continues to increase without further human $CO_2$ emissions. For brevity subsequent figures display only the $R_{\text{agg}}$ needed to balance atmospheric carbon verses cumulative carbon emissions. Figure 3.2 displays the fluxes between and the changes in mass of each of the major carbon pools before and after cessation of emissions for a selected balance experiment. This figure illustrates the changes in the magnitude of carbon fluxes as the Earth system transitions to a post fossil-fuel carbon cycle. Notably following the cessation of anthropogenic $CO_2$ emissions changes in carbon pool size become dominated by release of carbon from soils and uptake of carbon by the deep ocean. In addition to these two large fluxes their is a residual uptake of carbon by land plants an order of magnitude small than these two other fluxes.

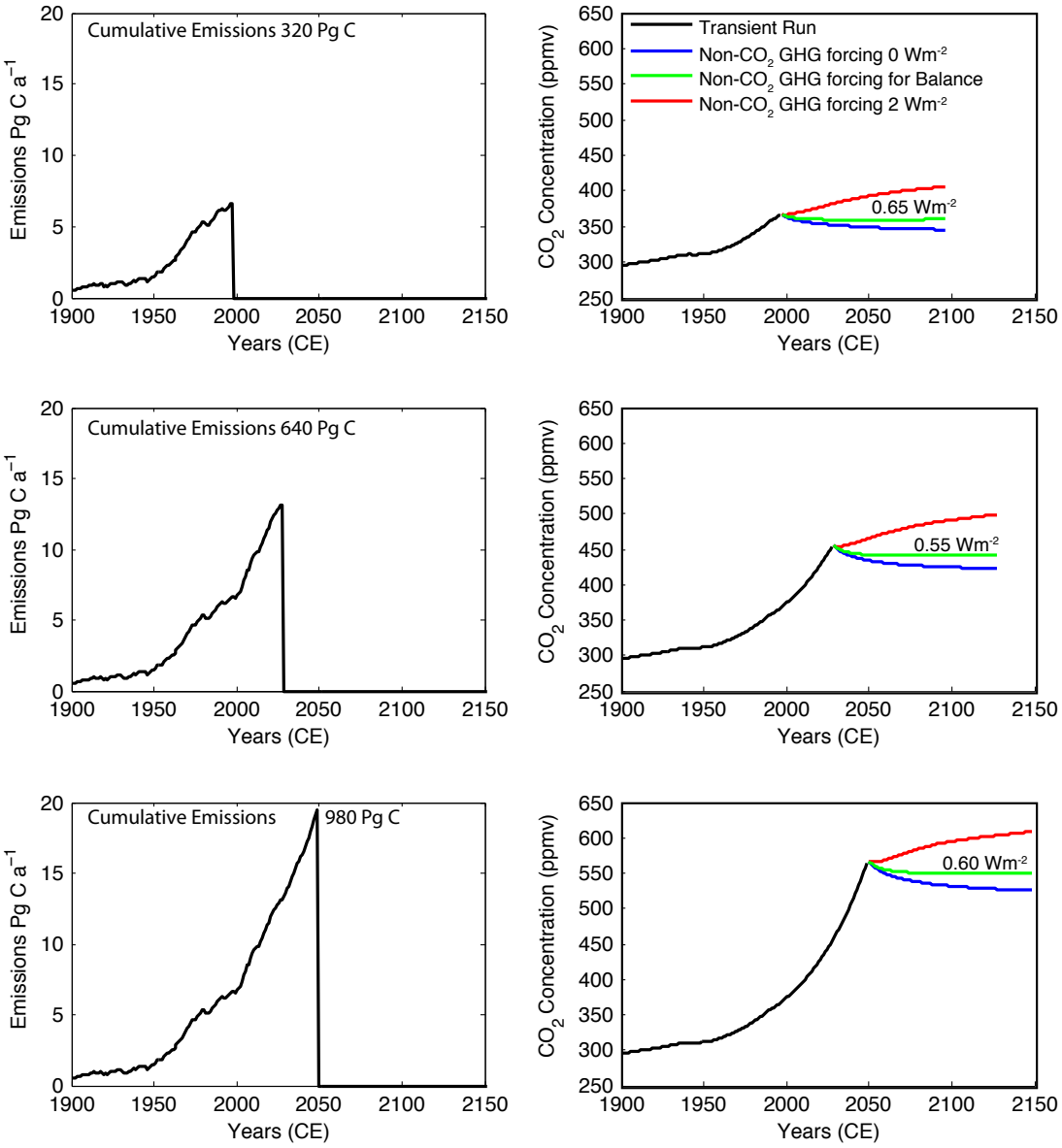


Figure 3.1: $CO_2$ emissions with time (left column) and $CO_2$ concentration with time for three selected cumulative emissions integration points. Atmospheric $CO_2$ concentrations with time after cessation of anthropogenic $CO_2$ emissions given for non-$CO_2$ greenhouse gas forcings at pre-industrial (0.0 W m$^{-2}$), balancing and 2.0 W m$^{-2}$ magnitudes.

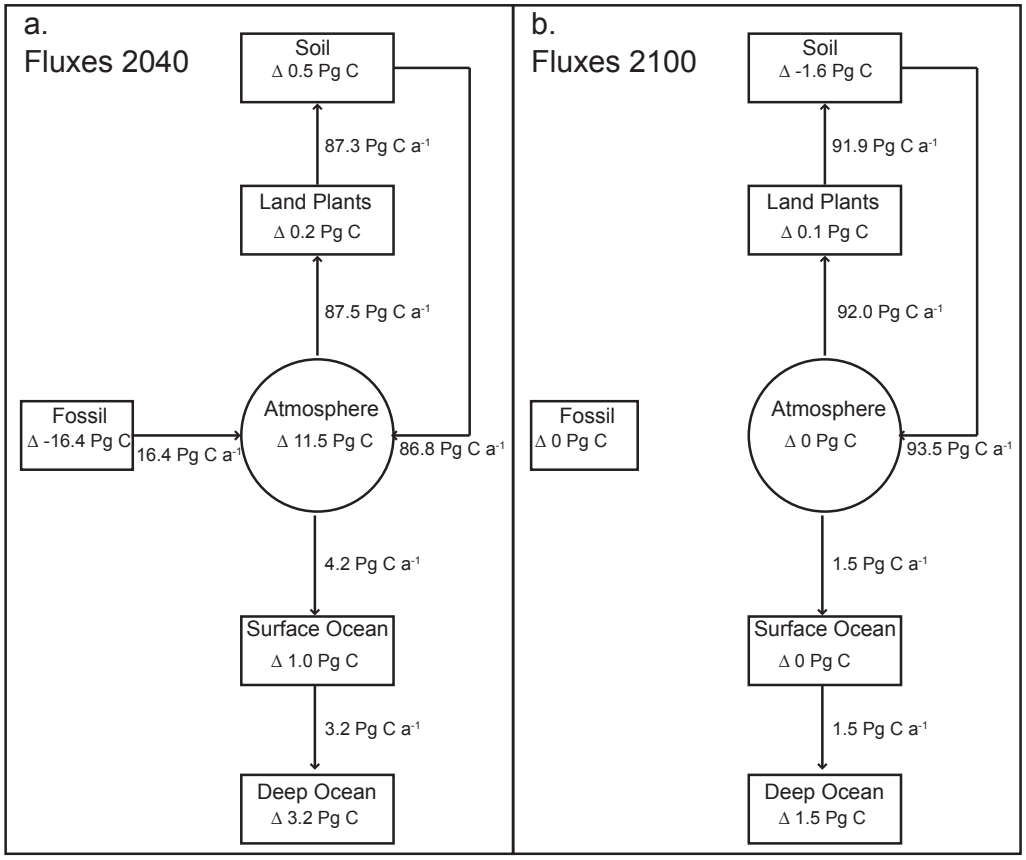


Figure 3.2: Net fluxes between, and changes in mass, of each of the major carbon pools. a) Averaged over a decade before cessation of fossil $CO_2$ emissions. b) Averaged over a decade 50 years after cessation of fossil $CO_2$ emissions. Fluxes are from the transient experiment following DEP 8.5, with anthropogenic $CO_2$ emissions ceasing in the year 2050. The surface ocean is taken at the top 250 m of the water column.

### 3.3.2 Balance experiments

Results for the pulse, ramp-up, and transient emissions experiments are shown in Figure 3.3. All of the curves have common characteristics, increasing from an $R_{\text{agg}}$ of zero (relative to pre-industrial times) at a cumulative emission of zero (relative to 1900), reaching a peak $R_{\text{agg}}$, between 160–980 Pg C of cumulative anthropogenic carbon emissions, and declining from this peak with higher cumulative carbon emissions. The highest $R_{\text{agg}}$ to induce balance is required for the pulse experiment and lowest $R_{\text{agg}}$ is required for the ramp-up experiment. This demonstrates that the rate at which carbon is emitted to the atmosphere contributes to the magnitude of $R_{\text{agg}}$ needed to balance terrestrial emissions and ocean uptake of carbon. That is, balance $R_{\text{agg}}$ is path dependent for the timescales considered here.

The transient experiment has a peak balance $R_{\text{agg}}$ of $0.65\,\text{W}\,\text{m}^{-2}$ at 320 Pg C and declines to $0.5\,\text{W}\,\text{m}^{-2}$ when following the DEP 4.5 and 6.0 emissions trajectories. For the DEP 8.5 trajectory $R_{\text{agg}}$ declines to $0.55\,\text{W}\,\text{m}^{-2}$ at 640 Pg C then increases again too stabilize at $0.6\,\text{W}\,\text{m}^{-2}$ for cumulative emissions up to 1920 Pg C. Also shown on Figure 3.3 c is the historical cumulative anthropogenic carbon emission – non-$CO_2$ greenhouse gas forcing trajectory. This line shows that the historical magnitude of non-$CO_2$ greenhouse gas forcing has been above the magnitude needed for $CO_2$ to continue to increase, if emissions were to cease, since 1900. That is, these model results suggest that the Earth has been in the regime of increasing $CO_2$ without further human $CO_2$ emissions for most of the industrial age.

The general shape of the curves in Figures 3.3 can be explained by the geographic distribution of soil carbon in the UVic ESCM. Figure 3.4 shows the regions where soil respiration is enhanced by increasing $R_{\text{agg}}$ from pre-industrial forcing to the balance forcing for selected cumulative emission integration points. The excess soil respiration needed to balance ocean uptake is largely derived from regions of decaying permafrost. The large jump in $R_{\text{agg}}$ needed to balance ocean uptake between 80 and 160 Pg C is therefore related to the quantity of climate warming needed to destabilize sequestered permafrost carbon.

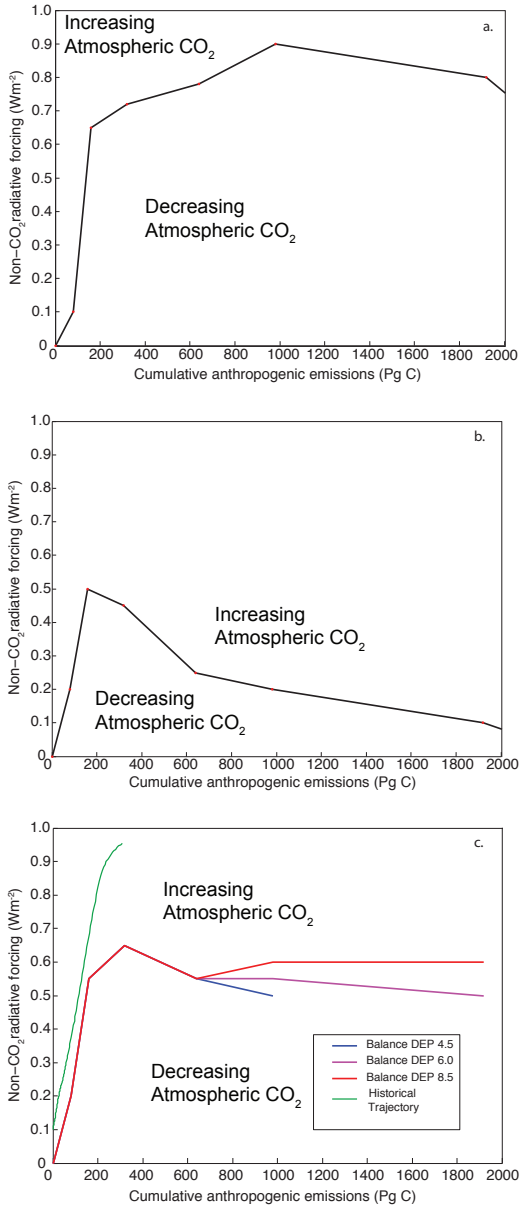


Figure 3.3: Non-$CO_2$ radiative forcing required to maintain a constant level of $CO_2$ in the atmosphere after cessation of emissions for a given quantity of cumulative anthropogenic carbon emissions. a.) Carbon emitted as a pulse over the course of one year. b.) Carbon emitted at 1% of cumulative emissions per year for 100 years. c.) Carbon emitted following a given Diagnosed Emissions Pathway (DEP). The green line shows the historical cumulative anthropogenic carbon emissions – non-$CO_2$ radiative forcing curve. The current radiative forcing from non-$CO_2$ greenhouse gasses is above the level needed to maintain balance after cessation of emissions.

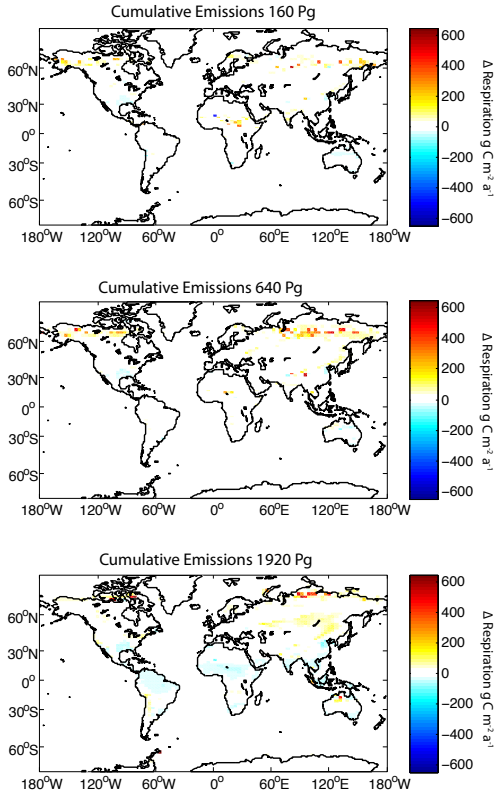


Figure 3.4: Difference in soil respiration between model simulation at balancing and pre-industrial magnitudes of non-$CO_2$ greenhouse gas forcing, for selected cumulative emission integration points. Maps are for the fifth decade after cessation of emissions. Notice that in each case most of the additional soil respiration caused by additional non-$CO_2$ greenhouse gas forcing originates from former permafrost soils. For cumulative emissions of 1920 Pg C increasing the magnitude of non-$CO_2$ greenhouse gas forcing reduces the rate of soil respiration in the tropics. This reduction in soil respiration is coincident with a reduction of net primary productivity in these regions. As soil carbon turn-over rates are high in the tropics a reduction in litter-fall will quickly lead to a reduction in soil respiration (once litter-fall and soil respiration are in equilibrium).

Inspection of the changes in carbon pool sizes for each of the experiments shows that uptake of carbon by vegetation makes a significant contribution to carbon uptake in the pulse experiment (15–40% of ocean uptake) and a negligible contribution in the other experiments. This explains why a higher $R_{\text{agg}}$ is needed to induce balance in this experiment than in the other two experiments. In the pulse experiment enhanced soil respiration must balance the uptake of carbon by both the oceans and terrestrial vegetation. Therefore, a larger $R_{\text{agg}}$ is required to further enhance soil respiration.

The difference between the shape of the balance curves in the ramp-up (Figure 3.3 b.) and the transient emissions experiment (Figure 3.3c.) is curious. Due to the presence of agriculture in the transient emissions experiment, this experiment has higher $CO_2$ concentrations at the same cumulative anthropogenic (fossil fuel) carbon emissions as the ramp-up experiment. All else being equal this should shift the curve to the left producing a lower balance $R_{\text{agg}}$ for the transient experiments beyond the peak $R_{\text{agg}}$ value. The experiments in fact exhibit the opposite behaviour. The difference in terrestrial Net Primary Production (NPP) between the ramp-up and transient emissions experiment provides an explanation for the higher balance $R_{\text{agg}}$ needed in the transient emissions experiment. For the cumulative anthropogenic carbon emissions integration point of 1920 Pg C, terrestrial NPP at the end of the balanced simulation is 100.4 $\text{Pg}\,\text{a}^{-1}$ C for the ramp-up experiment, 113.8 $\text{Pg}\,\text{a}^{-1}$ C for transient emissions DEP 8.5 experiment, and 106.7 $\text{Pg}\,\text{a}^{-1}$ C for the transient emissions DEP 6.0 experiment. This corresponds to balances in $R_{\text{agg}}$ of 0.1 $\text{W}\,\text{m}^{-2}$, 0.6 $\text{W}\,\text{m}^{-2}$, and 0.5 $\text{W}\,\text{m}^{-2}$ respectively. Since all of these values of terrestrial NPP are for stable $CO_2$ concentrations, the higher NPP must be coming from the transition of ecosystems into more carbon intense systems. This negative feedback can be seen in Figure 3.5, which maps the difference in terrestrial NPP between the ramp-up and transient emission experiments averaged over the decade beginning 90 years after cumulative anthropogenic carbon emissions reach 1920 Pg C. The figure shows distinct regions where NPP is higher in the transient emissions experiment than the ramp-up experiment. Specifically these are in central Eurasia, the Sahel and the subtropical region of South America and Africa. These regions are consistent with areas that are pastures in the transient experiment and natural ecosystems in the ramp-up experiment. These pasture regions have a higher NPP than the natural ecosystems they replaced and are associated with a build-up of stored soil carbon in these regions.

Figure 3.6 shows the estimated non-$CO_2$ greenhouse gas forcings from trace-gas concentrations prescribed for each RCP up to the year 2300. These estimated forcings

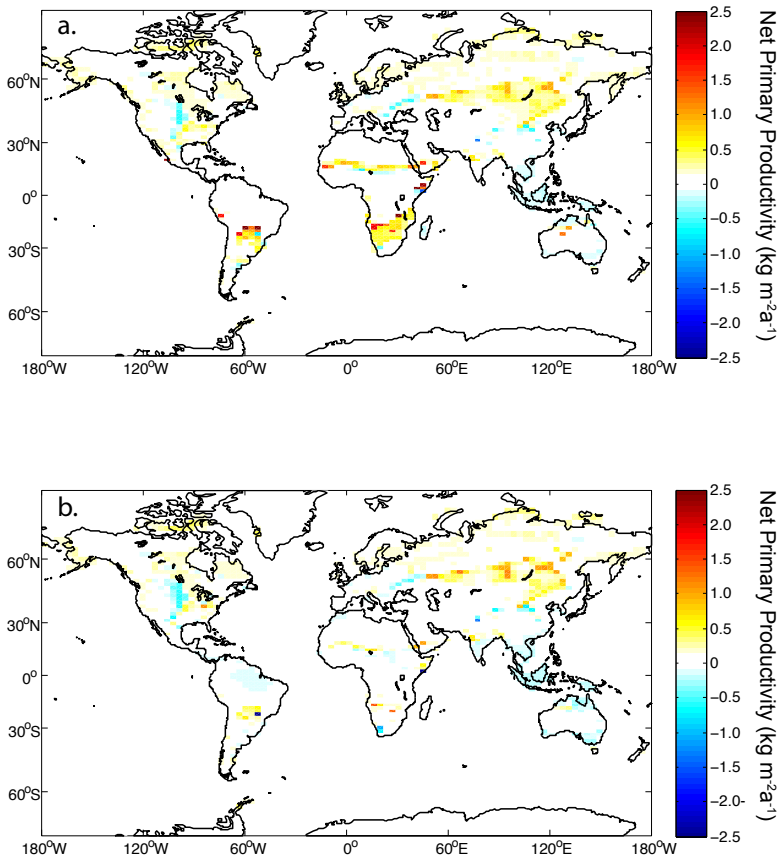


Figure 3.5: Difference in Net Primary Production (NPP) between the ramp up experiment and a.) transient emissions experiment following DEP 8.5 for cumulative anthropogenic carbon emissions of 1920 Pg C (Transient emission - Ramp up). b.) Same as **a.** except following DEP 6.0. Note that positive NPP anomalies are concentrated in central Eurasia, the Sahel, and the subtropics of Africa and South America.

for year 2300 range from 0.63 $\mathrm{W\,m^{-2}}$ under RCP 2.6 to 2.0 $\mathrm{W\,m^{-2}}$ for RCP 8.5. That is, the estimated non-$CO_2$ greenhouse gas forcing for the most optimistic RCP is about the same magnitude of radiative forcing needed to balance atmospheric $CO_2$ in the model experiments conducted here.

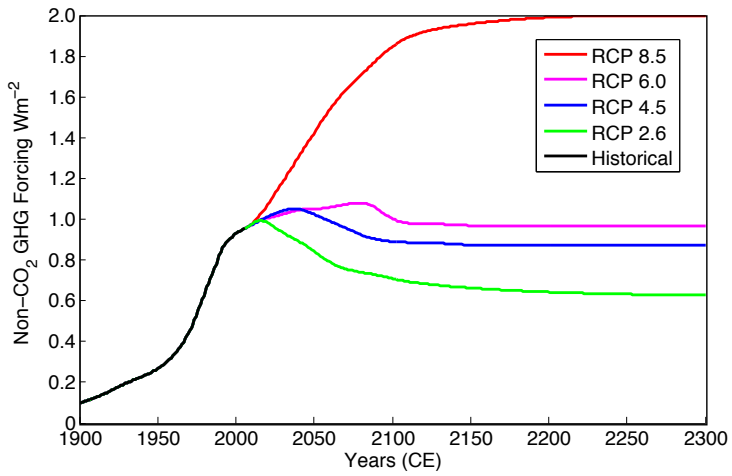


Figure 3.6: Estimated radiative forcing from non-$CO_2$ greenhouse gasses for trace-gas concentration prescribed for each of the four Representative Concentration Pathways (RCPs) (Moss et al., 2010). Note that even the most optimistic estimate for future non-$CO_2$ greenhouse gas forcing is consistent with approximately balancing ocean uptake of carbon with emissions from the terrestrial biosphere in the present simulations.

### 3.3.3 Unbalanced experiments

Results of the unbalanced experiments are shown in Tables 3.1, 4.1, and 3.3. Under a continued modern $R_{\text{agg}}$ of $0.95\,\text{W}\,\text{m}^{-2}$, the atmospheric $CO_2$ concentration increases an additional 11–22 ppmv before peaking in the 23rd or 24th century (Table 3.1). That is, $CO_2$ continues to build up very slowly in the atmosphere for hundreds of years after anthropogenic carbon emissions cease. The actual amount of carbon released by soils is substantial (167–400 Pg C) but most of this carbon is absorbed by the oceans (68–89%) (Table 4.1). Almost as much carbon is absorbed by land plants as builds up in the atmosphere. Under an $R_{\text{agg}}$ commensurate to that in RCP 8.5 ($2.0\,\text{W}\,\text{m}^{-2}$), soils release more carbon (400–570 Pg C) and the atmosphere takes up a larger fraction of this carbon (27-35%), but the oceans continue to take up the largest share of carbon (56–64%) (Table 3.3). The additional increase in $CO_2$ concentration is 64–86 ppmv, but the effects of this increase in $CO_2$ are minor compared to that of imposing an unbalanced radiative forcing of $2.0\,\text{W}\,\text{m}^{-2}$ on the Earth system. These results suggest that the consequences of being beyond the carbon-cycle balance point are mild for non-$CO_2$ greenhouse gas concentration observed in the contemporary atmosphere. After the cessation of anthropogenic carbon emissions, atmospheric $CO_2$ will continue to build up in the atmosphere but at a rate that is an order of magnitude slower than during the fossil fuel era.

Table 3.1: Peak $CO_2$ concentrations for a given quantity of cumulative anthropogenic carbon emissions, year of peak, and change in concentration relative to 20 years after shutdown.

| Cumulative Emissions (Pg C) | Year of Peak (CE) | Peak $CO_2$ (ppmv) | $\Delta$ $CO_2$ (ppmv) |
|---|---|---|---|
| Unbalanced 0.95 $W\,m^{-2}$ | | | |
| 80 | 2321 | 327 | 17 |
| 160 | 2360 | 342 | 15 |
| 320 | 2366 | 379 | 16 |
| 640 | 2241 | 460 | 12 |
| 980 | 2213 | 569 | 11 |
| 1920 | 2244 | 949 | 22 |
| | | | |
| Unbalanced 2.0 $W\,m^{-2}$ | | | |
| 160 | 2436 | 394 | 66 |
| 320 | 2347 | 431 | 64 |
| 640 | 2422 | 521 | 67 |
| 980 | 2341 | 639 | 70 |
| 1920 | 2249 | 1020 | 86 |

Table 3.2: Cumulative emissions from soils from year of cessation of anthropogenic carbon emissions to year of peak atmospheric $CO_2$. Also shown is the partition of this carbon to the atmosphere, land plants, and the oceans.

| Cumulative Emissions (Pg C) | Year of Peak (CE) | Soil Pool (Pg C) | Atmosphere Pool (Pg C) | Land Plants Pool (Pg C) | Ocean Pool (Pg C) |
|---|---|---|---|---|---|
| Unbalanced 0.95 $W\,m^{-2}$ | | | | | |
| 160 | 2360 | -166.8 | 29.7 | 5.6 | 113.9 |
| 320 | 2366 | -227.8 | 25.9 | 16.7 | 169.8 |
| 640 | 2241 | -240.3 | 11.4 | 18.6 | 203.3 |
| 980 | 2213 | -259.3 | 4.3 | 19.8 | 230.2 |
| 1920 | 2244 | -401.0 | 33.6 | 38.6 | 320.9 |
| | | | | | |
| Unbalanced 2.0 $W\,m^{-2}$ | | | | | |
| 160 | 2436 | -398.7 | 138.9 | 25.2 | 225.2 |
| 320 | 2347 | -407.8 | 135.2 | 23.7 | 247.7 |
| 640 | 2422 | -524.6 | 139.8 | 46.6 | 331.9 |
| 980 | 2341 | -565.0 | 152.8 | 44.6 | 363.4 |
| 1920 | 2249 | -569.5 | 183.9 | 27.5 | 355.6 |

Table 3.3: Fractional uptake by the atmosphere, land plants, and the oceans of carbon emitted by soils between cessation of anthropogenic carbon emissions and peak atmospheric $CO_2$ concentration.

| Cumulative Emissions (Pg C) | Year of Peak (CE) | Atmosphere Pool (%) | Land Plants Pool (%) | Ocean Pool (%) |
|---|---|---|---|---|
| Unbalanced 0.95 $W\,m^{-2}$ | | | | |
| 160 | 2360 | 18 | 14 | 68 |
| 320 | 2366 | 11 | 14 | 75 |
| 640 | 2241 | 5 | 10 | 85 |
| 980 | 2213 | 2 | 9 | 89 |
| 1920 | 2244 | 8 | 12 | 80 |
| | | | | |
| Unbalanced 2.0 $W\,m^{-2}$ | | | | |
| 160 | 2436 | 35 | 9 | 56 |
| 320 | 2347 | 33 | 6 | 61 |
| 640 | 2422 | 27 | 10 | 63 |
| 980 | 2341 | 27 | 9 | 64 |
| 1920 | 2249 | 32 | 6 | 62 |

### 3.3.4 Breakdown of assumptions

Not all of the attempts to find a carbon cycle balance point were successful. Figure 3.7 displays an attempt to balance at an integration point of 3840 Pg C for the transient emissions experiment following DEP 8.5. At the time anthropogenic $CO_2$ emissions cease in this simulation carbon emissions from the terrestrial biosphere are already larger than the ability of the oceans to absorb carbon. The terrestrial emissions soon fall off as the soil carbon pool is depleted (dropping 394 Pg C) and a strong afforestation feedback takes hold (adding 46 Pg C to land plants). Having exhausted the pool of soil carbon available for decay, terrestrial carbon emission become smaller than ocean uptake of $CO_2$, and atmospheric $CO_2$ concentration begins to decline. For this quantity of cumulative anthropogenic emissions, no constant level of non-$CO_2$ greenhouse gas forcing after cessation of emissions will produce a cancelation of terrestrial emissions and ocean uptake of carbon.

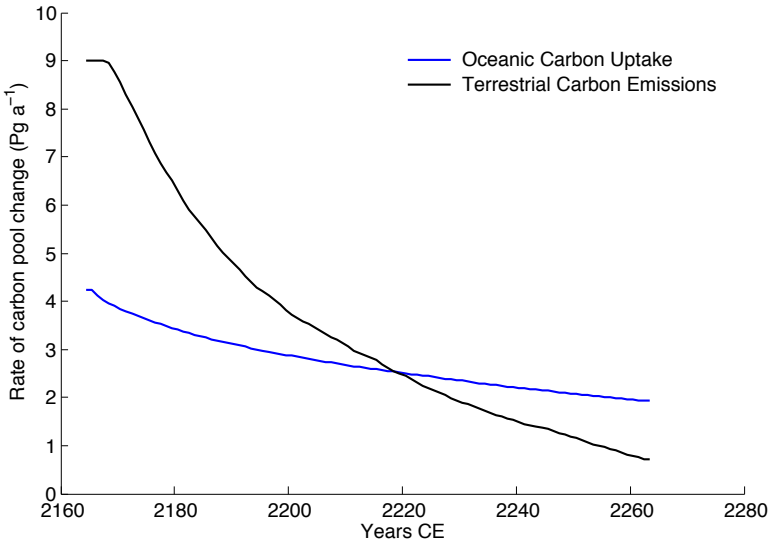


Figure 3.7: Rate of ocean uptake of carbon and terrestrial emissions of carbon for a simulation where the rates cannot be balanced. Opposite sign conventions are used for the two carbon fluxes to accommodate comparison of the magnitude of each. Notice that terrestrial emissions are already larger than ocean uptake when emissions cease. This example is from the transient emissions experiment for 3840 Pg of cumulative anthropogenic carbon emissions with a non-$CO_2$ radiative forcing of 3.0 W m$^{-2}$ after cessation of carbon emissions.

## 3.4 Discussion

### 3.4.1 Why is balancing atmospheric $CO_2$ possible?

A priori there is no reason to suspect the net emissions of $CO_2$ from the terrestrial land surface will balance the uptake of carbon by the oceans after cessation of anthropogenic $CO_2$ emissions. That this phenomenon does occur within the UVic ESCM for multiple cumulative carbon emissions and emissions trajectories begs for a simple mechanistic explanation. In this section a rudimentary description of ocean uptake of carbon and soil respiration will be invoked to argue that the functional form of the two processes, in addition to coincidences in the rate constants and carbon pool sizes of soil carbon and the surface ocean are what allow for balancing atmospheric $CO_2$.

As outlined in the introduction the flux of carbon into the surface ocean is proportional to the difference in $CO_2$ partial pressure between the atmosphere and the ocean. For a given location in the ocean this relationship can be described by:

$$\frac{\partial \mathrm{DIC}}{\partial t} = \frac{k_\mathrm{w}}{z_\mathrm{ml}} \left( [\mathrm{CO_2}]_\mathrm{sat} - [\mathrm{CO_2}]_\mathrm{w} \right), \tag{3.2}$$

where DIC is dissolved inorganic carbon, $k_\mathrm{w}$ is the piston velocity, $z_\mathrm{ml}$ is the thickness of the mixed layer, $[\mathrm{CO_2}]_\mathrm{sat}$ is the aqueous concentration of $CO_2$ at which the surface ocean would be in chemical equilibrium with the atmosphere, and $[\mathrm{CO_2}]_\mathrm{w}$ is the instantaneous concentration of $CO_2$ in ocean water (e.g. Najjar, 1992). The terms on right hand side are in turn functions of time, ocean stratification, ocean temperature, and other variables. $[\mathrm{CO_2}]_\mathrm{w}$ in particular is affected by the reaction of $CO_2$ with water and solutes into other species of DIC, and by marine organisms producing and consuming $CO_2$. Considering typical piston velocities (which vary an order of magnitude as a function of surface wind speed and other variables (e.g. Najjar, 1992)), and a typical mixed layer depth for the ocean, the rate constant of this relationship is on the order of 1-10$\times 10^{-7}\mathrm{s}^{-1}$ (e.g. Najjar, 1992). Recalling that only about 1 part in 200 of DIC is held as $\mathrm{CO_{2\,aq}}$ due to the carbonate buffering system of the ocean this rate constant reduces to 1-10$\times 10^{-9}\mathrm{s}^{-1}$ (e.g. Najjar, 1992).

Once carbon enters the surface ocean the biological pump and subduction of surface waters transport a portion of this carbon onto the ocean interior (e.g. Greenblatt and Sarmiento, 2004). Upwelling water from the deep ocean will partially compensate for this sink for carbon, however, due to the slow rate of ocean overturning transport of carbon into the deep ocean is expected to remain a sink of carbon for millennia

(e.g. Eby et al., 2009). The strength of the deep ocean carbon sink is dependent on the strength of the biological pump, the concentration of surface water DIC at the deep water formation sites, the rate of meridional overturning circulation, and the concentration of DIC in water upwelling from the ocean interior (e.g. Greenblatt and Sarmiento, 2004). If these factors were to remain constant in time then after an initial exponential decrease (as the surface ocean equilibrates with the atmosphere) the ocean uptake of carbon should asymptotically approach this background deep ocean uptake rate. However, it is a robust finding of ocean general circulation model simulations that the rate of meridional overturning circulation (MOC) is expected to decline in the first centuries of climate warming (Weaver et al., 2012), which implies that ocean uptake of carbon should decline in tandem with the slowing of the MOC.

The surface ocean holds approximately 700 Pg of dissolved inorganic carbon under contemporary conditions (Falkowski et al., 2000). If the solubility and carbonate chemistry of $CO_2$ were held constant, the surface ocean could hold another 700 Pg C for a doubling of atmospheric $CO_2$. However, the effects of $CO_2$ on solubility, carbonate chemistry, and ocean dynamics reduces this total to approximately 350-600 Pg C for a doubling of atmospheric $CO_2$, when simulated by ocean biogeochemical models (Greenblatt and Sarmiento, 2004). The surface ocean will absorb much of this total during a transient increase in atmospheric $CO_2$. Therefore, when anthropogenic $CO_2$ emissions cease the difference between the quantity of carbon the surface ocean has and the quantity of carbon the surface ocean needs (to be in equilibrium with the atmosphere) will be smaller. Once deep ocean processes dominate ocean uptake of carbon, the surface ocean is left with a perpetual deficit in the quantity of carbon needed to achieve equilibrium with the atmosphere.

Loss of carbon from soils occurs if soil respiration exceeds the rate of litter-fall into soils (Davidson and Janssens, 2006). As soil respiration is a function of soil temperature, many models show this transition occurring in the late 21st or 22nd century as climate warms (Davidson and Janssens, 2006). In non-permafrost soils approximately 100-200 Pg C of soil carbon are estimated to be vulnerable net soil respiration. Permafrost affected soils contain 1700 Pg C, about 800 Pg C of which is sequestered in frozen soils in the top 3 m of the soil column (Tarnocai et al., 2009). Together the terrestrial land surface has a total of approximately 900 to 1000 Pg C vulnerable to decay (but the quantity that actually becomes available to decay is dependent on the magnitude of surface temperature increase). The rate of soil respiration has been shown to be proportional to the quantity of soil carbon available for decay such that

given a pulse of soil carbon the quantity of carbon will be reduced asymptotically toward zero (Luo and Zhou, 2006). The rate constant for soil respiration for ideal moisture and temperature conditions varies by the chemical makeup of the organic mater available for decay and the microbial community conducting the decomposition. This rate constant has been measured to be between 1-10$\times 10^{-9} s^{-1}$ for typical mixtures of organic materials in soils (Luo and Zhou, 2006). The cold temperatures of former permafrost soils imply that effective rates constants for these soil are in the slow end of the range (e.g. Dutta et al., 2006). Results from MacDougall et al. (2012) shows that the UVic ESCM simulates a roughly linear release of sequestered permafrost carbon into active soil carbon pool for changes in surface temperature between 1 and 5 °C (see Figure 3.8). For a doubling of $CO_2$ (approximately a 3°C temperature increase), the results from MacDougall et al. (2012) show approximately a 400 Pg release of carbon to active soils from permafrost.

From these considerations one can see why it possible to balance the carbon cycle within the UVic ESCM for the century after cessation of carbon emissions. The phenomenon is conditional on the functional form of each process, rate constants, and quantity of carbon available for decay verses the quantity of carbon that the surface ocean requires to be in equilibrium with the atmosphere. Soil respiration has a negative exponential functional form, which after an initial period of rapid decline, can be approximated as a linearly declining emissions rate. Ocean uptake takes on a linear declining functional form once transport of carbon into the deep ocean becomes the dominant process (due to the slowing of meridional overturning circulation). Coincidentally the rate constants of uptake of carbon into the surface ocean and heterotrophic soil respiration are similar (larger for the ocean than land). In addition the quantity of carbon available for decay in the terrestrial land surface and the surface ocean's deficit in carbon are of similar magnitude (larger for the land than the ocean). By manipulating non-$CO_2$ greenhouse gas forcing one changes the rate of soil respiration (temperature dependant), controls how much carbon is liberated from permafrost carbon, and changes the partial pressure of $CO_2$ in ocean water (pulling the total ocean uptake of carbon and liberated permafrost carbon in opposite directions). These factors by coincidence happen to be close enough in value that manipulating non-$CO_2$ greenhouse gas forcing can generate an approximate balance between net emission of carbon from the terrestrial biosphere and uptake of carbon by the oceans for over a century.

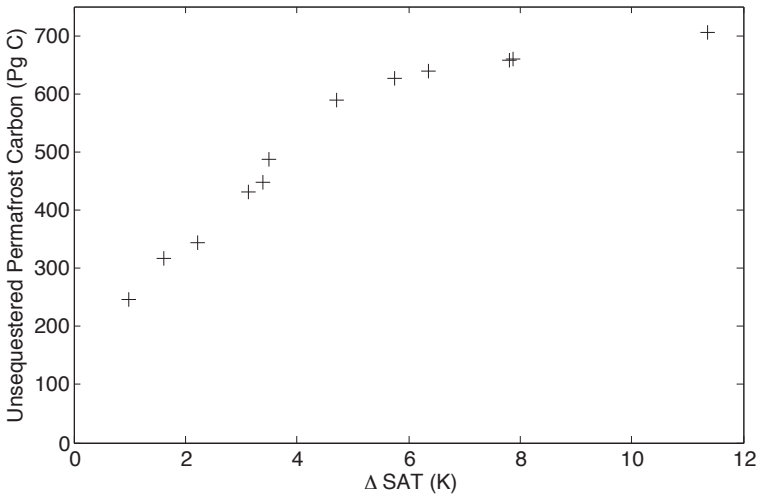


Figure 3.8: Change in Surface Air Temperature (SAT) verses release of carbon from the permafrost carbon pool to the active soil carbon pool, as simulated by the UVic ESCM for year 2300 following four emissions pathways (MacDougall et al., 2012). Note that between temperature increases of between 1 to 5°C the release of carbon from its sequestered state is nearly linear.

### 3.4.2 Model dependance

The results presented here are model dependent. The C$^4$MIP model intercomparison showed that carbon-cycle models have a range of simulated ocean uptake of carbon (between 4–10 Pg a$^{-1}$ C at 2100) and have varying responses from the terrestrial biosphere (Friedlingstein et al., 2006). If these type of balance experiments are conducted with other carbon-cycle models, different magnitudes of non-$CO_2$ greenhouse gas forcing, required to induce balance, would be expected. As discussed above the ability to balance the atmospheric carbon depends on several quantities within the Earth system being of coincident magnitude and functional form. Other Earth system models may simulate contrasting behaviour from the global carbon cycle.

The cloud, water vapour, albedo, and trace-gas feedbacks that determine planetary climate sensitivity have a similar effect as non-$CO_2$ greenhouse gasses (warming the surface while not increasing the ability of the ocean to absorb carbon). It is therefore expected that variations in climate sensitivity between models will also change the quantity of non-$CO_2$ greenhouse gasses needed to balance atmospheric $CO_2$. Low climate sensitivity models are expected to require more non-$CO_2$ greenhouse gas forcing to induce continued post-fossil fuel build up of atmospheric $CO_2$, than models with a higher climate sensitivity.

### 3.4.3 Timescale of balance

The model experiments conducted here consider the time-period up to 400 years after cessation of anthropogenic $CO_2$ emissions. The behaviour of the model at longer timescales is expected to be different. Balancing the atmospheric carbon pool requires that the quantity of carbon vulnerable for decay in soils be of the same order of magnitude as the quantity of carbon that the surface ocean requires to be in equilibrium with the atmosphere. However, the capacity of the full ocean to absorb carbon is immense (e.g. Falkowski et al., 2000) and the surface ocean deficit in carbon will exist long after the vulnerable pool of carbon has been depleted. At millennial time-scales it is expected that the permafrost carbon version of the UVic ESCM will behave much as earlier versions of the model (Eby et al., 2009) with the additional liberated permafrost carbon simply adding to the total anthropogenic carbon pulse.

### 3.4.4 Policy implications

Article 2 of the United Nations framework convention on climate change commits its signatories to "stabilization of greenhouse gas concentrations in the atmosphere at a level that would prevent dangerous anthropogenic interference with the climate system". The results presented here indicate that sharp reductions in the concentration of non-$CO_2$ greenhouse gasses may be required to prevent $CO_2$ from continuing to build up in the atmosphere (albeit slowly). That said, stabilizing atmospheric greenhouse gas concentrations may not be sufficient to prevent "dangerous anthropogenic interference with the climate system". Achieving that goal may require removal of greenhouse gasses from the atmosphere (e.g Hansen et al., 2008). Natural positive feedbacks between climate warming and wetland methane production imply that ceasing to emit industrial and agricultural methane will likely not return atmospheric methane concentration to their pre-industrial level (O'Connor et al., 2010). Ceasing production of methane from agricultural activities also appears unlikely if global food security is to be maintained. It is also possible irreversible damage to the caping formations of geological methane, and/or slow destabilization of methane clathrates could replace the current anthropogenic sources of methane (O'Connor et al., 2010). These factors could keep non-$CO_2$ greenhouse gas concentrations above quantity needed to stabilize atmospheric $CO_2$, even if anthropogenic sources of these gasses are eliminated.

### 3.4.5 Forcing and feedback uncertainties

The sudden cessation of anthropogenic $CO_2$ emissions is an implausible future emissions trajectory, and the model experiments conducted here are intended to be sensitivity experiments. However, if such an event where to occur uncertainties in the behaviour of several Earth system processes would affect whether atmospheric $CO_2$ concentration would continue to increase. The present day radiative forcing from anthropogenic aerosols is subject to considerable uncertainty (Murphy et al., 2009). The magnitude of this forcing and the forcing from non-$CO_2$ greenhouse gasses will determine the net change in radiative forcing upon cessation of aerosol emissions. The strength of the climate feedbacks that determine planetary climate sensitivity are also expected to strongly affect the rate at which carbon is released from permafrost soils (MacDougall et al., 2012). Balancing the atmospheric carbon pool is contingent on the existence of a vulnerable source of carbon within the terrestrial land surface (per-

mafrost carbon) to counteract the uptake of carbon by the oceans. Both the size and vulnerability of the permafrost carbon pool are subject to considerable uncertainties (Schuur and Abbott, 2011). All of these uncertainties will effect the magnitude of non-$CO_2$ greenhouse gas forcing required to induce a near balance in the atmospheric carbon pool.

## 3.5 Conclusions

Here we sought to answer the question: "if anthropogenic $CO_2$ emissions cease, will atmospheric $CO_2$ concentration continue to increase?" Our experiments show that for cumulative anthropogenic carbon emissions up to about 2000 Pg C there is a amount of non-$CO_2$ greenhouse gas forcing that will create a balance between emissions from the terrestrial biosphere and uptake of carbon by the oceans. If non-$CO_2$ greenhouse gasses are maintained above this amount then $CO_2$ will continue to build up in the atmosphere for centuries after the cessation of anthropogenic $CO_2$ emissions. If non-$CO_2$ greenhouse gasses are below this magnitude then atmospheric concentrations of $CO_2$ will decline after the cessation of emissions. That the simulated Earth is so close to the cross-over between decreasing and increasing atmospheric $CO_2$, appears to be a coincidence created by similar magnitudes in the quantity carbon that could be liberated from permafrost soils and the quantity of carbon that the surface ocean requires to be in equilibrium with the atmosphere.

The magnitude of non-$CO_2$ greenhouse gas forcing required to balance atmospheric $CO_2$ is a function of how much carbon has been emitted to the atmosphere and the rate at which it has been emitted. The historical trajectory of non-$CO_2$ greenhouse gas forcing has been above the simulated balancing magnitude since 1900. That is, if anthropogenic emissions were to cease tomorrow, the UVic ESCM projects that $CO_2$ would continue to build up in the atmosphere. However, the consequences of being in the regime of increasing $CO_2$ concentrations after the cessation of anthropogenic emissions are relatively mild. If current non-$CO_2$ greenhouse gas forcing is maintained indefinitely our admittedly model-dependent results suggest that we might expect an 11–22 ppmv increase in $CO_2$ after human emissions cease.

# Chapter 4

# Reversing climate warming by artificial atmospheric carbon-dioxide removal: can a Holocene-like climate be restored?

This chapter is based on the contents of the paper:
MacDougall, A. H., 2013: Reversing climate warming by artificial atmospheric carbon-dioxide removal: Can a holocene-like climate be restored? *Geophys. Res. Lett*, **40**, 5480–5485, DOI:10.1002/2013GL057467.

## 4.1 Introduction

Once net anthropogenic carbon emissions cease, the natural sources and sinks of carbon will govern the atmospheric concentration of $CO_2$. Long-term simulations using Earth system models suggest that over thousands of years carbon will be gradually incorporated into the oceans (e.g. Archer, 2005, Eby et al., 2009). However, long-term model simulations also indicate that most of the temperature anomaly created by burning of fossil fuels will persist even 10000 years into the future. The simulations of Eby et al. (2009) for example suggest that 70–80% of the peak surface temperature anomaly would remain by the year 12000 CE, for a large range of cumulative carbon emissions (160–5120 Pg C). Given these model findings any attempt to return atmospheric concentration of $CO_2$ to a "safe" level (after having greatly exceeded such a

threshold) will likely require synthetic removal of carbon from the atmosphere.

A number of previous model studies have performed simulations where anthropogenic carbon is removed from the atmosphere (e.g. Cao and Caldeira, 2010, Held et al., 2010, Samanta et al., 2010, Boucher et al., 2012, Zickfeld et al., 2013). These studies have been designed to explore the reversibility of climate change with respect to various metrics of the Earth system, such as surface temperature or thermosteric sea-level rise (e.g. Zickfeld et al., 2013), or to separate the fast from the slow components of climate warming (Held et al., 2010). Each of these previous studies has imposed highly idealized rates of atmospheric $CO_2$ removal. Cao and Caldeira (2010) and Held et al. (2010) prescribed instantaneous returns to pre-industrial $CO_2$ concentrations, while Samanta et al. (2010) and Zickfeld et al. (2013) prescribe linear reductions in $CO_2$ concentrations. Boucher et al. (2012) transitions from a 1% increases in atmospheric $CO_2$ concentration a year to a 1% decreases in atmospheric $CO_2$ concentration a year, creating a very abrupt transition from large positive carbon emissions to large negative carbon emissions.

Boucher et al. (2012) employed the complex Earth system model (ESM) HadGEM2-ES and documents the most extensive examination of hysteresis within an ESM. The study found that most metrics of the Earth-system exhibit hysteresis both with respect to temperature and atmospheric $CO_2$ concentration. Zickfeld et al. (2013) documents part of a model intercomparison of Earth system models of intermediate complexity (EMICs) carried out in preparation for the fifth assessment report of the Intergovernmental Panel on Climate Change (IPCC AR5). For two of the model experiments the EMICs were forced with a prescribed return to pre-industrial forcing over a period of 100 and 1000 years beginning in year 3000 CE. All of the EMICs simulated surface temperature and thermosteric sea-level anomalies with respect to the pre-industrial era that persisted for centuries after the return to pre-industrial $CO_2$ concentrations. Of interest is that two of the EMICs (including the UVic ESCM) suggested that more carbon would have to be removed from the atmosphere than had originally been emitted to the atmosphere to return to a pre-industrial $CO_2$ concentration.

Several technologies have been proposed to remove $CO_2$ from the atmosphere (e.g. Shepherd, 2009). Of those proposed, only bio-energy carbon capture and storage (BECS) (Azar et al., 2006) and chemical open-air capture of $CO_2$ (Keith et al., 2006) are considered technologically both feasible and capable of removing sufficient quantities of carbon to reverse the change in atmospheric $CO_2$ concentration (Matthews,

2010). Of the Representative Concentration Pathways (RCPs) used in IPCC AR5 (Moss et al., 2010), only the lowest (RCP 2.6) envisions large scale deployment of $CO_2$ removal technology (in the form of BECS). However, global net primary productivity, a desire not to further compromise fragile ecosystems, and the need to grow sufficient food to feed the human population imposes a limit to the extent that BECS can be deployed (e.g. Shepherd, 2009). To achieve the kind of negative emissions needed to reverse the higher RCPs chemical open-air capture, powered by a carbon neutral energy source, would likely need to be deployed (Matthews, 2010).

For the model experiments described below a set of novel future climate scenarios are introduced that prescribe a gradual return to pre-industrial $CO_2$ concentrations, land-use and non-$CO_2$ radiative forcing. That is, these scenarios describe a future where a decision has been made to restore the Earth to pre-industrial atmospheric composition and land-use in hopes of restoring a Holocene-like climate. The scenarios are used to force the University of Victoria Earth System Climate Model (UVic ESCM), which is used to diagnose carbon emission compatible with the scenarios, in addition to examining the reversibility of various metrics of the Earth-system, including the Greenland ice-sheet.

## 4.2 Methods

### 4.2.1 Future scenarios

Four future scenarios where designed based on the RCPs used in IPCC AR5 (Moss et al., 2010). Each of the scenarios follows an RCP exactly up until that RCP reaches its peak $CO_2$ concentration. After peak $CO_2$ each of the scenarios prescribes a decline in atmospheric $CO_2$ concentration in an exact mirror image to the original rise in $CO_2$ concentration (Figure 4.1 a.). Non-$CO_2$ greenhouse gases decline linearly to their pre-industrial forcing beginning in the year of peak $CO_2$ and reaching their pre-industrial forcing in the same year $CO_2$ reaches 280 ppmv (Figure 4.1 b.). Sulphate emissions are taken to be zero once $CO_2$ concentration begins to decline (Figure 4.1 c.). Land use is also reversed in these simulations, with land being abandoned in the opposite order that it was acquired until the land use of 1850 is restored (Figure 4.1 d.). The pattern of land use change causes a complication for the scenario based on RCP 4.5, where large scale reforestation occurs before peak $CO_2$ is reached. In the derived scenario a period of deforestation occurs after atmospheric $CO_2$ begins to decline.

These scenarios are named the Mirrored Concentration Pathways (MCPs) and are distinguished with the same number as the RCP each is derived from. The peak $CO_2$ concentration occurs in year 2053, 2130, 2151, and 2251 for MCPs 2.6, 4.5, 6.0, and 8.5 respectively.

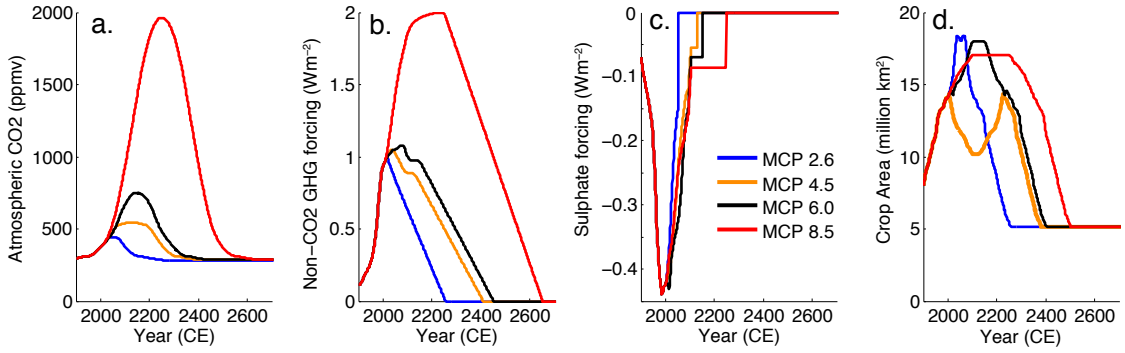


Figure 4.1: Forcing for each of the Mirrored Concentration Pathways (MCPs). Note that all of the MCPs except MCP 2.6 reach peak $CO_2$ concentration after the year 2100 CE.

**Rational for mirrored future scenarios**

The scenarios introduced here are an attempt to extend climate warming reversal experiments to an idealized but more plausible transition from net positive to net negative carbon emissions. The assumption that atmospheric $CO_2$ concentration decline will mirror its prior increase is intentionally simple, however, this assumption does follow intuitive economic logic. That is, carbon extraction begins slowly as $CO_2$ removal machines with a finite lifespan are deployed at some rate. The rate of extraction grows as the machines become more numerous and new machines become more efficient. As $CO_2$ concentration approaches its pre-industrial concentration the extraction rate slows as old machines are no-longer replaced to avoid having obsolete infrastructure when the goal of 280 ppmv $CO_2$ concentration is reached. Although it may be possible to reduce atmospheric $CO_2$ faster than its original increase, such a scenario risks inducing a rate of global cooling greater than the original warming rate. Given the challenges of adapting to a quickly changing climate it seem unlikely that a high rate of cooling would be desirable. The MCPs are therefore a simple approximation of a fast but plausible return to pre-industrial forcing.

The mirrored $CO_2$ paths of the MCPs are to some extent similar to the $CO_2$ paths in the reversal experiments of Samanta et al. (2010) and Boucher et al. (2012). However, the MCPs account for the historic trajectory of $CO_2$ emissions and non-$CO_2$ influences on radiative forcing, neglected in previous reversibility studies.

To return to a pre-industrial forcing it is necessary to return to pre-industrial land use. An exact reversal of land use as envisioned by the MCPs is implausible. However, assuming a continued increase in agricultural yields until the mid 21st century (e.g. Fischer et al., 2009) it should be possible to feed a population of under ten billion people on a fraction of the global land surface similar to that used for agriculture in 1850 (e.g. Fischer et al., 2009).

### 4.2.2 The UVic ESCM

The UVic ESCM is a coupled climate model of intermediate complexity with a full three dimensional ocean GCM (Weaver et al., 2001), complex land surface (Meissner et al., 2003), thermodynamic-dynamic sea-ice model, and simplified energy and moisture balance atmosphere (Weaver et al., 2001). The model has both a terrestrial and an oceanic carbon cycle. The terrestrial carbon cycle is simulated using the TRIFFID dynamic vegetation model (Cox et al., 2001, Matthews et al., 2004).

The inorganic ocean carbon cycle is simulated following the protocols of the ocean carbon-cycle intercomparison project (Orr et al., 1999). Ocean biology is simulated using a nutrient-phytoplankton-zooplankton-detritus ecosystem model (Schmittner et al., 2008). Ocean sedimentary processes are simulated using an Oxic-only model of sediment respiration (Archer, 1996). An extended description of the UVic ESCM is found in Appendix A.2.

Two variants of the UVic ESCM are used for the experiments in this manuscript: 1) the frozen ground version of the UVic ESCM which includes a deep soil column extending to 250 m depth, soil hydrology in the top 10 m of soil, full freeze-thaw physics, and a representation of the permafrost carbon pool (Avis et al., 2011, MacDougall et al., 2012); and 2) the dynamic ice-sheet version of the UVic ESCM which couples the Pennsylvania State University ice-sheet model into the UVic ESCM providing for simulation of the Greenland and Antarctic ice-sheets and ice shelves (Fyke et al., 2011). Both variants of the UVic ESCM are forced with each of the MCPs. The frozen ground version is used to diagnose $CO_2$ emissions compatible with each MCP and to simulate the metrics of the Earth-system displayed below, except for eustatic sea-level rise. The ice-sheet version is used in its Greenland only configuration to estimate the stability and ice loss from the Greenland ice-sheet under each MCP.

To generate an uncertainty range for the model estimates the climate sensitivity of the UVic ESCM is varied by artificially modifying the outgoing longwave radiation (Zickfeld et al., 2008). Each MCP was simulated three times, once each for climate sensitivities of 2, 3.2, and 4.5 °C for a doubling of atmospheric $CO_2$ concentration. This range covers the "likely" uncertainty range for climate sensitivity from the fourth assessment report of the IPCC (Hegerl et al., 2007). The central value (3.2 °C) is the inherent climate sensitive of the frozen ground version of the UVic ESCM.

## 4.3 Results

Various metrics of the Earth-system are shown in figure 4.2 for each MCP and climate sensitivity. In every simulation surface air temperature shows an asymmetric decline toward pre-industrial temperatures following the peak $CO_2$ concentration. None of the simulations show a full recovery to 19th century temperatures by the end of the 30th century (Figure 4.2 a.), with a residual climate warming of 0.1–1.7 °C for the full range of simulations. Similar to previous studies (e.g. Samanta et al., 2010, Boucher et al., 2012) the simulated northern sea-ice extent closely follows surface

temperature with a recovery beginning soon after temperatures begin to fall (Figure 4.2 d.). Permafrost area shows a delayed recovery after surface temperatures begin to fall. In MCP 8.5 permafrost area continues to decline for over a century after peak surface air temperature before commencing a slow recovery. Only under MCP 2.6 does permafrost area reach its 1990s extent by the year 3000 CE (Figure 4.2 f.). We note that in every simulation the meridional overturning circulation returns stronger that its pre-industrial strength (Figure 4.2 e.). The thermosteric contribution to sea-level peaks no more than 150 years after the peak surface temperatures are reached, after-which it begins a slow decline (Figure 4.2 h.). Consistent with previous studies (e.g. Boucher et al., 2012) ocean surface pH very closely follows atmospheric $CO_2$ concentration, to the extent that the model simulations under each climate sensitivity are indistinguishable (Figure 4.2 c.).

The simulated Greenland ice-sheet remains stable under the three lower MCPs despite the high sensitivity of the ice-sheet component used in the UVic ESCM to variations in climate sensitivity (Fyke et al., 2011). Under MCP 6.0 with a climate sensitivity of 4.5°C the ice-sheet losses 0.26 m sea-level equivalent before re-stabilizing after $CO_2$ is restored to 280 ppmv. Under the high concentration pathway (MCP 8.5) the ice sheet contributes substantially to sea-level rise, adding 2.69 m to sea level under the high climate sensitivity simulation. The contribution to sea level from the Greenland ice-sheet is simulated to be largely irreversible on the millennial time-scale considered in this study. Under the middle two MCPs the ice-sheet has regained less that 10% of the mass it had lost by the end of the simulations in the year 3000 CE. The UVic ESCM has a relatively low arctic amplification, another parameter that the ice-sheet component is very sensitive to (Fyke, 2011). Simulations with a higher polar amplification could result in substantially larger contribution to sea level rise from the Greenland ice-sheet.

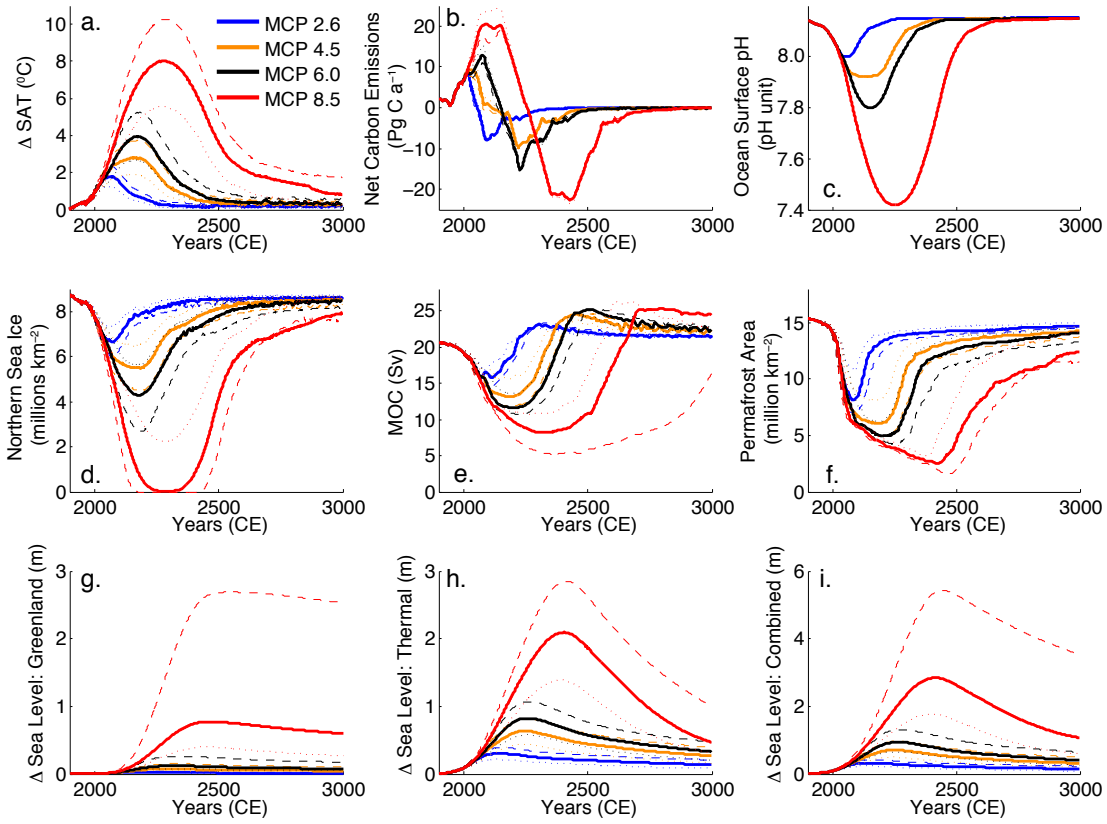


Figure 4.2: Earth-system metrics as simulated by the UVic ESCM under each of the four MCPs. Dotted lines are simulations with a climate sensitivity of 2.0 °C, solid lines are simulations with a climate sensitivity of 3.2 °C, and dashed lines are simulations with a climate sensitivity of 4.5 °C. Metrics in panels a.–f. and h. where generated using the frozen ground version of the UVic ESCM, panel g. is from the dynamic ice-sheet version of the model, and panel i. is a metric combining output from both version of the model. Note that the combined sea-level rise includes only contributions from thermosteric rise and Greenland, and does not include contributions from Antarctica, small glaciers and ice-caps, or ground-water mining.

Table 4.1: Cumulative fossil fuel carbon emissions and cumulative carbon drawdown for each of the MCPs. Results are for model runs with a climate sensitivity of 3.2 °C

| Scenario | Fossil Emissions (Pg C) | Drawdown (Pg C) | Ratio (%) |
|---|---|---|---|
| MCP 2.6 | 584 | 896 | 153 |
| MCP 4.5 | 911 | 1389 | 152 |
| MCP 6.0 | 1513 | 2112 | 140 |
| MCP 8.5 | 3898 | 4899 | 127 |

Table 4.1 displays the total fossil emissions and total drawdown for each of the simulations with a climate sensitivity of 3.2°C. Consistent with the behaviour of the UVic ESCM in the EMIP5 intercomparison (Zickfeld et al., 2013) more carbon needs to be removed from the atmosphere than was originally emitted to the atmosphere to restore a pre-industrial $CO_2$ concentration. However, with the addition of the permafrost carbon pool model component the quantity of carbon that must be removed has grown to between 127–153% of that originally emitted to the atmosphere (for the medium climate sensitivity simulations). For the low climate sensitivity model runs the quantity of carbon that must be removed is between 115–130% of that originally emitted to the atmosphere and for the high climate sensitivity model runs between 140–181%. In MCPs 2.6, 4.5, and 6.0 vertually all of the excess carbon originates from soils dominantly from former permafrost regions. Under MCP 8.5 the ocean contributes approximately 18% of the excess carbon, presumably due to large remnant warming of the oceans under this scenario.

The permafrost carbon pool will presumably gradually reform once permafrost begins recovering. Rates of permafrost carbon pool formation in Alaska following deglaciation were on the order of 7 g C $m^{-2}$ $a^{-1}$ for non-peatland soils (Marion and Oechel, 1993). Assuming a similar rate following restoration of pre-industrial forcing and assuming a permafrost area of approximately 16 million $km^2$ one would expect burial of about 0.15 Pg C $a^{-1}$ into permafrost soils. For MCP 4.5 this implies that it would take on the order of 3000 years to restore the permafrost carbon pool. However, $^{14}C$ based estimates of age of certain deposits of permafrost carbon indicate ages of over 30000 years (Zimov et al., 2006), implying that a 3000 year restoration time for the permafrost carbon pool may be optimistic.

To provide a quantitative sense of the time scales for restoring a Holocene-like climate significant events simulated for MCP 4.5 with climate sensitivity 3.2°C are

described below. Under MCP 4.5 atmospheric $CO_2$ concentration peaks in the year 2130. Surface air temperature peaks two decades latter at 2.8°C above the pre-industrial temperature. Ocean pH and northern sea-ice are restored to their 1990 states by 2280 and 2450 respectively. Sea level peaks in 2251 and in the year 3000 surface air temperature is 0.3°C above the pre-industrial temperature. Diagnosed net negative emissions begin soon after $CO_2$ concentration peaks and reach their apex of -9.7 Pg C $a^{-1}$ in year 2220. The apex negative emissions are very close to the magnitude of present day positive fossil fuel emissions (Olivier et al., 2012). Negative emissions gradually decline over the following centuries until 2630 when direct human interference in atmospheric composition ends.

## 4.4 Discussion

### 4.4.1 A Holocene-like climate

Recent paleoclimate reconstructions of the Holocene suggest that globally temperatures rose rapidly flowing the end of the last ice-age, plateaued between 9000 and 5000 years Before Present (BP) at approximately 0.4°C above mid 20th century temperatures (Marcott et al., 2013). Beginning at about 5000 BP temperatures gradually declined until the rise of industrial civilization resulted in rapid anthropogenic warming (Marcott et al., 2013). Present day surface air temperatures may not yet have exceeded the full range of those estimated for the Holocene (Marcott et al., 2013).

If one assumes an upper bound of Holocene-like surface temperature estimates to be those as much as 1°C above the pre-industrial surface air temperature (e.g. Marcott et al., 2013), all but one of the simulations present here suggests a restoration of a Holocene-like climate by the year 3000 (MCP 8.5 with a climate sensitivity of 4.5°C is the exception). Given that in our simulations the oceans cool slower than the land surface there are likely to be large differences between the restored climate and the pre-industrial climate at the continental and region scale.

### 4.4.2 The effectiveness of removing carbon

Many of the problems associated with climate warming originate from the rate of temperature change as opposed to its absolute magnitude (e.g Thomas et al., 2004). Although the rate of temperature reduction during the carbon removal stage of the

MCPs is slower than the prior rate of temperature increase, the simulated rate of cooling is substantial enough to warrant concern. However, if rates of cooling were found to be too fast carbon could simply be removed at a slower rate. It is likely that the ability to adapt to a cooling climate would be a key consideration in setting the rate of atmospheric carbon removal in addition to the economic and technological feasibility of carbon removal.

Restoring atmospheric $CO_2$ concentrations to their pre-industrial level implies totally decarbonizing the global economy followed by developing the infrastructure to remove carbon from the atmosphere. Matthews (2010) estimated that the economic scale of carbon removal technology would be of similar scale to the fossil fuel powered industry. Therefore, a society that decided to restore a Holocene-like climate would have to devote a significant fraction of its industrial output to removing carbon from the atmosphere.

From the model experiments presented above and those published in literature (e.g. Cao and Caldeira, 2010, Held et al., 2010, Samanta et al., 2010, Boucher et al., 2012, Zickfeld et al., 2013) the only components of the Earth-system to demonstrate a lack of reversibility are those associated with ice-sheets, and even they may recover over many thousands of years. Whether this reversibility is a feature of the natural Earth-system or some artifact of our modelling methods is a question requiring further study. State-of-the-art Earth-system models do not yet simulate complex ecosystem dynamics. These systems are of the most concern for reversibility (e.g Thomas et al., 2004) as the extinction of biological species is not easily reversed. Despite the technological feasibility of reversing the physical and chemical aspect of climate warming on a millennial time scale, irreversible damage to the biosphere from climate change remains an enduring concern (Barnosky et al., 2011).

## 4.5 Conclusions

Here novel future scenarios were developed to investigate a gradual return to pre-industrial radiative forcing to assess the possibility and time-frame of restoring a Holocene-like climate.The four scenarios follow the RCPs up until each RCPs reaches its peak $CO_2$ concentration after-which atmospheric $CO_2$ is reduced in a mirrored image to its original increase. The scenarios were used to force the UVic ESCM under a range of model climate sensitivities. The simulations suggest that a Holocene-like climate can be restored under all but the highest emissions and climate sensitivity

permutation by the year 3000 CE. Due primarily to a strong permafrost carbon feedback in the model more carbon needs to be removed from the atmosphere than was originally emitted to restore a pre-industrial atmospheric $CO_2$ concentration. Removing carbon from the atmosphere was able to re-stabilize the simulated Greenland ice-sheet. However, the ice-sheet regrows slowly regaining less than 10% of its lost mass by the year 3000 CE under the middle two scenarios. These results suggest that even with monumental effort to remove $CO_2$ from the atmosphere, humanity will be living with the consequences of fossil fuel emissions for a very long time.

# Chapter 5

# The origin and limits of the near proportionality between climate warming and cumulative $CO_2$ emissions

## 5.1 Introduction

The radiative forcing from an increase in atmospheric $CO_2$ concentration is close to a logarithmic function of concentration (Wigley, 1987). The equilibrium surface temperature response to a change in radiative forcing has been shown to be proportional to the magnitude of radiative forcing (e.g. Hansen et al., 1997). However, in models the response of the global average surface temperature to cumulative emissions of $CO_2$ has been shown to be roughly linear in simulations of historical and future climate (e.g. Matthews et al., 2009). A relationship that Earth system models suggest will hold until approximately 2000 Pg of carbon (Pg C) have been emitted to the atmosphere (e.g. Matthews et al., 2009, Allen et al., 2009, Zickfeld et al., 2012, Gillett et al., 2013, Allen and Stocker, 2013). This linear relationship, the slope of which has been designated as the Transient Climate Response to [cumulative $CO_2$] Emissions (TCRE) (Collins et al., 2013, Planton, 2013), is a highly convenient metric for climate policy as it establishes a simple relationship between the cause of warming ($CO_2$ emissions) and the expected magnitude of warming, that is independent of when carbon is emitted (e.g. Matthews et al., 2009, Allen et al., 2009, Zickfeld et al.,

2012, Gillett et al., 2013, Allen and Stocker, 2013). TCRE is formally defined as "The transient global average surface temperature change per unit cumulated $CO_2$ emissions" (Planton, 2013). The path-independent of surface temperature change allows budgets of cumulative carbon emissions to be established for the climate system stay below a chosen threshold of warming. For these reasons TCRE features prominently in the fifth assessment report of the Intergovernmental Panel on Climate Change (IPCC AR5) (IPCC, 2013, Collins et al., 2013).

TCRE combines information about the airborne fraction of carbon, climate sensitivity, carbon cycle feedbacks, and planetary heat uptake into a single parameter value (Matthews et al., 2009). Inter-model differences in the magnitude of these metrics lead to different values of TCRE. TCRE is distinct from the notion of climate sensitivity, in that climate sensitivity is the global mean increase in temperature one would expect once the Earth system comes into equilibrium with the radiative forcing from a doubling of atmospheric $CO_2$ concentration, while TCRE also takes into account that not all emitted $CO_2$ will remain in the atmosphere and that there is a time lag between the imposition of radiative forcing and reaching the equilibrium temperature response (Matthews et al., 2009). In general models with a higher climate sensitivity will also have a higher TCRE. TCRE is usually defined in terms of fossil fuel emissions with carbon cycle feedbacks and land-use change emissions implicitly taken into account in the value of TCRE (Matthews et al., 2009, Collins et al., 2013, e.g.).

The origin of the near constant nature of TCRE remains a subject of scientific interest (e.g. Matthews et al., 2009, Gregory et al., 2009, Raupach, 2013). The leading hypothesis at present is that the decline in radiative forcing from a unit of $CO_2$ added to the atmosphere (due to the logarithmic nature of the forcing) is compensated by an increase in the airborne fraction of $CO_2$ (Matthews et al., 2009, Gregory et al., 2009). Why this cancelation should remain so precise over such a large range of cumulative carbon emissions remains poorly explained. Matthews et al. (2009) suggests that the link between ocean heat uptake and ocean uptake of carbon, which are driven by the same deep-ocean mixing processes on long-timescales, is the origin of this precise cancelation of competing factors. However, Matthews et al. (2009) does not provide a detailed analysis to support this inference. Raupach (2013) suggests that the linearity of TCRE arises from exponential eigenmodes in linearized carbon-climate system. This form of eigenmode when applied to a system produce a response of the same shape, and therefore according to Raupach (2013) leads to a near constant TCRE.

Here a simple analytical model of the climate system is invoked to argue that TCRE largely arises from a cancelation of the diminishing radiative forcing from a unit of $CO_2$ added to the atmosphere and the diminishing flux of heat into the the oceans. The property of the ocean whereby the ocean-borne fraction of carbon is a function of $CO_2$ emission rate is also necessary for stabilizing TCRE. This analytical analysis draws on Earth system model experiments where carbon is emitted to the atmosphere at a constant rate. These model experiments allow examination of TCRE under condition of both strong and weak positive carbon cycle feedbacks from the terrestrial land surface. In cases where such feedbacks are strong TCRE losses its path independence and becomes near constant over a much narrower window of cumulative carbon emissions.

## 5.2 Modelling methods and experiment design

### 5.2.1 Model description

The University of Victoria Earth System Climate Model (UVic ESCM) is a coupled climate model of intermediate complexity with a full three dimensional ocean general circulation model (Weaver et al., 2001), complex land surface (Meissner et al., 2003), thermodynamic-dynamic sea-ice model, and simplified energy and moisture balance atmosphere (Weaver et al., 2001). The model has both a terrestrial and an oceanic carbon cycle. The terrestrial carbon cycle is simulated using the Top-down Representation of Interactive Foliage and Flora Including Dynamics (TRIFFID) dynamic vegetation model (Cox et al., 2001, Matthews et al., 2004). The inorganic ocean carbon cycle is simulated following the protocols of the ocean carbon-cycle intercomparison project (Orr et al., 1999). Ocean biology is simulated using a nutrient-phytoplankton-zooplankton-detritus ecosystem model (Schmittner et al., 2008). Ocean sedimentary processes are simulated using an Oxic-only model of sediment respiration (Archer, 1996). The frozen ground version of the UVic ESCM is used for simulations described in this manuscript. This version of the UVic ESCM includes a deep soil column extending to 250 m depth, soil hydrology in the top 10 m of soil, full freeze-thaw physics, and a representation of the permafrost carbon pool (Avis et al., 2011, MacDougall et al., 2012). See Appendix A.2 for an extended model description.

### 5.2.2 Experiment design

The UVic ESCM was forced under scenarios where $CO_2$ was emitted at a constant rate until a total of 1920 Pg C was emitted to the atmosphere. Emission rates where set at 2, 4, 8, 12, and 16 Pg C $a^{-1}$. After the desired total of carbon had been emitted to the atmosphere, $CO_2$ emissions were set to zero for the remainder of the simulation. Simulations commenced from a pre-industrial climate and were continued for 1000 model years. Forcing from non-$CO_2$ greenhouse gasses, sulphate aerosols, land use changes, and volcanic events were set to their pre-industrial averages throughout these simulations. To explore the effect of carbon cycle feedback strength on the TCRE, the climate sensitivity of the UVic ESCM (to a doubling of $CO_2$ concentration) was varied to 2.0, 3.2, and 4.5°C following the method of Zickfeld et al. (2008). This methods takes advantage of the simplified atmospheric model component of the UVic ESCM such that outgoing longwave radiation to space is altered as a function of the change in global mean surface temperature, to emulate variable strength of the physical climate feedbacks. These experiments are designated the constant emission rate experiments.

A second set of model experiments were conducted by forcing the UVic ESCM with the Representative Concentration Pathways (RCPs) used in IPCC AR5 (e.g. Moss et al., 2010). Carbon emissions compatible with each RCP where diagnosed from these model runs to examine the effect of the permafrost carbon feedback on the magnitude of the TCRE and allowable emissions for each RCP. Simulations of the RCPs were conducted with the UVic ESCM's inherent climate sensitivity of 3.2°C (for a doubling of atmospheric $CO_2$ concentration).

## 5.3 Analytical analysis

For this analysis two well established relationships are used: 1) that temperature change is proportional to radiative forcing,

$$Q = \lambda \Delta T + \Delta F, \tag{5.1}$$

(e.g. Wigley and Schlesinger, 1985) and 2) that TCRE is defined as follows,

$$\Lambda = \frac{\Delta T}{E}, \tag{5.2}$$

(Matthews et al., 2009), where $Q$ is radiative forcing, $\lambda$ is the climate feedback parameter, $\Delta T$ is the change is surface air temperature, $\Delta F$ is the planetary heat uptake (which is dominated by ocean heat uptake), $\Lambda$ is TCRE, and $E$ is the cumulative emitted carbon. For convenience emission rate will initially be assumed to be constant. That is,

$$E = rt, \tag{5.3}$$

where $r$ is the rate of $CO_2$ emissions and $t$ is time. In section 5.3.1 we will relax this assumption and consider exponentially increasing emissions of $CO_2$. For the convenience of the reader all constants are defined in text where they are first used as well as in table 5.1.

Table 5.1: Parameters used in this manuscript, their units and the typical values of the parameters used in calculations.

| Parameter | Value | Units | Definition |
|---|---|---|---|
| $R$ | 5.3 | $\mathrm{W\,m^{-2}}$ | Radiative forcing from e-fold increase in $CO_2$ concentration |
| $r$ | 4 | $\mathrm{Pg\,C\,a^{-1}}$ | $CO_2$ emission rate |
| $\lambda$ | 1 | $\mathrm{W\,m^{-2}\,K^{-1}}$ | Climate feedback parameter |
| $\alpha$ | 0.45 | – | Airborne fraction of carbon |
| $C_\mathrm{o}$ | 600 | Pg C | Original carbon content of the atmosphere |
| $\phi$ | 0.0125 | $\mathrm{W^{-2}\,m^4\,K^{-2}a^{-1}}$ | Ocean heat uptake parameter |
| $\epsilon$ | 0.0133 | $\mathrm{a^{-1}}$ | e-fold time for $CO_2$ emission rate |
| $\beta$ | 1 | $\mathrm{Pg\ a^{-1}}$ | Initial $CO_2$ emission rate |
| $\theta$ | 0.0049 | $\mathrm{W\,m^{-2}Pg^{-1}\,C}$ | Linearized radiative forcing from Gregory et al. (2009) |

In most analytical analysis of the climate system $\Delta F$ has been approximated as $\Delta F = \kappa \Delta T$ (e.g. Hansen et al., 1997, Gregory et al., 2009). This relationship is mathematically convenient as $\kappa$ can be treated as a negative feedback to climate warming and is directly comparable to $\lambda$ (e.g. Gregory et al., 2009). Despite this convenience it is well understood that $\kappa$ is not constant in time and will diminish toward zero as the climate system comes into equilibrium with the imposed radiative forcing (e.g. Wigley and Schlesinger, 1985, Hansen et al., 1997, Gregory et al., 2009). To take this effect into account here we will use the approximation that ocean heat

uptake can be parameterized as heat diffusion into a semi-infinite half space:

$$\Delta F = \frac{K \Delta T}{\sqrt{\pi k t}} \tag{5.4}$$

(Carslaw and Jaeger, 1986), where $K$ is thermal conductivity, $k$ is thermal diffusivity and $t$ is time. To reduce the number of constants we define:

$$\frac{1}{\sqrt{\phi}} = \frac{K}{\sqrt{\pi k}}. \tag{5.5}$$

This approximation of ocean heat flux has been used at least once before by Wigley and Schlesinger (1985) but fell out of use a generation ago. Fitting this parameterization to temperature and planetary heat uptake model output from the Climate Model Intercomparison Project phase Five (CMIP5) (Taylor et al., 2012) yields a good fit in most cases, with correlation coefficients of between 0.74 and 0.94 (Table 5.2). The inter-model range of $\phi$ is 0.011 to 0.137 $\mathrm{W^{-2}\,m^4\,K^{-2}a^{-1}}$, however the value from the UVic ESCM (0.0125 $\mathrm{W^{-2}\,m^4\,K^{-2}a^{-1}}$) will be used in calculations presented here. In the UVic ESCM the value of $\phi$ varies very little by model experiment or imposed model climate sensitivity.

Table 5.2: $\phi$ values and correlation coefficients for the semi-infinite half space parameterization fitted to eleven climate models that participated in CMIP5. The models were selected for having full ocean general circulation models and for having stored the planetary heat imbalance as a model output. The model experiment examined is the instant quadrupling of $CO_2$ experiment.

| Model Name | $\phi$ | Correlation Coefficient |
|---|---|---|
| BCC-CSM1.1 | 0.137 | 0.93 |
| CanESM2 | 0.011 | 0.78 |
| CCSM4 | 0.061 | 0.82 |
| CNRM-CM5 | 0.186 | 0.94 |
| CSIRO-MK3.6.0 | 0.100 | 0.89 |
| GFDL-CM3 | 0.072 | 0.94 |
| INMCM4 | 0.080 | 0.93 |
| IPSL-CM5A-LR | 0.029 | 0.74 |
| IPSL-CM5A-MR | 0.045 | 0.91 |
| MIROCS | 0.077 | 0.91 |
| NorESM1-M | 0.03 | 0.74 |

Treating ocean heat uptake as a negative feedback to climate change has proved to be a useful way of conceptualizing the physics of the climate system (e.g. Hansen et al., 1997, Gregory et al., 2009). To this end, it is useful to retain the ocean heat uptake efficiency $\kappa$ here defined as:

$$\kappa(t) = \frac{1}{\sqrt{\phi t}}. \tag{5.6}$$

The radiative forcing from $CO_2$ is approximated using the classical logarithmic relationship:

$$Q = R \ln\left(1 + \frac{\alpha r t}{C_o}\right), \tag{5.7}$$

(Wigley, 1987), where $R$ is the radiative forcing for an e-fold increase in atmospheric $CO_2$ concentration, $\alpha$ is the airborne fraction of emitted carbon, and $C_o$ is the original quantity of carbon in the atmosphere.

Combining the above equations, the relationship for the change in surface temperature can be shown to be the following:

$$\Delta T = \frac{Q}{\lambda}\left(\frac{1}{1 + \frac{1}{\sqrt{\phi\lambda^2 t}}}\right). \tag{5.8}$$

Substituting in equation 5.7 for $Q$ we find,

$$\Delta T(t) = \frac{R}{\lambda}\ln\left(1 + \frac{\alpha r t}{C_o}\right)\left(\frac{1}{1 + \frac{1}{\sqrt{\phi\lambda^2 t}}}.\right), \tag{5.9}$$

Now by substituting equation 5.9 into the definition of TCRE (equation 5.2) we find the time dependent relationship for TCRE,

$$\Lambda(t) = \frac{R\alpha}{\lambda C_o}\ln\left(1 + \frac{\alpha r t}{C_o}\right)\left(\frac{C_o}{\alpha r t}\right)\left(\frac{1}{1 + \frac{1}{\sqrt{\phi\lambda^2 t}}}\right). \tag{5.10}$$

We can now replace time ($t$) with emissions ($E$) to find TCRE as a function of cumulative carbon emissions,

$$\Lambda(E) = \frac{R\alpha}{\lambda C_o}\ln\left(1 + \frac{\alpha E}{C_o}\right)\left(\frac{C_o}{\alpha E}\right)\left(\frac{1}{1 + \sqrt{\frac{r}{\phi\lambda^2 E}}}\right). \tag{5.11}$$

In order to understand how multiplying three functions of $E$ together is yielding a near constant value, an approximation for ln is needed. The taylor series based on the area hyperbolic tangent can be shown to be a good approximation for values of ln relevant for the climate problem. Recall this approximation takes the form:

$$\ln(z) = 2\left(\operatorname{arctanh}\left(\frac{\mathrm{z}-1}{\mathrm{z}+1}\right)\right) = 2\left(\frac{z-1}{z+1} + \frac{1}{3}\left(\frac{z-1}{z+1}\right)^3 + \frac{1}{5}\left(\frac{z-1}{z+1}\right)^5 + \cdots\right), \tag{5.12}$$

(Jeffrey and Zwillinger, 2000). For the values in table 5.1 the first term of this approximation can reproduce the logarithmic factor of equation 5.11 with a 3% error at $E = 1000$ Pg C and with a 7% error at $E = 2000$ Pg C. Invoking this approximation equation 5.11 can be reduced too:

$$\Lambda(E) \approx \frac{R\alpha}{\lambda C_o}\left(\frac{2\alpha E}{2C_o + \alpha E}\right)\left(\frac{C_o}{\alpha E}\right)\left(\frac{1}{1+\sqrt{\frac{r}{\phi\lambda^2 E}}}\right). \tag{5.13}$$

Combining the second and the third factor this relationship simplifies too:

$$\Lambda(E) \approx \frac{R\alpha}{\lambda C_o}\left(\frac{1}{1+\frac{\alpha E}{2C_o}}\right)\left(\frac{1}{1+\sqrt{\frac{r}{\phi\lambda^2 E}}}\right), \tag{5.14}$$

and therefore,

$$\Lambda(E) \approx \frac{R\alpha}{\lambda C_o}\left(\frac{1}{1+\sqrt{\frac{r}{\phi\lambda^2 E}}+\frac{\alpha E}{2C_o}+\sqrt{\frac{\alpha^2 r E}{4C_o^2\phi\lambda^2}}}\right). \tag{5.15}$$

TCRE is approximately a constant over a large rage of cumulative carbon emissions. This implies that the derivative of TCRE with respect to $E$ is near zero for values of $E$ up to 2000 Pg C. The derivative of TCRE with respect to $E$ is:

$$\frac{d\Lambda(E)}{dE} = -\frac{R\alpha}{\lambda C_o}\left(\frac{\frac{\alpha}{2C_o} - \sqrt{\frac{r}{4\phi\lambda^2}}\frac{1}{E^{1.5}} + \frac{\alpha}{4C_o}\sqrt{\frac{r}{4\phi\lambda^2 E}}}{\left(1+\sqrt{\frac{r}{\phi\lambda^2 E}}+\frac{\alpha E}{2C_o}+\sqrt{\frac{\alpha^2 r E}{4C_o^2\phi\lambda^2}}\right)^2}\right). \tag{5.16}$$

This derivative (computed with the values in table 5.1) is plotted in figure 5.1. The figure shows that for the values in table 5.1 $\frac{\mathrm{d}\Lambda}{\mathrm{dE}}$ reaches zero at 677 Pg C. For cumu-

lative carbon emissions near this point TCRE will be near constant.

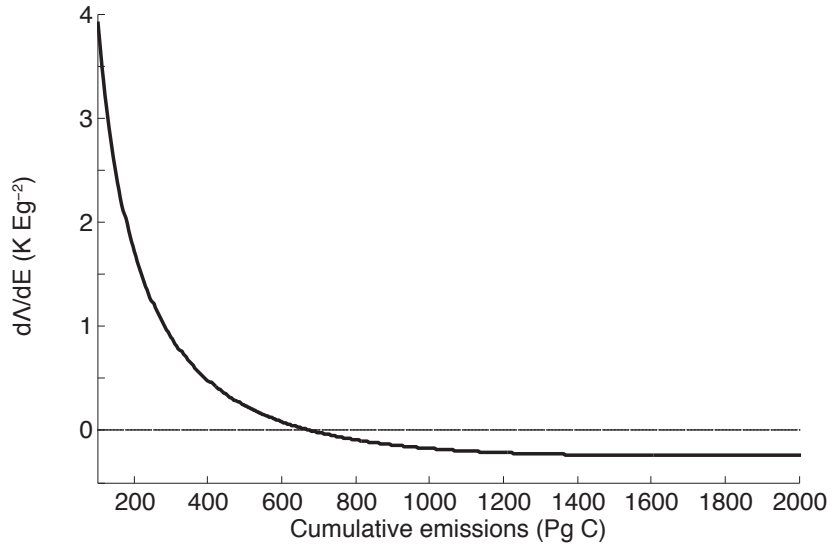


Figure 5.1: First derivative of TCRE ($\Lambda$) computed for values in table 5.1. Note that the derivative reaches zero at 677 Pg C.

Another way of expressing this is that the sum of the terms $\sqrt{\frac{r}{\phi\lambda^2 E}}, \frac{\alpha E}{2C_o}$ and $\sqrt{\frac{\alpha^2 rE}{4C_o^2\phi\lambda^2}}$ from equation 5.15 is nearly constant over a large range of values. By comparing the first derivatives of these terms we can see how the parameters compensate to create TCRE. As these derivatives need to nearly cancel one another out we can set them as the similarity:

$$\sqrt{\frac{r}{\phi}}\frac{1}{E^{1.5}} \sim \frac{\alpha}{C_o} + \frac{\alpha}{C_o}\sqrt{\frac{r}{\phi}}\frac{1}{\sqrt{E}}. \tag{5.17}$$

Notably this relationship is a function of the rate of $CO_2$ emissions and cumulative carbon emissions such that the two terms will be closer in value if $r$ is small when $E$ is small and if $r$ is large when $E$ is large.

This avenue of analysis has the advantage that these terms have easily inferred physical meaning. By looking back to equation 5.6 one can see that the term $\sqrt{\frac{r}{\phi\lambda^2 E}}$ is equivalent to $\frac{\kappa(E)}{\lambda}$. This term is therefore the ratio of the ocean heat uptake efficiency to the climate feedback parameter. The derivative of this term is the change in the ocean heat uptake efficiency (with respect to cumulative carbon emissions) normalized to the climate feedback parameter. The term $\frac{\alpha E}{2C_o}$ is simply the increase in atmospheric

$CO_2$ content relative to double the original carbon content of of the atmosphere. The third term $\sqrt{\frac{\alpha^2 rE}{4C_o^2\phi\lambda^2}}$ is the non-linear coupling between the first two terms.

Figure 5.2 a. and b. shows examples of the function for $\Delta T(E)$ and $\Lambda(E)$ derived above (equations 5.9 and 5.11) compared to functions for $\Delta T(E)$ and $\Lambda(E)$ derived in Gregory et al. (2009). In Gregory et al. (2009) ocean heat uptake and radiative forcing from $CO_2$ were both linearized such that:

$$\Lambda \approx \frac{\theta\alpha}{\lambda+\kappa}, \tag{5.18}$$

where $\theta$ is the linearized value for radiative forcing. Also shown in figure 5.2 is a parameterization where the logarithmic forcing for $CO_2$ (equation 5.7) is substituted in for $\theta$ to demonstrate the effect of the non-linearity of radiative forcing from $CO_2$ on the parameterization of Gregory et al. (2009). The figure shows that the parameterization derived above reproduces the near proportionality between temperature change and cumulative carbon emissions.

### 5.3.1 An exponential increase in emissions

The simplifying assumption that carbon is emitted at a constant rate used in the previous section clearly does not represent the situation in the modern world where emissions have been increasing approximately exponentially (e.g Boden et al., 2011). To explore this situation the above equations were resolved under the condition that:

$$E \approx \frac{\beta}{\epsilon}e^{\epsilon t}, \tag{5.19}$$

where $\epsilon$ is the e-folding time for emissions and beta is the initial rate of emissions. Substituting this into equation 5.10 we find:

$$\Lambda(E) = \frac{R\alpha}{\lambda C_o}\ln\left(1+\frac{\alpha E}{C_o}\right)\left(\frac{C_o}{\alpha E}\right)\left(\frac{1}{1+\sqrt{\frac{\epsilon}{\phi\lambda^2\ln(\frac{E\epsilon}{\beta})}}}\right). \tag{5.20}$$

Applying the approximation for the logarithm used above we find:

$$\Lambda(E) \approx \frac{R\alpha}{\lambda C_o}\left(\frac{1}{1+\sqrt{\frac{\epsilon}{\phi\lambda^2\ln(\frac{E\epsilon}{\beta})}}+\frac{\alpha E}{2C_o}+\frac{\alpha E}{2C_o}\sqrt{\frac{\epsilon}{\phi\lambda^2\ln(\frac{E\epsilon}{\beta})}}}\right). \tag{5.21}$$

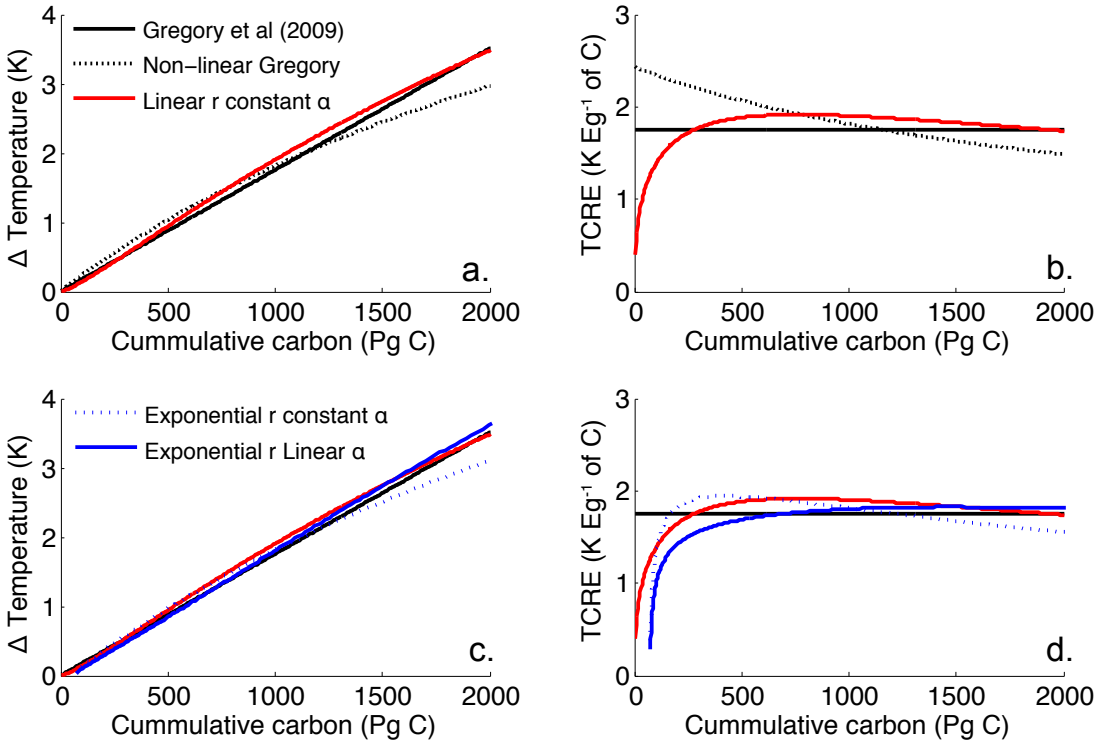


Figure 5.2: Temperature verses cumulative carbon emissions curves (a. and c.) and TCRE curves (b. and d.) for various analytical approximations of the climate system. $r$ is the rate of carbon emissions and $\alpha$ is the airborne fraction of carbon.

The exponential increase in emissions does not affect the radiative forcing part of this relationship and therefore does not have an effect on the accuracy of the approximation of the logarithm used to simplify the relationship.

From figure 5.2 c. and d. one can see that the ratio of temperature change to cumulative carbon emissions deviates significantly from a constant in the case of exponentially increasing $CO_2$ emissions. Given that Earth system models find TCRE to be nearly constant until approximately 2000 Pg C have been emitted to the atmosphere, there must be another factor changing to compensate for the decline in $\sqrt{\frac{\epsilon}{\phi\lambda^2 \ln(\frac{c\epsilon}{\beta})}}$.

The most intuitive suspect for that changing factor is the airborne fraction ($\alpha$) which in models is known to decline as cumulative carbon emissions rise (e.g. Zickfeld et al., 2013). Results from the constant rate experiments performed with the UVic ESCM help illuminate this problem. Shown in figures 5.3, 5.4, and 5.5 are the airborne, ocean-borne, and land-borne fractions of carbon for the constant rate experiments with the permafrost carbon pool of the UVic ESCM turned on and turned off. From the figures it is clear that in the UVic ESCM ocean uptake of carbon is effectively a function of the rate of carbon emissions, as is the airborne fraction of carbon in experiments with weak terrestrial carbon cycle feedbacks. Taking into account that airborne fraction is a function of the rate of carbon emissions we can recover the near constant nature of TCRE (Figure 5.2 c. and d.). These results support the hypothesis of Matthews et al. (2009) that it is the ocean's diminishing ability to absorb heat and carbon that creates TCRE.

### 5.3.2 The TCRE window

The derivatives in equation 5.17 only fully cancel one another out at a single point:

$$\frac{\alpha}{C_o} + \frac{\alpha}{C_o}\sqrt{\frac{r}{\phi}}\frac{1}{\sqrt{E}} - \sqrt{\frac{r}{\phi}}\frac{1}{E^{1.5}} = 0. \tag{5.22}$$

For other values of cumulative carbon emissions the cancelation between these terms is only approximate. Furthermore the further one gets from the cancelation value the less constant TCRE becomes. Therefore, it may be useful to define a "TCRE window" where TCRE is approximately constant. The upper and lower bounds of this window are arbitrary but pragmatically defining the window as the region where TCRE is within 95% of its peak value (which is where the terms in equation 5.22 are

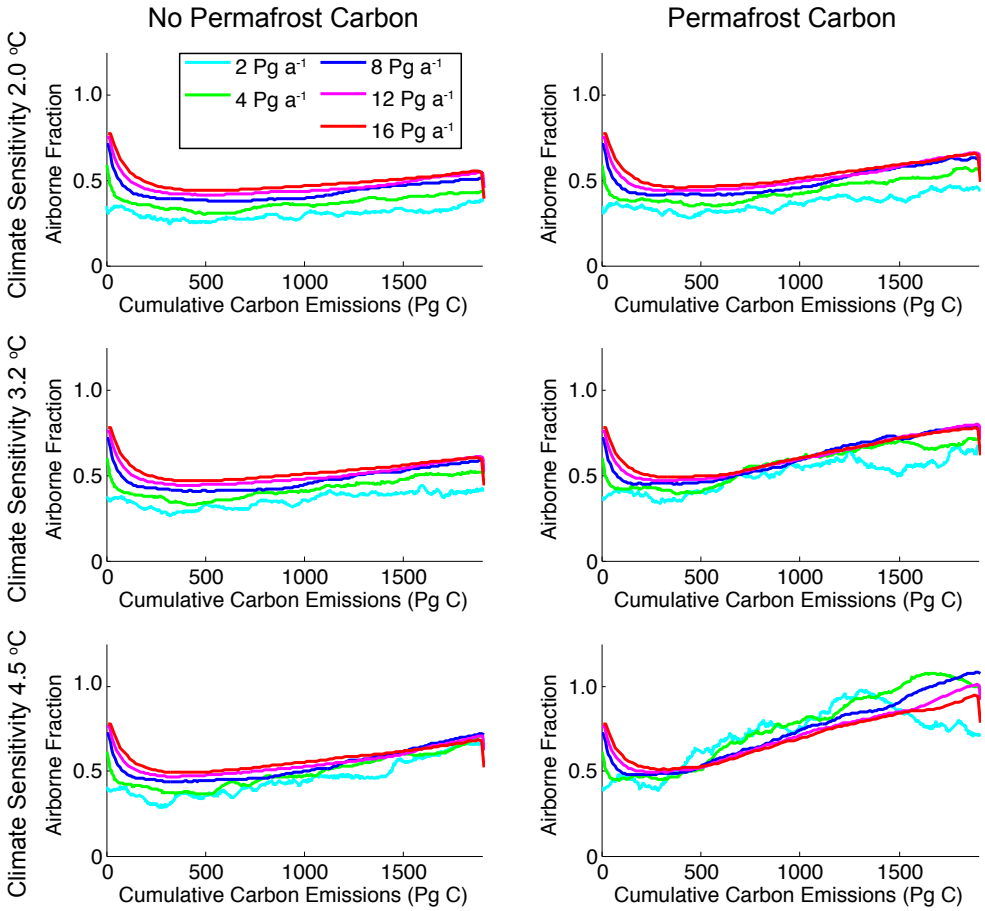


Figure 5.3: Airborne fraction of carbon for each of the constant rate experiments carried out with the UVic ESCM. Note that airborne fraction of carbon rises faster as a function of cumulative $CO_2$ emissions for simulation with permafrost carbon and for simulation with a higher climate sensitivity to a doubling of $CO_2$.

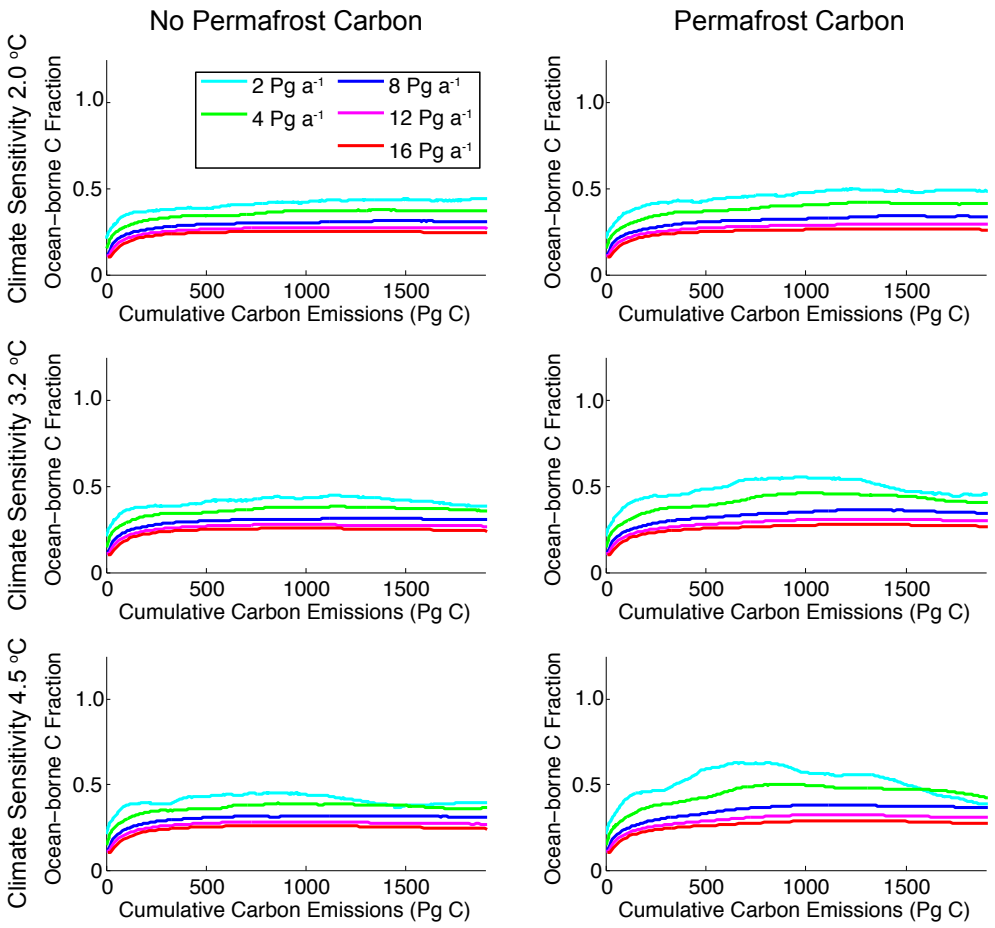


Figure 5.4: Ocean-borne fraction of carbon for each of the constant rate experiments carried out with the UVic ESCM. Note that ocean-borne fraction of carbon is approximately a function of carbon emission rate

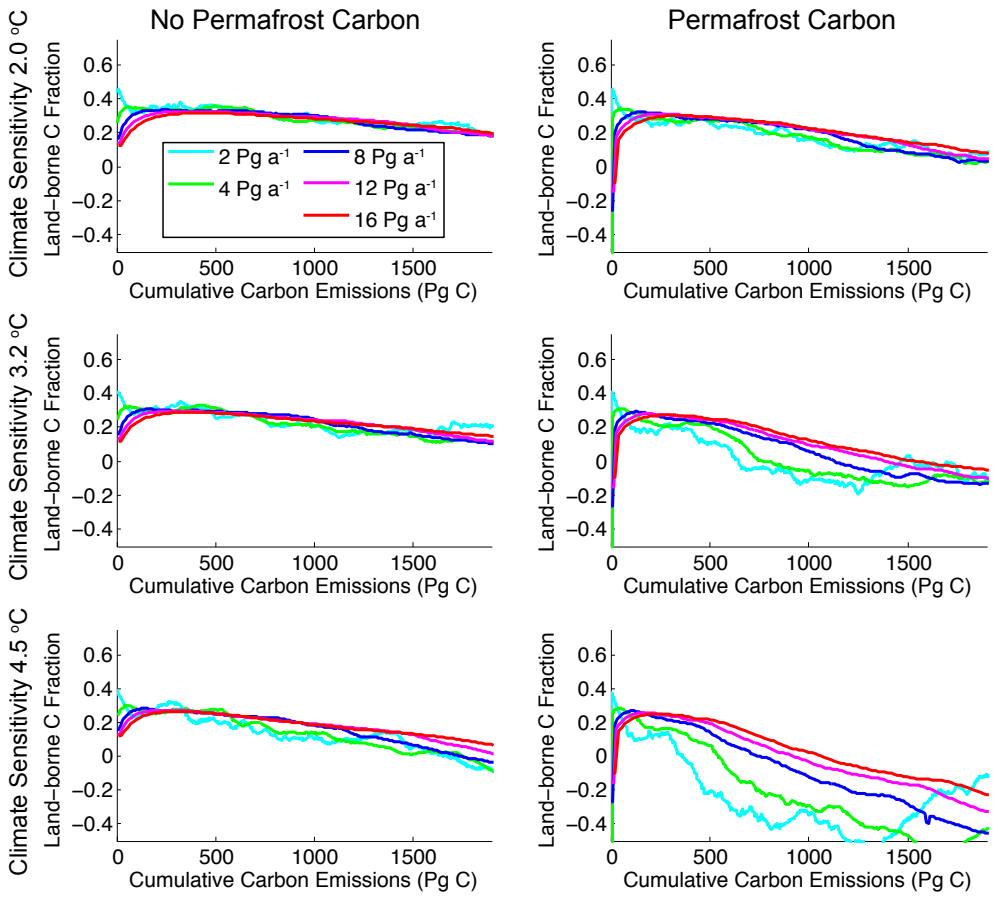


Figure 5.5: Land-borne fraction of carbon for each of the constant rate experiments carried out with the UVic ESCM. Note that land-borne fraction of carbon becomes more rate dependent and steeply declining in simulations with permafrost carbon and simulations at a higher climate sensitivity.

zero). The cumulative carbon emissions consistent with the values of TCRE 95% of peak can be solved for numerically. For the parameter values in in table 5.1 the TCRE window is between of 200 to 2100 Pg C of cumulative emissions, roughly reproducing the near-linear region inferred from Earth system model simulations.

The notion of a TCRE window also provides a means to examine the parameter sensitivity of the linearity of the temperature-cumulative carbon curve. Figure 5.6 shows the results of such an analysis. Each of the four parameters in equation 5.22 were varied through a plausible range of values while all of the other parameters were held at their values from table 5.1. The TCRE window becomes smaller as airborne fraction of carbon increases (Figure 5.6a.) and becomes larger as the rate of emissions is increased (Figure 5.6b.). That is, the TCRE is linear over a smaller range of cumulative carbon emissions when a larger fraction of carbon remains in the atmosphere. This intuitively makes sense as the logarithmic form of the radiative forcing will become dominant at lower cumulative emission when a higher fraction of carbon remains in the atmosphere. The value of ocean heat uptake parameter $\phi$, which varied over on order of magnitude between climate models (Table 5.2), also strongly effects the TCRE. Higher values of $\phi$ correspond to a slower uptake of heat by the oceans and a narrower TCRE window (Figure 5.6c.).

The initial quantity of carbon in the atmosphere is not a variable as its value is known (596 Pg C). However, examining variations in this quantity allows one to question whether the existence of a near constant TCRE depends of what point in Earth history an industrial civilization happened to emerge. Varying the initial quantity of carbon in the atmosphere strongly affects the TCRE window with both upper and lower bounds increasing as the initial quantity of carbon is increased (Figure 5.6d.). This suggests that as long as the semi-infinite half space parameterization for planetary heat uptake holds for a given climate state that there will be a region where a temperature verses cumulative carbon curve will be nearly linear. That is, TCRE may be a general feature of the Earth system and not a fortuitous fluke of compensating parameter values.

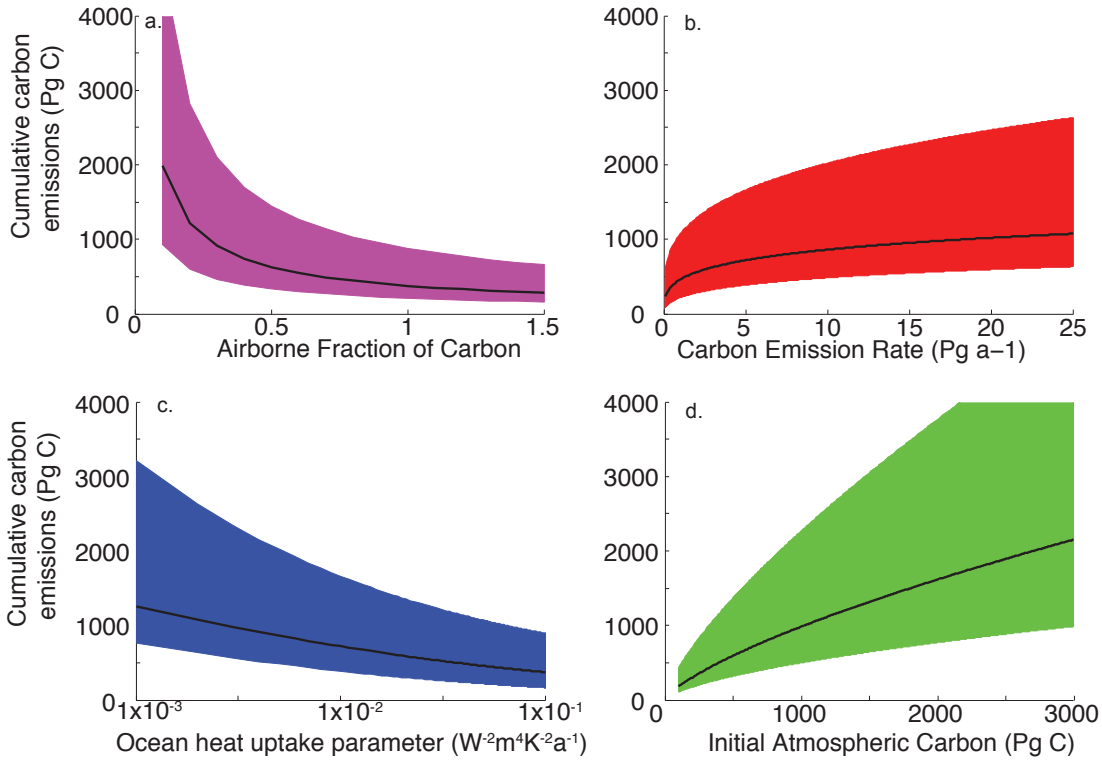


Figure 5.6: Range of values for which TCRE is approximately constant as functions of variations in parameter values. The solid black line is the point where terms in equation 5.17 exactly cancel one another out. The shaded region indicates the region where TCRE is approximately constant. Note that the horizontal axis for the ocean heat uptake parameter (c.) is logarithmic.

## 5.4 Model results

### 5.4.1 Constant rate experiment

Figure 5.7 displays temperature verses cumulative carbon emission curves for the constant emission rate experiments for the three climate sensitivities used and for model runs with and without the permafrost carbon feedback. The permafrost carbon pool is a large previously poorly quantified reservoir of carbon within the Earth system (e.g. Schuur et al., 2008). This carbon cycle feedback has the potential to disrupt the near linear temperature cumulative carbon emissions relationship by releasing large quantities of carbon into the atmosphere. If the permafrost carbon feedback (or any other strong terrestrial carbon cycle feedback) is strong enough to disrupt the ocean derived relationship between airborne fraction of carbon and rate of carbon emissions, then presumably the near constant nature of TCRE could also break down.

By comparing figure 5.7 and figure 5.5 one can see that the degree to which TCRE remains a constant is related to the strength and emissions rate dependance of the terrestrial carbon cycle feedback to climate change. In simulations with a climate sensitivity of 2.0°C the land-borne uptake of carbon is an emissions rate independent function of cumulative carbon emissions, stabilizing at about 0.3 and gradually declining to 0.2 at 2000 Pg C for the simulation without the permafrost carbon. For the simulation with permafrost carbon, land-borne uptake declines from about 0.3 to 0.1 at 2000 Pg C. The temperature verses cumulative carbon emissions curves for these two sets of simulations are emission rate independent with a near constant TCRE.

For simulations with a climate sensitivity of 3.2°C and with no permafrost carbon the land-borne fraction of carbon is emission rate independent and gradually declining like the set of simulations with a climate sensitivity of 2.0°C. Likewise, the temperature verses cumulative carbon emissions curves for these simulations is emission rate independent with a constant TCRE. For the simulations with permafrost carbon the magnitude of the land-borne fraction of carbon becomes dependent on carbon emission rate, with steeper declines for slower emissions rates of carbon. This clearly affects the temperature verses cumulative carbon emissions curves, which in this set of simulations diverge by emission rate and have more variable TCRE at low emission rates. This emission rate dependance is likely a manifestation of the time lag inherent in the permafrost carbon feedback. That is, when a permafrost region

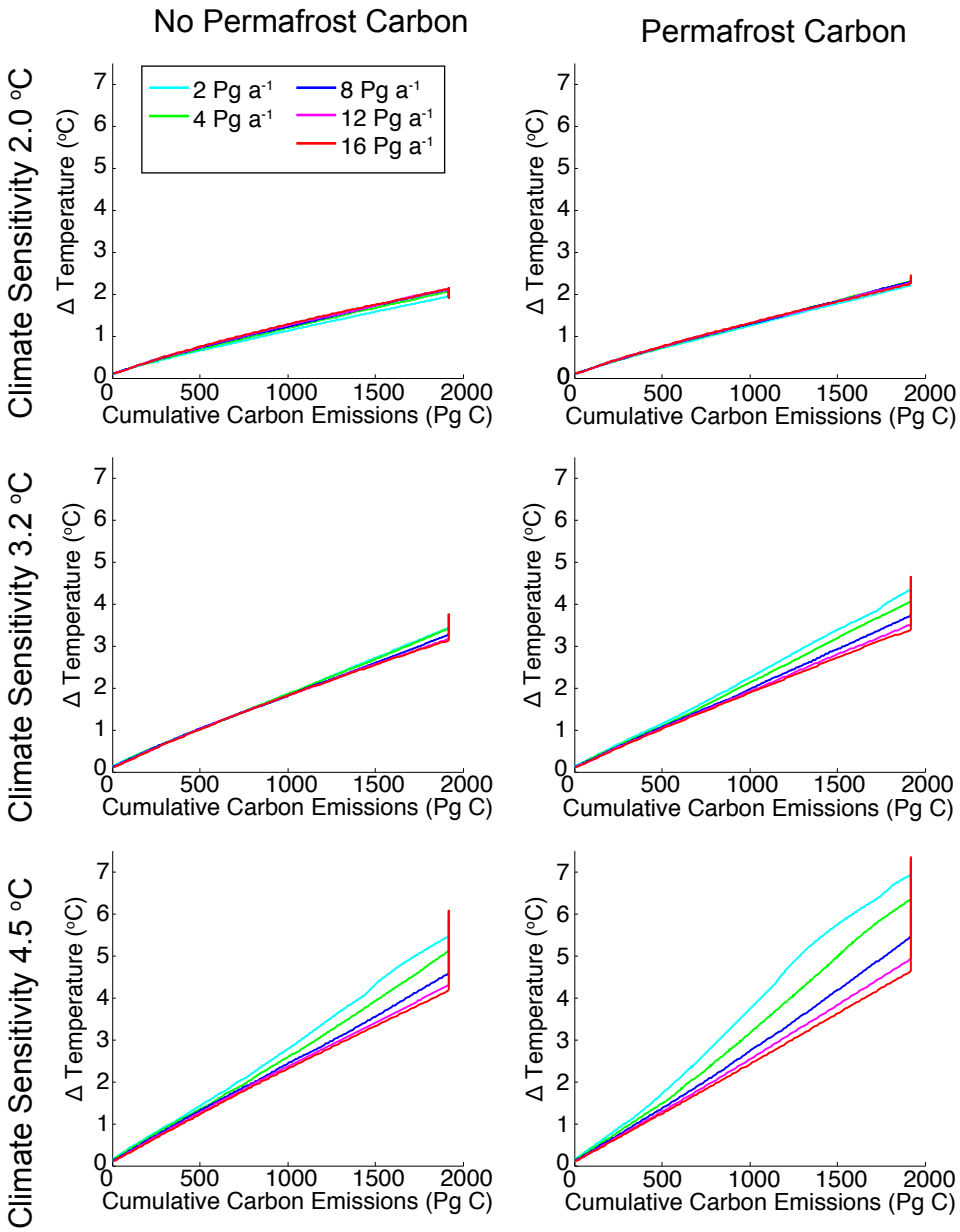


Figure 5.7: Temperature verses cumulative carbon emissions curves for constant rate experiment simulations carried out with the UVic ESCM. Note that TCRE becomes non-constant and path dependent for simulations with strong terrestrial carbon cycle feedbacks. The vertical line seen at the right of the panels represents the residual warming that occurs after emissions cease. Notably the peak temperature anomaly seen after emissions cease remains independent of $CO_2$ emissions rate, even in cases with large transient differences in temperature.

is warmed it takes time for soils to thaw and for carbon to decay such that there is a long time-lag between forcing the system and carbon release from the system (e.g. Schuur et al., 2008). In the simulations with a slower rate of emission more time has elapsed at a given quantity of cumulative carbon emissions, meaning that the permafrost soils are closer to being in equilibrium with there new climate and that more carbon has been released from these soils.

For the simulations with a climate sensitivity of 4.5°C strong rate dependent terrestrial carbon cycle feedbacks are seen in simulations with and without permafrost carbon (these feedbacks are stronger in the simulations with permafrost carbon). This corresponds with non-linear temperature verses cumulative carbon emissions curves for both simulations with and without permafrost carbon, especially for simulations with a low emissions rate.

An interesting feature of temperature verses cumulative carbon emissions curves is the vertical line where emissions cease. This represents the continued change in surface temperature after emissions cease. All emission rate curves end at the same point. That is, the simulations all end at the same equilibrium temperature (dependent on the climate sensitivity) even in simulations where there are large transient differences in temperature as a function of cumulative carbon emissions.

### 5.4.2 Permafrost carbon and the RCPs

MacDougall et al. (2012) described model experiments with the permafrost carbon version of the UVic ESCM forced with emissions derived from the RCPs. However, that study did not examine the effect of the permafrost carbon feedback on the TCRE of the RCPs nor did it provide carbon emissions compatible with each RCP. Compatible carbon emissions are calculated by prescribing atmospheric carbon content from a given RCP while using the UVic ESCM to simulated uptake of carbon by the oceans and the terrestrial land surface. This allows for anthropogenic emissions of carbon to be solved for as the final unknown variable in the global carbon mass balance. Figure 5.8 shows temperature verses cumulative carbon curves for each of the four RCPs with and without the permafrost carbon component of the model turned on. In either case the curves are roughly linear with a TCRE of 1.9 $\mathrm{K\,Eg^{-1}}$ C for the simulations without permafrost carbon and a TCRE of 2.2 $\mathrm{K\,Eg^{-1}}$ C for the simulations with permafrost carbon. TCRE for the RCPs includes not only the effects of $CO_2$ from fossil fuels but also non-$CO_2$ radiative forcings and land use changes. The

most interesting feature to arise from the addition of the permafrost carbon pool in the RCP simulations is the "tail" features that the temperature curves gain for RCPs 2.6, 4.5 and 6.0. These tails represent the continued warming of the system once atmospheric $CO_2$ has been stabilized or in the case of RCP 2.6 begins to decline. The reverse slopes of the tails, most pronounced for RCP 2.6, indicate that net negative emissions are necessary to achieve these scenarios.

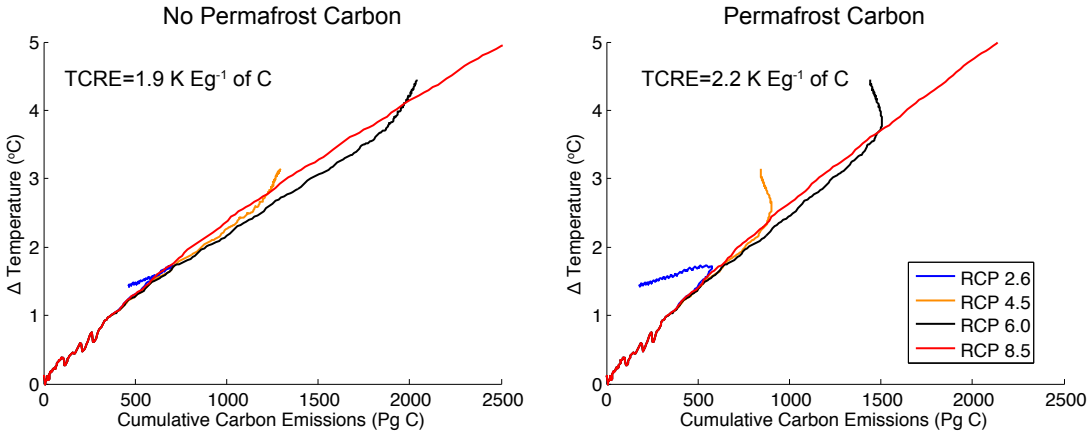


Figure 5.8: Temperature verses cumulative carbon emissions curves for simulations of the Representative Concentration Pathways (RCPs) carried out with the UVic ESCM.

Table 5.3 shows the diagnosed compatible emissions for the RCPs with and without permafrost carbon between 2012 and 2100 CE for the frozen ground version of the UVic ESCM. For reference the same quantities published in the summary for policy makers of IPCC AR5 (IPCC, 2013) are also shown. The table suggests that the inclusion of the permafrost carbon feedback reduces the remaining cumulative emissions compatible with each RCP for the remainder of the 21st century by 155-280 Pg C. Figure 5.9 shows the diagnosed emissions pathways compatible with each RCP for simulations with and without permafrost carbon. The figure shows that the permafrost carbon feedback necessitates lower peak emissions and faster elimination of net $CO_2$ emissions for compatibility with the RCP prescribed $CO_2$ pathway. RCPs 4.5 and 6.0 now require negative emissions in the 22nd century and RCP 2.6 requires elimination of net $CO_2$ emission in 2058 CE and peak negative emissions of -2.5 Pg C $a^{-1}$ in 2084 CE.

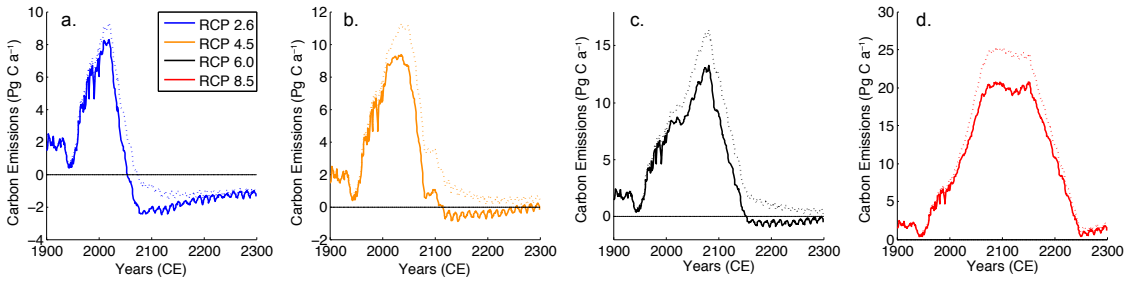


Figure 5.9: Diagnosed emissions pathways for each RCP for the UVic ESCM with (solid lines) and without (dotted lines) permafrost carbon. Note that there is a different scale for the vertical axis in each panel. Also note that the addition of the permafrost carbon feedback necessitates lower allowable peak emissions and a faster elimination of net carbon emissions for compatibility with each RCP.

Table 5.3: Compatible emission for each RCP taking the permafrost carbon feedback to climate change into account. Values are cumulative carbon emissions between 2012 and 2100 CE. AR5 range taken from IPCC (2013). All values are in Pg of carbon. Ranges in final column were computed by varying the climate sensitivity of the UVic ESCM between 2.0 and 4.5°C for a doubling of atmospheric $CO_2$.

| Scenario | AR5 Range | UVic ESCM value without permafrost carbon | UVic ESCM value including permafrost carbon |
|---|---|---|---|
| RCP 2.6 | 140 to 410 | 260 | 105 (9 to 216) |
| RCP 4.5 | 595 to 1005 | 702 | 503 (367 to 650) |
| RCP 6.0 | 840 to 1250 | 1113 | 920 (760 to 1062) |
| RCP 8.5 | 1415 to 1910 | 1722 | 1440 (1222 to 1654) |

## 5.5 Discussion

As a metric of climate change TCRE's most important quality is that provides a simple way of relating the cause of climate change ($CO_2$ emissions) to the most used index of climate change (global mean near surface temperature change). Despite the rate dependence added by the inclusion of the permafrost carbon pool into the UVic ESCM, TCRE retain its simplicity for the RCP simulations and therefore retains its principle utility.

From the analysis above it appears that the hypothesis for the near constant nature of TCRE proposed by Matthews et al. (2009) is largely correct. There is in fact a compensation between declining radiative forcing from a unit of $CO_2$ and diminishing uptake of heat and carbon by the ocean. These two oceanic effects, however, act in a surprisingly independent way. In the case of a constant rate of $CO_2$ emission it is the diminishing rate of ocean heat uptake that compensates for the diminishing radiative forcing per unit atmospheric $CO_2$. In this case the ocean carbon uptake is stable an therefore stabilizes the airborne fraction of carbon. In the more realistic case of exponentially increasing $CO_2$ emissions, a second compensation between airborne fraction of carbon and the $CO_2$ emission rate effect on ocean heat uptake becomes important. As the rate of $CO_2$ emissions increases the ocean takes up a diminishing fraction of carbon. This leads to a stronger radiative forcing from $CO_2$ at given cumulative emissions but also increases the rate of ocean heat uptake, compensating in such a way maintain a near constant TCRE.

The parameterization of ocean heat uptake as heat flow in a semi-infinite half space is a mathematically useful but ultimately a gross over simplification of a complex phenomenon. The logarithmic approximation of the radiative forcing from $CO_2$ is also a simplification of complex physics (Wigley, 1987), which for some of the analysis in this chapter I have here further simplified using an approximation of the logarithm. The results presented here should therefore be interpreted with appropriate caution.

If the reduction in compatible emissions from the permafrost carbon feedback for each RCP shown in Table 5.3 are borne out in the natural world, then staying below the politically defined 2°C warming threshold will necessitate substantial negative emissions during the latter half of the present century. Such negative emissions may be technologically feasible (e.g. Chapter 4) but would likely require a degree of international cooperation that has not been evident in recent human history.

## 5.6 Conclusions

The transient climate response to emissions is a useful metric of climate warming that emerges as a near constant in Earth-system model simulations of climate change up until approximately 2000 Pg C have been emitted to the atmosphere (Matthews et al., 2009, Collins et al., 2013). Here we have conducted an analytical analysis of the climate system using a parameterization of ocean heat uptake as heat flux into a semi-infinite half space to derive an analytical expression of TCRE. This analysis shows that TCRE is near constant where the change in the ocean heat uptake efficiency with respect to cumulative carbon emissions (relative to the climate feedback parameter) is the same order of magnitude as the sum of one half the airborne fraction of carbon (relative to the initial carbon content of the atmosphere) and the derivative of a cross term. This cancelation produces a window where TCRE is nearly constant. In the more realistic case of exponentially increasing emissions of $CO_2$, the property of the ocean whereby the ocean-borne carbon fraction is a declining function of emissions rate helps compensate for the increased ocean heat uptake (as a function of cumulative carbon emissions) at higher emission rates.

Supporting this analytical analysis are numerical modelling experiments, conducted with the the frozen ground version of the UVic ESCM. The model when forced with a constant emissions rate of $CO_2$ suggests that strong feedbacks from the terrestrial carbon cycle (enhanced by the existence of the permafrost carbon pool) lead to emission rate dependence in the TCRE. These emission rate dependancies are of academic interest but do not result in significant changes in the linearity of temperature verses cumulative carbon emissions curves of the RCPs. Overall I reason that the near proportionality between temperature and cumulative carbon emissions is a feature of the Earth system in its current configuration and therefore a useful metric of climate warming.

# Chapter 6

# Conclusions and future directions

## 6.1 Conclusions

The uptake of over half of anthropogenically emitted $CO_2$ by the oceans and terrestrial biosphere has greatly mitigated the effect of human activities on global climate (Ciais et al., 2013). As human emission of $CO_2$ are expected to continue far into the future even under optimistic future scenarios (IPCC, 2013) there is great interest in whether natural processes will continue to remove carbon from the atmosphere. This dissertation has been an effort to improve the understanding of the potential future behaviour of the carbon cycle in light of the recently quantified reservoir of carbon held in permafrost soils. In addition, an effort has been made to understand why global mean temperature increase is nearly proportional to cumulative $CO_2$ emissions in virtually all Earth system model simulations.

In the introduction to this dissertation the scientific work was framed in terms of five questions. Below I will summarize the conclusions drawn from investigating these questions.

1. The permafrost carbon feedback to climate change is simulated to have a strength of 0.25 °C (0.1 to 0.75)°C by the year 2100 CE independent of emission pathway followed in the 21st century. This range is contingent on the size of the permafrost carbon pool and the simulated model climate sensitivity. After 2100 the projected strength of the feedback diverges by emission pathway with a full range of between 0.15 to 1.70°C for all scenarios, permafrost carbon density, and modelled climate sensitivities. The upper bound of this temperature range is simulated for the lower two emission pathways under high climate sensitivity.

The permafrost carbon feedback reduces the diagnosed compatible emissions for achieving each RCP relative to model simulations without permafrost carbon. For model simulations with a climate sensitivity of 3.2°C (for a doubling of atmospheric $CO_2$ concentration) compatible emissions are reduced by 155 to 280 Pg C between 2012 and 2100 CE depending on the concentration pathway followed.

2. If $CO_2$ emissions were to suddenly cease, the UVic ESCM suggests that whether or not $CO_2$ would continue to build up in the atmosphere is contingent on climate sensitivity and the concentration of non-$CO_2$ greenhouse gasses in the atmosphere. For a given model climate sensitivity there is a threshold value of radiative forcing from non-$CO_2$ greenhouse gasses above which $CO_2$ will continue to build up in the atmosphere for centuries after cessation of anthropogenic $CO_2$ emissions. This threshold value varies depending on the total quantity of cumulative $CO_2$ emissions and the history of the rate of emissions. For a UVic ESCM integration with an inherent climate sensitivity of 3.2°C the threshold value for the RCP derived emission scenarios is approximately $0.6\,\mathrm{W\,m^{-2}}$ of non-$CO_2$ greenhouse gas radiative forcing. This value is lower than the present non-$CO_2$ greenhouse gas forcing ($0.95\,\mathrm{W\,m^{-2}}$) and equivalent to the value for the most optimistic RCP in 2100 (Moss et al., 2010). The consequences of being above this threshold value are mild, with the model projecting a further 11-22 ppmv rise in atmosphere $CO_2$ concentration after emissions cease if present-day non-$CO_2$ greenhouse gas forcing is maintained indefinitely.

3. If technologies were developed and deployed to remove carbon from the atmosphere simulations with the UVic ESCM suggest that a Holocene-like climate could be restored by the end of the present millennium (except under a high climate sensitivity and high emission scenario). The scenarios simulated imposed a decline in atmospheric $CO_2$ concentration as a mirror image to its prior increase after the peak in $CO_2$ concentration is reached following each RCP. I argue that these scenarios, while idealized, emulate a fast but plausible decline in atmospheric $CO_2$ concentration. The UVic ESCM forced with these scenarios projects that more carbon must be removed from the atmosphere than was originally emitted to it. This is primarily a consequence of the permafrost carbon feedback as reincorporation of carbon into permafrost soils is a process that occurs on millennial time-scales, while carbon in permafrost soils can be

released on centennial time scales.

4. The proportionality between cumulative $CO_2$ emissions and global mean temperature change seen in most Earth system model simulations appears to arises from two factors: I) the stability of the airborne fraction of emitted carbon provided by the ocean uptake of carbon begin nearly a function of $CO_2$ emission rate; and II) the diminishing heat uptake by the oceans compensating for the reduced radiative forcing per unit mass $CO_2$ at high atmospheric $CO_2$ concentrations.

5. Strong terrestrial carbon cycle feedbacks can disrupt the proportionality between cumulative $CO_2$ emissions and global mean temperature change. Such emission from the land surface make the value of the transient climate response to [cumulative $CO_2$] emissions (TCRE) dependent on the rate and path of emissions. However, within the range of emission rates project for the RCPs the permafrost carbon feedback is not strong enough to disrupt TCRE.

Overall, the addition of the permafrost carbon pool to the UVic ESCM alters model behaviour in ways that if representative of the natural world will make stabilizing climate or reversing climate change more difficult than has previously been foreseen.

## 6.2 Future directions

Since I began this project in May 2011 rapid progress has been made quantifying the size, spatial distribution, and chemical properties of the permafrost carbon pool (e.g. Schädel et al., 2014, Grosse et al., 2013, Hugelius et al., 2013). Incorporating this improved understanding of permafrost carbon into Earth system models should be a priority. In the context of the UVic ESCM the newly available spatial maps of permafrost carbon density with depth to 3 m could be incorporated into the model to replace the current assumption of a uniform permafrost carbon density.

For the purposes of an Earth system model it is important that a parameterization of cryoturbation be incorporated into the UVic ESCM. I chose at the beginning of this project to prescribe the permafrost carbon pool as a uniform density carbon pool in millennially frozen soil. This choice was made so that the permafrost carbon pool would accurately represent the quantity of carbon in permafrost soils, which I

believed was more important for this project than closing the carbon cycle. At that time attempts to parameterize uptake of carbon into permafrost soils had resulted in substantial underestimates of the quantity of carbon in these soils (e.g. Koven et al., 2011). However, if the model is to be applied to paleoclimate simulations or millennial scale recovery simulations a process based representation of the incorporation of carbon into permafrost soils will be needed. Another priority for model development is to link the decomposition of permafrost carbon with methanogenesis once the wetland methanogenesis component of the model is operational.

The goal of Earth system modelling is to improve the understanding of the Earth system and how human activities affect its functioning. As human technologies continue to advance our effect on the biogeochemical cycles that keep the planet habitable for complex life is likely to grow. In the past seventy years humanity has faced three existential crisis related to our growing powers: the threat of nuclear winter, depletion of stratospheric ozone, and anthropogenic climate change. Modelling played a key role in foreseeing each of these crisis before they came to pass. By continuing to advance Earth system models more crisis may be foreseen before they occur. Crisis that are foreseen may be averted and every crises that is averted extends the lifetime of this grand uncontrolled experiment that is industrial civilization.

# Appendix A

# Additional Information

## A.1 Supplementary material for: Significant contribution to climate warming from the permafrost carbon feedback

### A.1.1 UVic ESCM soil carbon component

The frozen ground version of the UVic ESCM has a soil component with fourteen layers of exponentially increasing thickness to a total depth of 250 m. Only the top six layers (to a depth of 3.35 m) are active in the carbon cycle. The terrestrial carbon cycle in the UVic ESCM is simulated using the Top-down Representation of Interactive Foliage and Flora Including Dynamics (TRIFFID) dynamic global vegetation model (Matthews et al., 2004, Meissner et al., 2003, Cox et al., 2001). Litter from land plants is transferred into soil layers as a decreasing fraction with depth and is only allowed to enter soil layers that are above a threshold temperature of 1°C (except the top layer of soil). To achieve stability the threshold at which soil respiration is turned on and at which fresh carbon is allowed to enter a soil layer cannot be the same (if they are the same soil layers that are infinitesimally above freezing will accumulate near-infinite quantities of carbon during model spin-up). The TRIFFID soil respiration component is implemented in each soil layer. When soil carbon is respired, it is instantaneously transferred to the atmosphere. The TRIFFID soil respiration parameterization has been modified to ensure that soil respiration cannot occur below 0°C. A parallel set of model experiments were conducted using an unmodified version of the soil respiration parameterization. The results from these experiments are only slightly different from

those presented here. The TRIFFID soil respiration parameterization uses only a single carbon pool with a globally uniform $Q_{10}$ of 2 ($Q_{10}$ is a measure of change in the rate of a chemical or biochemical reaction given a 10 K change in temperature) and a reaction rate of $3.5\times10^{-9}s^{-1}$. These respiration parameters are close to the weighted average of the labile and recalcitrant fractions for incubation experiments using permafrost derived soil carbon Dutta et al. (2006). To take into account that permafrost carbon contains a relatively large fraction of highly recalcitrant carbon, 15% of frozen permafrost carbon is not allowed to decay.

### A.1.2 UVic ESCM permafrost dynamics component

The permafrost dynamics of the frozen ground version of the UVic ESCM were succinctly described in Avis et al. (2011) and described in detail in Avis (2012). This model setup is briefly recalled here. The UVic ESCM has spatially variable thermal and hydraulic properties based on the material properties of soil interpolated (to the UVic ESCM grid spacing) from the International Satellite Land Surface Climatology Project, Initiative II (ISLSCP-II) soil database (Scholes and de Colstoun, 2012). The water content of the top eight soil layers (10 m) varies in time as rainfall and melt water percolate through the subsurface. Soil layers below 10 m are considered hydraulically inactive (bedrock). The thermal conductivity of the soil is a function of the air, water, and ice content of the soil in addition to the sand, silt and clay fraction of the soil. The carbon content of the soil also affects the thermal and hydraulic conductivity of the soil following the method of Lawrence and Slater (2008). Freezing and thawing within the soil are governed by relations to minimize Gibbs free energy. Heat is transported through the soil via thermal conduction and advection of ground water. Water that percolates to the deepest hydraulically active soil layer is routed to the appropriate river system. Plants extract water from the soil layers where their roots are located.

The degradation of permafrost under each RCP as simulated by the frozen ground version of the UVic ESCM was described in Avis et al. (2011) and Avis (2012). As the present study varies the climate sensitivity of the model and uses emissions pathways in place of concentration pathways, the degradation of permafrost will be slightly different from those previous efforts. The reduction in permafrost extent for each DEP is shown in Figure A.1. Each DEP shows a gradual decline in permafrost extent in the 20th century followed by a rapid decline in the 21st century. Except for DEP

2.6 the reduction in the extent of permafrost continues throughout the 22nd and 23rd centuries. In some ensemble members of DEP 2.6 (including the median member) permafrost extent recovers after the 21st century.

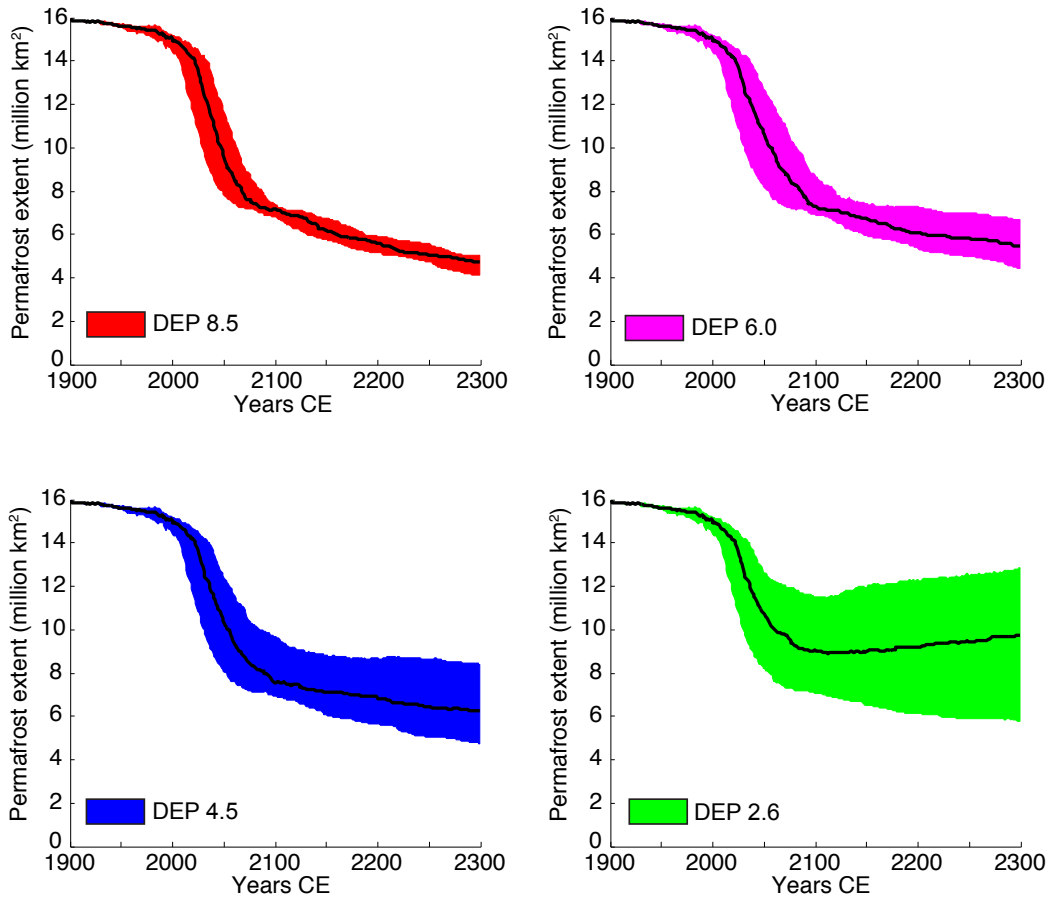


Figure A.1: Extent of permafrost under four future emissions pathway. Median values for each range are shown as a black line.

Table A.1 compares the loss of permafrost area in the UVic ESCM simulations under the DEPs to the loss of permafrost area for models used in the fifth assessment repost of the intergovernmental panel on climate change (IPCC AR5). The initial northern hemisphere area of permafrost in the UVic ESCM is 15.94 million km$^2$ which is smaller than the accepted value of 18.78 million km$^2$ for this quantity in the natural world (e.g. Tarnocai et al., 2009). From Table A.1 one can see that the UVic ESCM overestimates permafrost loss relative to the IPCC AR5 models for DEP 2.6,

Table A.1: Relative reduction in permafrost area in the UVic ESCM and for models assessed in IPCC AR5 for year 2100 (relative to pre-industrial).

| Concentration or Emissions Pathway | AR5 (%) | UVic ESCM (%) |
|---|---|---|
| RCP/DEP 2.6 | 37 ± 11 | 43 (28 to 56) |
| RCP/DEP 4.5 | 51 ± 13 | 53 (39 to 57) |
| RCP/DEP 6.0 | 58 ± 13 | 54 (46 to 57) |
| RCP/DEP 8.5 | 81 ± 12 | 55 (54 to 57) |

underestimates loss for DEP 8.5, and is in the range of the IPCC AR5 models for DEP 4.5 and 6.0.

### A.1.3 Diagnosed emissions pathways

Climate model simulations conducted in preparation for the 5th Assessment Report of the Intergovernmental Panel on Climate Change use the Representative Concentration Pathways (RCP) to force simulations of future climate (Moss et al., 2010). RCPs define a $CO_2$ concentration–time curve for each pathway instead of specifying $CO_2$ emissions with time (Moss et al., 2010). However, if atmospheric $CO_2$ concentration is allowed to evolve freely in response to the permafrost carbon feedback, $CO_2$ emissions with time are needed. The UVic ESCM can be configured to be forced with a $CO_2$ concentration pathway while diagnosing anthropogenic emissions of $CO_2$ as a residual from the simulated carbon cycle. Such simulation were performed for RCPs 2.6, 4.5, 6.0, and 8.5 to generate Diagnosed Emissions Pathways (DEPs) designated with numbers corresponding to the RCP from which each was diagnosed. The diagnosis was performed using the frozen ground version of the UVic ESCM with permafrost carbon turned off and using the model's inherent climate sensitivity (of 3.2°C).

The four DEPs are displayed in Figure A.2 a. In DEP 2.6, $CO_2$ emissions peak at 9.7 $\mathrm{Pg\,C\,a^{-1}}$ in the year 2021, emissions decline to zero by 2077, and negative emissions are maintained to the end of the pathway in 2300. In DEP 4.5, $CO_2$ emissions peak at 11.7 $\mathrm{Pg\,C\,a^{-1}}$ in the year 2037 and sharply decline after 2050, settling down to tail emissions of 0.5 $\mathrm{Pg\,C\,a^{-1}}$ by the late 22nd century. In DEP 6.0 emissions peak at 17.0 $\mathrm{Pg\,C\,a^{-1}}$ in the year 2082 and decline in the first half of the 22nd century. In DEP 8.5 emissions peak at 26.3 $\mathrm{Pg\,C\,a^{-1}}$ in 2102, are held at near constant levels until 2200 then decline in the first half of the 23rd century. Figure A.2 b shows the cumulative emissions for each of the DEPs.

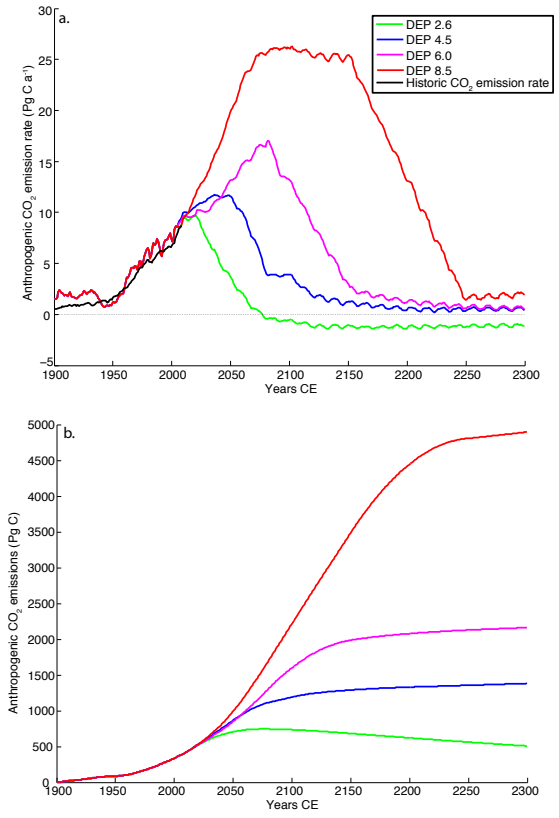


Figure A.2: Emissions pathways diagnosed from representative concentration pathways 2.6, 4.5, 6.0 and 8.5. a. Anthropogenic carbon emissions rate. b. Cumulative anthropogenic carbon emissions. Note that DEP 2.6 requires negative carbon emissions. Historical emissions are from Boden et al. (2011). The periodic variations seen in panel a. are a consequence of the variation in external radiative forcing from the solar cycle.

### A.1.4 The permafrost carbon pool

Tarnocai et al. (2009) estimated the size of the permafrost carbon pool as 1672 Pg C in the northern hemisphere north of 45°. Of this 1024 Pg C was estimated to reside in the top 3 m of soil, 407 Pg C in the yedoma deposits in Siberia, and 241 Pg C in deep-deltaic deposits. In the UVic ESCM deep deposits are not accounted for due to their localized nature. Only carbon down to a depth of 3.35 m is simulated. The simulated quantity of soil carbon in permafrost regions varies depending on the assumed density of frozen permafrost carbon, and the given climate sensitivity of the model (due to feedbacks between climate sensitivity and the carbon cycle). Table A.2 shows the simulated quantity of permafrost carbon north of 45° N for each combination of climate sensitivity and permafrost carbon density for the decade 1990-1999. In the UVic ESCM permafrost carbon is simulated south of 45° N in the high Himalayas and the fringes of Antarctica, this permafrost carbon amounts to about 150 Pg C (depending on permafrost carbon density and climate sensitivity).

Figure A.3 compares the simulated carbon density in the UVic ESCM to ISLSCP-II carbon density data (Scholes and de Colstoun, 2012) interpolated to the grid of the UVic ESCM. The ISLSCP-II data exists only for the top 1.5 m of soil, therefore for comparison the simulated soil carbon density is given only to this depth. From the figure one can see that the UVic ESCM reproduces soil carbon density to the correct order of magnitude, but with a much more spatially uniform distribution than the contemporary world. The UVic ESCM biases the distribution of soil carbon toward the northern fraction of the permafrost zone. This region is projected to thaw last, therefore distribution of carbon may cause the UVic ESCM to underestimate the rate of loss of carbon from permafrost early on, and overestimate the loss of carbon in the latter parts of the simulation.

Figure A.4 show global and permafrost region averaged carbon density profiles with depth for the decades 1990–1999 and 2290–2299. One can see that the general shape of the profiles is consistent, with high carbon density near the surface and declining concentrations with depth. The carbon density in the top soil layer in the permafrost region is implausibly high, at close to 200 $\mathrm{kg\,m^{-3}}$. This is a consequence of the model's method of distributing plant litter carbon to soil layers. Recall that the model distributes plant litter as a decreasing function with depth into soil layers above 1°C, unless all of the layer are below this threshold in which case plant litter is deposited in the top layer of soil. This creates the spuriously high soil carbon density

in the top soil layer. In reality this carbon should be more smoothly distributed in the uppermost soil layers. However, since these layers quickly respond to surface temperature changes there should be only minor differences in soil respiration rates.

Table A.2: Simulated soil carbon in permafrost affected soils north of 45° N for the decade 1990-1999.

| Climate Sensitivity (°C) | Permafrost Carbon Density ($kg\,m^{-3}$) | Active Carbon (Pg C) | Frozen Carbon (Pg C) | Total Carbon (Pg C) |
|---|---|---|---|---|
| 2.0 | 15.8 | 365 | 505 | 869 |
| 3.0 | 15.8 | 353 | 505 | 858 |
| 4.5 | 15.8 | 332 | 505 | 837 |
| 2.0 | 21.0 | 366 | 673 | 1039 |
| 3.0 | 21.0 | 353 | 673 | 1026 |
| 4.5 | 21.0 | 330 | 673 | 1003 |
| 2.0 | 26.3 | 365 | 841 | 1206 |
| 3.0 | 26.3 | 351 | 841 | 1192 |
| 4.5 | 26.3 | 330 | 841 | 1171 |

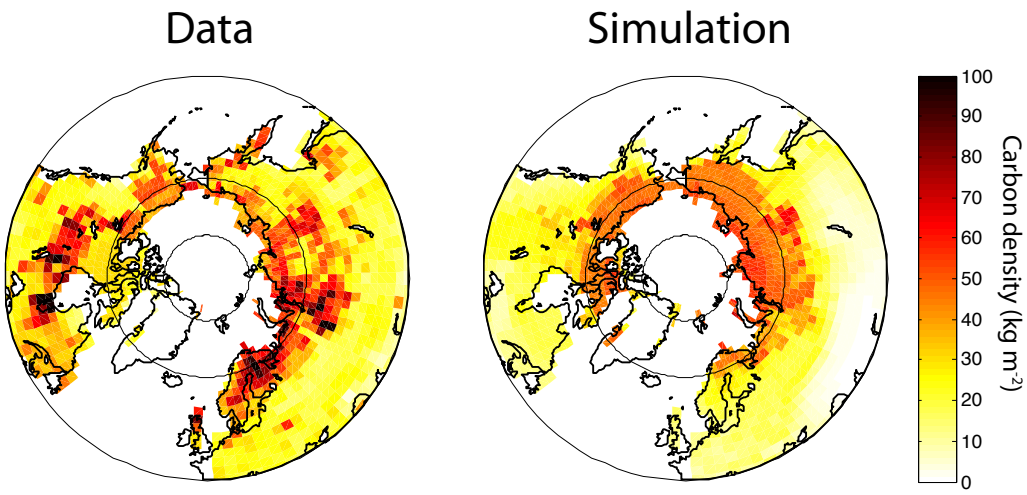


Figure A.3: Carbon density in the top 1.5 m of soil for International Satellite Land Surface Climatology Project, Initiative II (ISLSCP-II) carbon density data (Scholes and de Colstoun, 2012), interpolated to the grid of the UVic ESCM (Data), and the simulated carbon density in the UVic ESCM in the top 1.5 m of soil (Simulated).

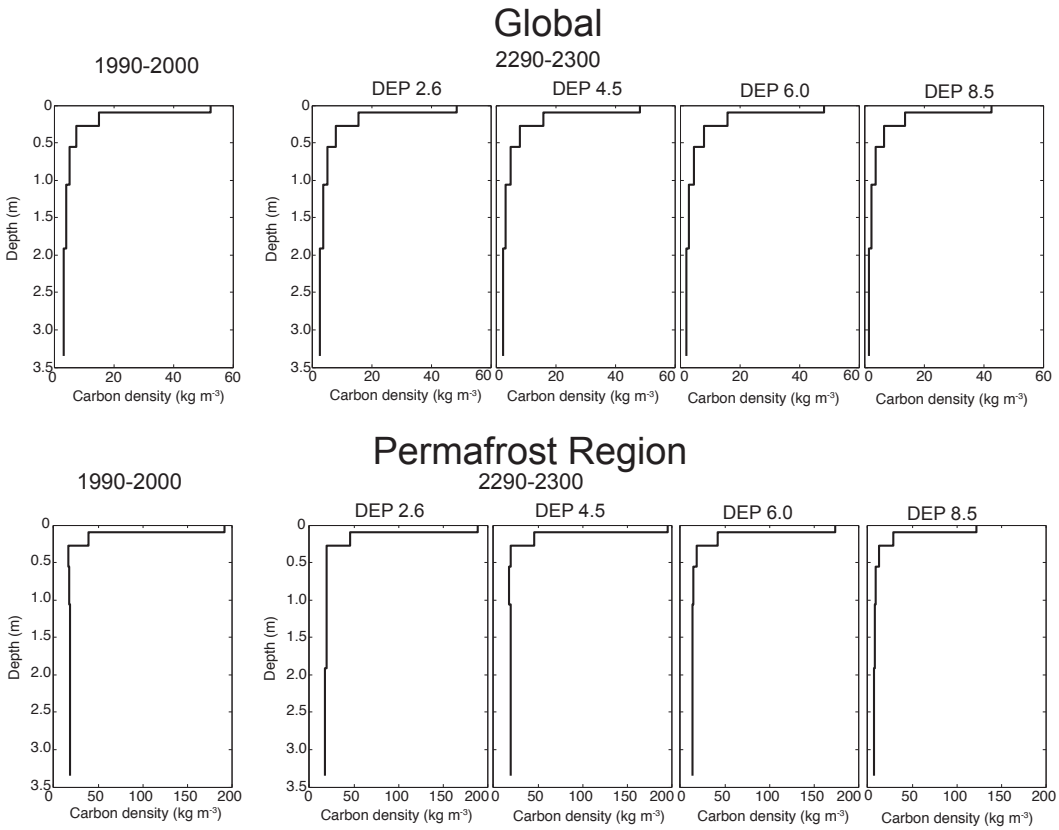


Figure A.4: Global and permafrost region carbon density depth profiles for UVic ESCM. Profiles given for decades 1990–1999 and 2290-2299 for each DEP.

### A.1.5 Permafrost carbon and the carbon cycle

Figure A.6 displays the $CO_2$ anomaly with respect to baseline runs with no permafrost carbon for each of the DEPs. Higher emissions pathways result in more carbon being liberated from the permafrost. In Figure 2.2 the effect of adding permafrost carbon to the carbon cycle is shown for DEPs 4.5 and 8.5. Figure A.7 shows the same quantity for DEPs 2.6 and 6.0. Figure A.8 displays the rate at which the terrestrial carbon pools contribute carbon to the atmosphere in a given year (negative values indicate a carbon sink). In every model simulation the terrestrial land surface transitions from a sink to a source of carbon to the atmosphere by 2150. The terrestrial land surface remains a source of carbon to the atmosphere until 2300 in most simulations. Peak

carbon emissions from the terrestrial land surface vary by anthropogenic emissions pathway, but are of the same order as 20th century anthropogenic carbon emissions.

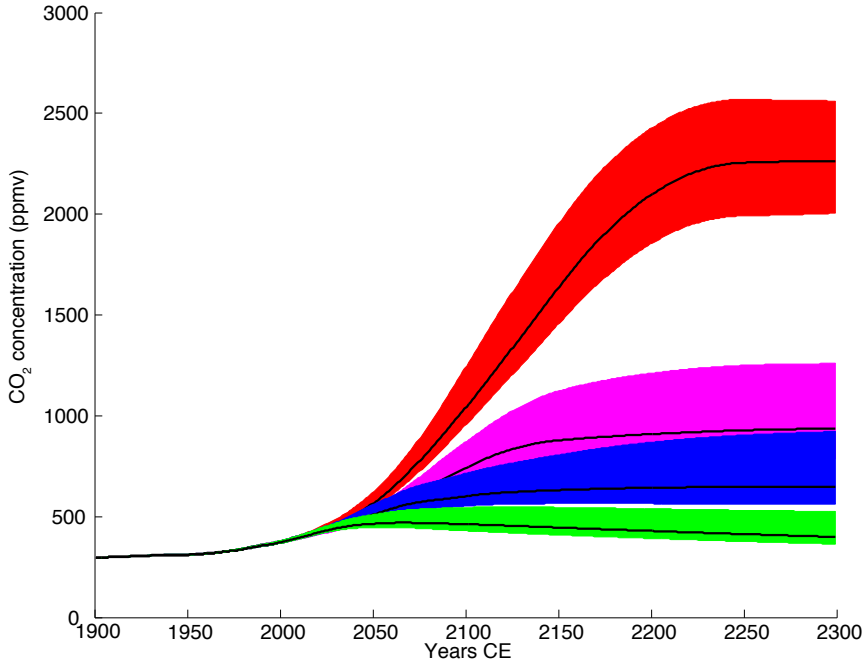


Figure A.5: Absolute $CO_2$ concentration for each all DEP simulations with permafrost carbon. Median values for each range are shown as a black line.

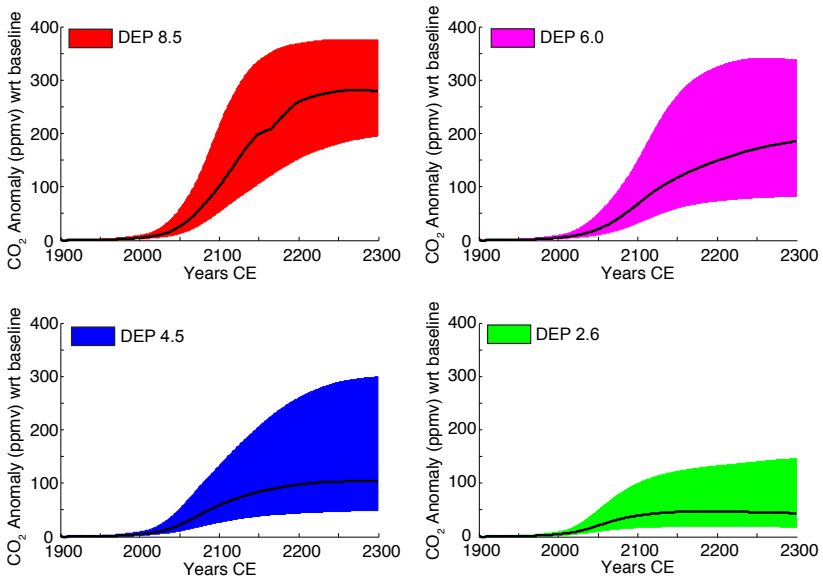


Figure A.6: Anomaly in $CO_2$ concentration with respect to baseline runs with no permafrost carbon, for each DEP. Median values for each range are shown as a black line.

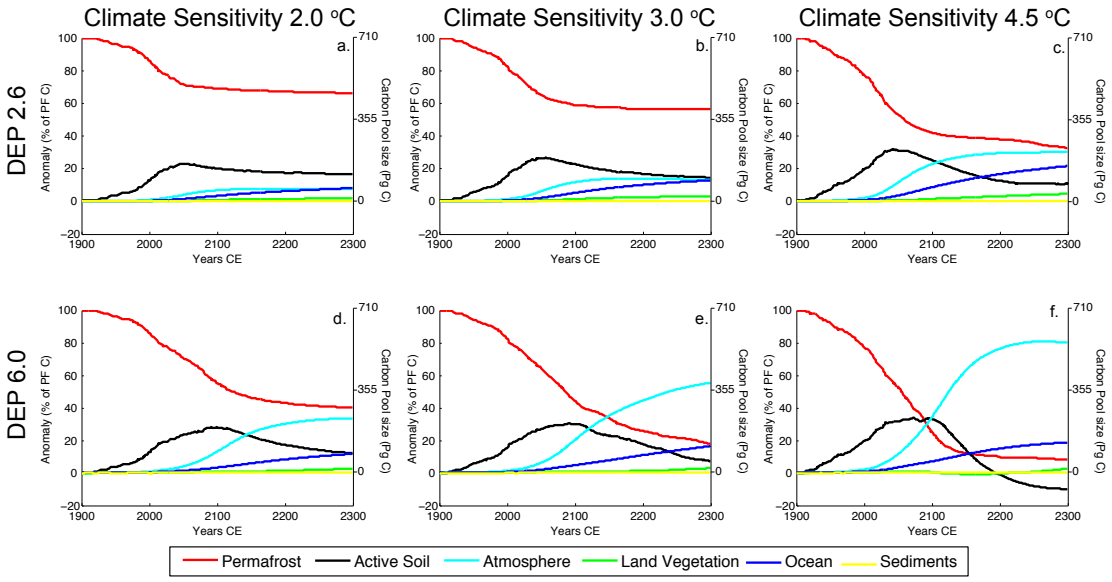


Figure A.7: Changes in the size of each Earth system carbon pool in response to the addition of permafrost carbon to the UVic ESCM. That is, the difference in the size of each carbon pool between simulations with and without permafrost carbon. All values are relative to the initial size of the frozen permafrost carbon pool (and a summation of all of the pools adds up to 100% for each year).

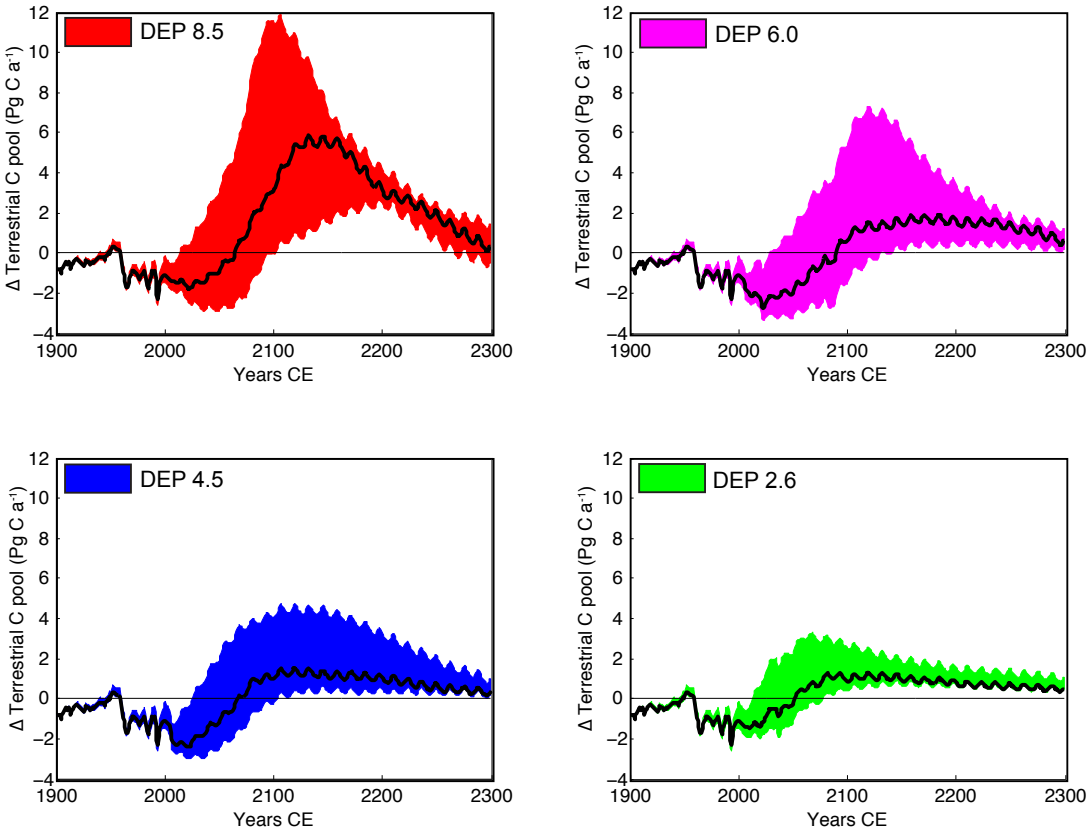


Figure A.8: Carbon emissions (or uptake) from terrestrial carbon pools. Negative values indicate a carbon sink with respect to the atmosphere, positive values a source of carbon to the atmosphere. The periodic variations in emissions rate are a consequence of the variation in external radiative forcing from the solar cycle.

### A.1.6 Absolute temperature change

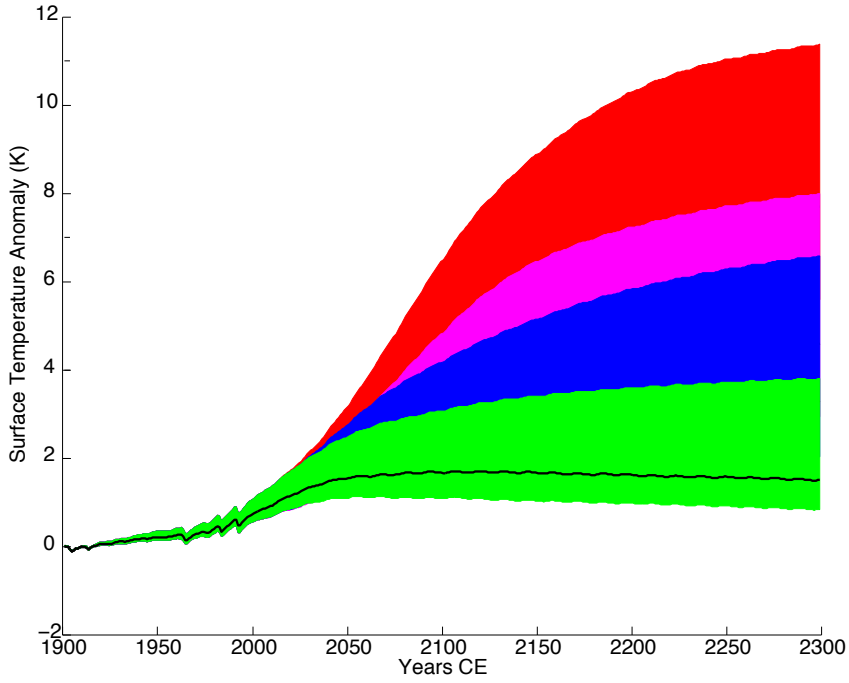


Figure A.9: Absolute Surface Air Temperature (SAT) anomaly for each all DEP simulations with permafrost carbon. Median values for each range are shown as a black line.

### A.1.7 Industrial shutdown experiment

To explore under what conditions the permafrost carbon feedback becomes self-sustaining (drives itself forwards indefinitely), a series of experiments were conducted wherein DEP 8.5 is followed until a given date when industrial emissions are immediately eliminated. That is, anthropogenic $CO_2$ and sulphate emissions are set to zero. Figure A.10 displays the results of these experiments when industrial activity is shutdown in 2013 (Fig. A.10 column 1) or 2050 (Fig. A.10 column 2). In either case, the climate sensitivity of the model determines whether the feedback becomes self-sustaining. For a climate sensitivity of 2.0°C carbon emissions from terrestrial carbon pools are smaller than the ability of the ocean to absorb carbon and the concentration of $CO_2$ in the atmosphere falls. For a climate sensitivity of 3.0°C carbon emissions from terrestrial carbon pools and the absorption of carbon by the ocean are

almost balanced. As a result concentrations of $CO_2$ in the atmosphere are near constant. For a climate sensitivity of 4.5°C the release of carbon from terrestrial carbon pools exceeds the ability of the oceans to absorb carbon and the concentration of $CO_2$ in the atmosphere continues to increase indefinitely after cessation of anthropogenic emissions.

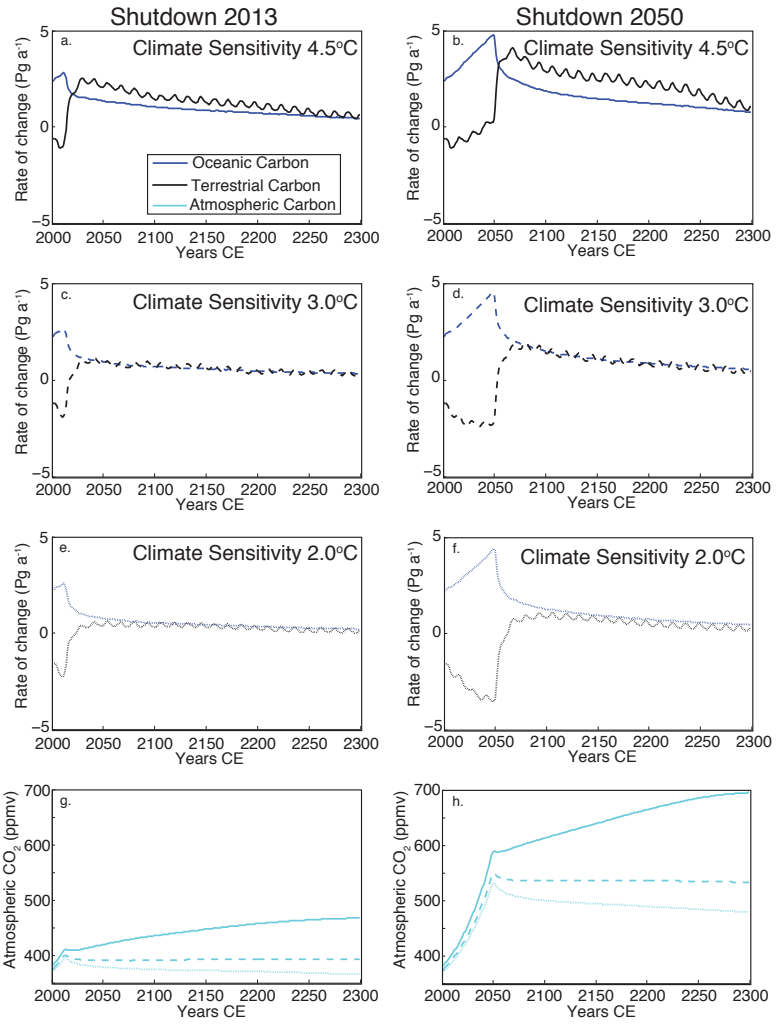


Figure A.10: Response of the carbon-cycle to a shutdown of industrial activity under varying climate sensitivities. Dotted lines indicate a climate sensitivity of 2.0°C, dashed lines a climate sensitivity of 3.0°C and solid lines a climate sensitivity of 4.5°C. a.–f. Rate of change of oceanic and terrestrial carbon pools. The terrestrial and oceanic carbon pools are displayed using opposite sign conventions to accommodate comparison of the magnitude of the rates of change. For the ocean positive is into the ocean and for the terrestrial biosphere positive is towards the atmosphere. The sudden increase in the rate of carbon release from the terrestrial carbon pool when anthropogenic emissions are shutdown is caused by the termination of $CO_2$ fertilization of land vegetation. g.,h. Atmospheric $CO_2$ concentrations in response to shutdown of industrial activity. The periodic variations emission rate from terrestrial carbon pool are a consequence of the variation in external radiative forcing from the solar cycle.

### A.1.8 Comparison to previous efforts

There have been several previous efforts to quantify the strength of the permafrost carbon feedback using terrestrial land surface models forced with GCM output (Zhuang et al., 2006, Schaefer et al., 2011, Koven et al., 2011) and one effort using a one dimensional carbon-cycle emulator (Schneider von Deimling et al., 2012). Each of these studies used different models to estimate the permafrost carbon feedback and consequently produce wide-ranging estimate of its strength. Zhuang et al. (2006) used the Terrestrial Ecosystem Model (TEM) to estimate $CO_2$ and $CH_4$ fluxes from high latitudes during the 21st century. The TEM is capable of simulating vegetation dynamics, enhanced soil respiration, nitrogen dynamics and the effects of fire. The model is forced with output from the MIT-IGSM. The study is somewhat ambiguous about how much carbon they simulate in the permafrost region under the present climate but from the citation given (Jobbágy and Jackson, 2000) it is constrained to 144–294 Pg C. Under their simulations, between 7 to 17 Pg C is released to from permafrost regions.

Schaefer et al. (2011) used the SiBCASA land surface model to estimate $CO_2$ fluxes from the permafrost region and consequently the strength of the permafrost carbon feedback. The model is capable of simulating freeze-thaw processes, enhanced soil respiration, vegetation dynamics, but not fire or nitrogen dynamics. The model is forced with output from three GCMs under the A1B scenario. The estimated permafrost carbon pool in this study is 414 Pg C of which 313 Pg C is frozen under the present climate. These simulations estimate that 103 $\pm$35 Pg C will be released from permafrost soils by 2100 and 190 $\pm$64 by 2200.

Koven et al. (2011) used the ORCHIDEE model to estimate $CH_4$ and $CO_2$ fluxes from the region north of 60°N for the 21st century. The model simulates vegetation dynamics, freeze-thaw processes, methanogenesis in deep soils, release of heat by microbial respiration, and contains a prognostic simulation of vertical mixing of carbon but does not include nitrogen dynamics or the effects of fire. The model forced with output from the Institut Simon Pierre Laplace Climate model 4 under the A2 scenario. This version of ORCHIDEE is the only globally resolved model to parameterize the formation of the permafrost carbon pool and simulated an initial such pool of 476 Pg C. The model produced a best guess of 62 $\pm$7 Pg C released from permafrost soils by 2100.

Schneider von Deimling et al. (2012) used the MAGIC6 reduced complexity carbon cycle model to estimate fluxes of $CH_4$ and $CO_2$ from northern high latitudes. The model is a highly parameterized statistical model which must be calibrated to the output of dynamically based highly resolved carbon cycle models. The model can only simulate the gradual thickening of the active layer and does not account for talik formation. The model is prescribed a frozen permafrost carbon pool of 600–1000 Pg C of which 33–114 Pg C are released from soil by 2100.

Of these previous efforts the UVic ESCM is most similar to Schaefer et al. (2011) effort in that it does not simulate $CH_4$ production and uses the same method to prescribe carbon into permanently frozen soil layers. Unlike the previous efforts, the UVic ESCM does not need to be forced with output from a GCM or be calibrated to highly resolved carbon cycle models but instead generates its own climatological fields. This allows the UVic ESCM to complete the feedback loop and simulate the effect of the permafrost carbon feedback on further driving the permafrost carbon feedback and other carbon-climate feedbacks within the model. The UVic ESCM is coupled to a full oceanic carbon cycle model component which allows the model to simulate the uptake of carbon by the ocean and to calculate the airborne fraction of carbon released from the permafrost.

The UVic ESCM estimates an additional release from all soils of 68 to 508 Pg C by 2100 relative to the baseline runs with no permafrost carbon. The initial carbon pool in permafrost soils and the active layer above them is 837–1206 Pg C in the UVic ESCM . Considering the UVic ESCM's much larger initial permafrost carbon pool in a relative sense our estimate of 8%–42% reduction in the size of the pool by 2100 is comparable with the Schaefer et al. (2011) estimate of 16%–33% and the Koven et al. (2011) estimate of 13%–16% reduction by 2100.

## A.2 Extended modelling methods description

### A.2.1 Introduction

The University of Victoria Earth System Climate Model (UVic ESCM) is a climate model of intermediate complexity developed at the University of Victoria in the late 20th century (Weaver et al., 2001). Since the model's release to the public in 2001 the model has been further developed to better represent processes within the Earth system, and is now used by several modelling groups worldwide.

The model consists of a full three dimensional ocean general circulation model (Modular Ocean Model 2), coupled to a energy and moisture balance atmosphere, a thermodynamic-dynamic sea ice model (Weaver et al., 2001), and a complex land surface scheme (Meissner et al., 2003, Avis, 2012). The model contains a full realization of the global carbon cycle. The ocean carbon cycle is represented with an inorganic ocean carbon chemistry scheme(Weaver et al., 2001), in addition to a nutrient-phytoplankton-zooplankton-detritus ocean biology scheme (Schmittner et al., 2008). The slow negative feedback between ocean alkalinity and calcite deposition is simulated using an oxygen only representation of respiration of organic matter in sediments (Archer, 1996). The terrestrial carbon cycle is simulated with a dynamic vegetation model and a soil-carbon respiration component (Matthews et al., 2004). Added to this scheme is a representation of the permafrost carbon pool (Chapter 2). A schematic diagram of the UVic ESCM is show in figure A.11. The model is forced by incoming solar radiation and prescribed surface wind fields. This appendix contains a more detailed description of the present state of the UVic ESCM than the descriptions given in each of the paper-derived chapters (Chapters 2, 3, 4, and 5).

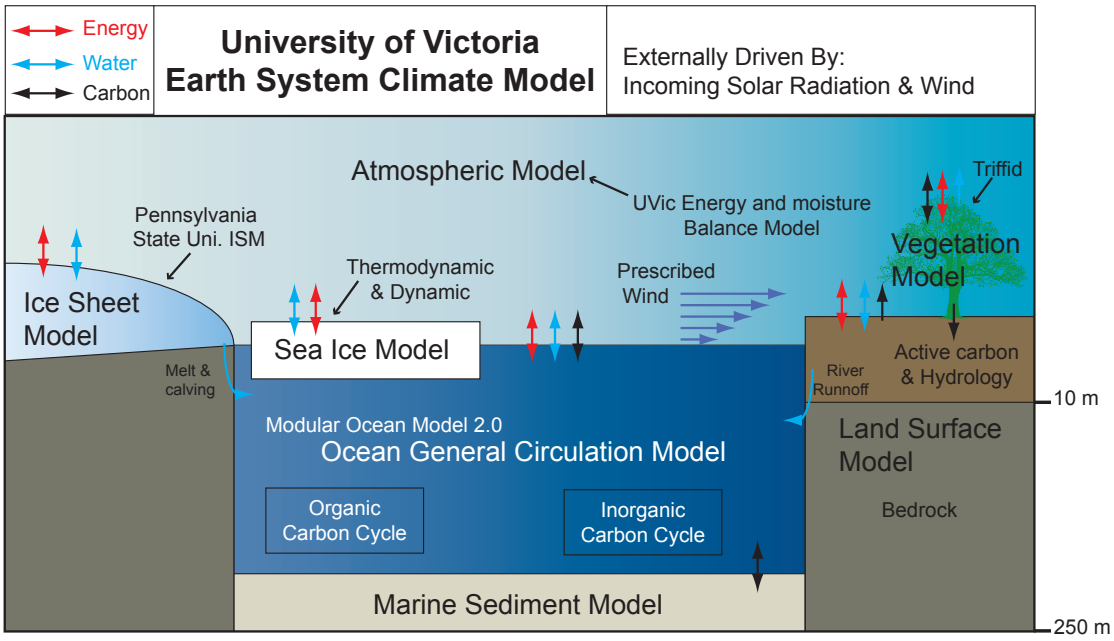


Figure A.11: Schematic diagram of the University of Victoria Earth System Climate Model. Fluxes of energy, water, and carbon are show with arrows.

### A.2.2 Physical climate components

#### Atmosphere

The UVic ESCM uses a simplified energy and moisture balance atmosphere. This simplified atmospheric component is what makes the UVic ESCM a climate model of intermediate complexity, and what gives the model its high computational efficiency. This model component carries out the main climatological functions of the atmosphere, without simulating the fluid motions of air. The simulated functions are: transporting heat and moisture from the tropics towards the poles, and solving energy balance equation at the planetary surface and top of the atmosphere. The simplified atmosphere component allows the model to simulate climate but not day to day weather or internal climate variability (Weaver et al., 2001).

Atmospheric heat transport is simulated via fickian diffusion. Moisture is transported both by diffusion and by advection that is driven by the prescribed surface wind fields. At each grid cell and each atmospheric time-step the atmospheric energy balance is modified by absorbed incoming solar radiation, latent heat flux, outgoing longwave radiation, absorbed longwave radiation emanating from the surface, and sensible heat flux from the surface (Weaver et al., 2001). Sensible heat flux is calculated using the bulk aerodynamic approach, a parameterization that relates sensible heat flux to humidity, wind speed and atmospheric temperature. The outgoing longwave radiation flux is simulated using the parameterization of Thompsom and Warren (1982) which relates outgoing longwave to near surface air temperature and relative humidity (Weaver et al., 2001).

A convenient consequence of the simplified atmospheric model component is that the outgoing longwave radiation to space can easily be altered within the model framework. This feature of the atmospheric model has been exploited (originally by Zickfeld et al. (2008)) as a means to change the equilibrium climate sensitivity of the UVic ESCM. The present version of the UVic ESCM has an inherent climate sensitivity of 3.2 °C for a doubling of atmospheric $CO_2$ concentration but this can be changed to any value within the full range of uncertainty for climate sensitivity (1-9 °C) (Zickfeld et al., 2008) using the following parameterization:

$$L^{\star}_{\mathrm{out}}(t) = L_{\mathrm{out}}(t) - K_{\mathrm{cs}}(T_s(t) - T_{\circ}), \tag{A.1}$$

where $L^{\star}_{\mathrm{out}}$ is the modified outgoing longwave radiation, $t$ is time, $L_{\mathrm{out}}$ is the unaltered

outgoing longwave radiation, $T_s$ is the global average surface air temperature, $T_\circ$ is the preindustrial surface temperature and $K_{\rm cs}$ is a constant. By performing a series of model integrations with varying values of $K_{\rm cs}$ a relationship between $K_{\rm cs}$ and equilibrium climate sensitivity can be established. The ability to perform model experiments with varying values of climate sensitivity is invaluable for evaluating the uncertainty in carbon-cycle climate feedbacks. This feature of the UVic ESCM has been exploited repeatedly in the model experiments document in this thesis (Chapters 2, 4, and 5).

### Ocean

The ocean component of the UVic ESCM is the the model component with the highest fidelity to observed physical reality. However, the model experiments documented in this thesis do not focus on ocean circulation and therefore the description of the ocean model provided here is brief. The ocean component of the model is the Geophysical Fluid Dynamics Laboratory Modular Ocean Model 2.2 (Pacanowski, 1995). The ocean model is based on the Navier Stokes equations of fluid motion (subject to Boussinesq and hydrostatic approximations). The model has 19 vertical layers of unequal thickness, smoothly varying in thickness from 50 m at the surface to 518 m for the deepest interval (Weaver et al., 2001). The ocean component is forced with surface wind stress fields and surface buoyancy.

Sea ice is simulated using a thermodynamic-dynamic sea ice model (Weaver et al., 2001). The sea ice is assumed to have no heat capacity and to be in instantaneous balance with external forcing. The parameterization accounts for sea ice as a sub-grid scale competent, with sea-ice occupying a prognostically determined fraction of the ocean grid-cell. Sea ice dynamics are simulated using a momentum balance which accounts for wind and ocean stress on the ice and the internal deformation of the ice.

### Land surface

The UVic land surface scheme used in the present version of the UVic ESCM is a highly modified variant of the Met Office Surface Exchange Scheme (MOSES) (Avis, 2012). The land surface itself is composed of sub-grid scale tiles of six surface types, five plant function types and bare ground. The surface energy balance is computed for each tile based on the varying albedo, aerodynamic roughness, and moisture availability of the tile. A weighted average of the six values is computed based on the

fraction of the grid cell that each surface type covers. Subsequent to weighting, the surface energy balance is passed to the atmospheric component of the model. If snow is present, it is assumed to uniformly cover the grid cell. Snow affects the surface energy balance by changing the albedo of the surface and by changing the aerodynamic roughness of the surface by modifying the effective vegetation height (Avis, 2012).

The sub-surface scheme consists of 14 vertical layers extending down to a depth of 250 m. The layers are of unequal thickness and become exponentially thicker with depth. The top layer has a thickness of 0.1 m. The top 8 layers (10 m) are active in model hydrology and top 6 layers (3.25 m) are active in the carbon cycle. In the hydraulically active layers the subsurface is prescribed porosity and permeability based on the sand, soil, silt, and organic matter content of the grid cell. These gridded data are interpolated from the International Satellite Land Surface Climate Project Initiative II (Scholes and de Colstoun, 2012). Water flows in the subsurface based on Darcy's law of fluid flow in a permeable solid. Water enters the soil column from the surface and is removed via evapouration at the surface or uptake into plant roots distributed through the subsurface Avis (2012). The deepest hydraulically active layer is assumed to be gravity drained. Water drained from the subsurface is directed into the river scheme and instantly deposited in the proper river outlet. In soils valence forces from soil particles depresses the freezing point of water such that water freezes over a range of temperatures. To take this into account the UVic ESCM subsurface component solves for the fraction of frozen or unfrozen soil water based on equations that minimize Gibbs free energy (Avis, 2012).

The temperature of the subsurface is determined by temperature-gradient driven heat diffusion, latent heat released or absorbed by the phase change of water, and transport of heat via the vertical movement of groundwater. The surface boundary condition is the surface temperature as determined by surface energy balance and the bottom boundary condition is a prescribed geothermal heat flux (Avis, 2012).

### A.2.3 Carbon Cycle

#### Ocean carbon cycle

The ocean carbon cycle in the UVic ESCM is simulated with modules for inorganic carbon chemistry, ocean biology, and carbonate sediment deposition and dissolution. The difference in partial pressure of $CO_2$ between the surface ocean and the atmosphere is what drives atmosphere-ocean flux of $CO_2$ (e.g. Greenblatt and Sarmiento,

2004). Once dissolved in ocean water $CO_2$ goes into equilibrium with other species of dissolved inorganic carbon, with the net effect being that relatively little carbon is held as $CO_{2(aq)}$. This equilibrium reaction is:

$$CO_2 + CO_3^{2-} + H_2O \longleftrightarrow 2\,HCO_3^{-}. \tag{A.2}$$

The UVic ESCM simulates this chemistry following the protocols of the ocean carbon-cycle model intercomparison project (Orr et al., 1999). Dissolved inorganic carbon is treated as a passive tracer by the model and carried throughout the ocean following ocean circulation (Weaver et al., 2001).

Ocean biology is simulated using a simple marine ecosystem model developed by (Schmittner et al., 2008). The marine ecosystem model consists of two types of phytoplankton (nitrogen fixing and non-nitrogen fixing), zooplankton and detritus. Inorganic dissolved oxygen, nitrate and phosphate drive and interact with ocean biology. Phytoplankton grow based on nutrient and light availability, and temperature. The zooplankton consume phytoplankton and both contribute to detritus which sinks into the deep ocean. Calcium carbonate is treated as a ocean tracer, it is taken up by plankton and transported to the deep ocean as a fixed fraction of detritus. The inclusion of ocean biology allows the model to simulate ocean anoxia, the biological pump, the alkalinity pump and combined with terrestrial biology, global net primary productivity.

The third component of the UVic ESCM ocean carbon-cycle is the carbonate sediment deposition and dissolution module. This component takes into account the slow feedback between ocean pH and carbonate sediment dissolution. As more $CO_2$ is added to ocean water the equilibrium of equation A.2 shifts as the ocean has a finite quantity of $CO_3^{2-}$ anions. This shift increases the relative fraction of dissolved inorganic carbon held as $CO_{2(aq)}$ and consequently lowers ocean pH. This lowering of pH in turn changes the stability of $CaCO_3$ and leads to dissolution of ocean sediments composed of calcite. This dissolution releases more $CO_3^{2-}$ anions into the ocean. The UVic ESCM simulates this process using a oxygen only model of sediment respiration based on the model of Archer (1996). Critical to this simulation is that pH conditions within the pore spaces of ocean sediments have higher concentration of $CO_{2(aq)}$ than ocean water due to microbial decomposition of organic matter within the sediments.

**Terrestrial carbon cycle**

The terrestrial carbon cycle in the UVic ESCM is simulated using the Top-down Representation of Interactive Foliage and Flora Including Dynamics (TRIFFID) developed by the Hadley Centre (Cox et al., 2001). TRIFFID is composed of five plant function types: broadleaf trees, needleleaf trees, shrubs, C3 grasses, and C4 grasses. These plant function types compete with one-another for space in each grid cell based on the Lotka-Voterra equations (Cox, 2001). Photosynthesis is simulated using the method of Collatz et al. (1991). The simulated plants take up carbon through photosynthesis and distributed acquired carbon to plant growth and autotrophic respiration. Simulated plants have leaf, wood and root carbon pools with specified turnover times for each. Dead carbon is transferred to the soil carbon pool as litter-fall.

The distribution and respiration of soil carbon has been modified in the present version of the UVic ESCM to accommodate the multi-layer subsurface and the effect of freezing on soil respiration. Soil respiration is taken to be a function of carbon quantity, soil temperature and soil moisture content:

$$R_s = \kappa_s C_s f_\Theta f_T \tag{A.3}$$

where $R_s$ is soil respiration, $\kappa_s$ is a rate constant, $C_s$ is the soil carbon density, $f_\Theta$ and $f_T$ are respectively moisture and temperature dependent functions. Soil respiration is computed independently for each of the top six subsurface layers based on the local temperature and moisture conditions.

The temperature function has been modified from previous version of the UVic ESCM to take into account that very little soil respiration occurs below the freezing point of water (Luo and Zhou, 2006) and now takes the form:

$$f_T = \begin{cases} Q_{10}^{0.1(T_{\text{soil}}-25)}, & \text{for } T_{\text{soil}} > 0 \\ 0, & \text{if } T_{\text{soil}} <= 0 \end{cases} \tag{A.4}$$

where $Q_{10}$ is taken to be 2.0 and $T_{\text{soil}}$ is soil temperature.

Carbon from the litter-pool is added to soil layers as an exponentially decreasing function of depth. The parameter values of this function change depending how many of the soil layers are frozen. The model is not allowed to allocate carbon soil layers that are below 1°C. Through trial and error it was discovered that the threshold that soil respiration stops and the threshold where carbon cannot be allocated to a soil

layer must be separated to avoid soil layers the are infinitesimally above freezing from acquiring near infinite quantities of carbon during model spin-up.

#### Permafrost Carbon Pool

The UVic ESCM used in the four paper derived chapters presented in this thesis includes a representation of the permafrost carbon pool. This large previously neglected pool of organic carbon is represented in the UVic ESCM using the algorithm of Schaefer et al. (2011). The model was modified to keep track of which soil layers are frozen and unfrozen. The model is spun-up and integrated with a millennial length paleoclimate simulation. Soil layers that remain frozen throughout the entire transient simulation are assigned a uniform permafrost carbon density. After the permafrost component is turned on, carbon in layers that thaw is reassigned to the control of the active soil carbon module and allowed to decay like any other soil carbon. If the layer were to refreeze decay would be halted as soil respiration cannot occur below the freezing point of water.

This method of adding the permafrost carbon pool to the a land surface model is not prognostic and cannot easily be applied to paleoclimate simulations or reversibility simulations. Other researchers have devised parameterizations that allow soil carbon to diffuse into permafrost layers which allows models to prognostically create a permafrost carbon pool during model spin-up (Koven et al., 2011). However, to date these methods have not been able to reproduce the size of the permafrost carbon pool, underestimating its size by $\frac{1}{2}$ (Koven et al., 2011) to $\frac{2}{3}$ (Burke et al., 2012). For this reason I have continued to use the Schaefer et al. (2011) method of initializing the permafrost carbon pool as I believe it is important for the purposes of the experiments conducted in this dissertation to correctly represent the size of the permafrost carbon pool. Further work to invent new parameterizations that better take into account the processes that incorporate carbon into permafrost soils should be a priority for model development.

### A.2.4 Acquisition of the UVic ESCM

The UVic ESCM is made available to the public through the UVic Climate Modelling Group website: http://climate.uvic.ca/model/. If the website is unavailable please contact the author at his permanent email address andrewhughmacdougall@gmail.com.

# Bibliography

Allen, M. R., D. J. Frame, C. Huntingford, C. D. Jones, J. A. Lowe, M. Meinshausen, and N. Meinshausen, 2009: Warming caused by cumulative carbon emissions towards the trillionth tonne. *Nature*, **458 (7242)**, 1163–1166.

Allen, M. R. and T. F. Stocker, 2013: Impact of delay in reducing carbon dioxide emissions. *Nature Climate Change*, doi:10.1038/nclimate2077.

Archer, D., 1996: A data-driven model of the global calcite lysocline. *Global Biogeochemical Cycles*, **10 (3)**, 511–526.

Archer, D., 2005: Fate of fossil fuel $CO_2$ in geologic time. *Journal of Geophysical Research*, **110 (C9)**, C09S05.

Arora, V. K., et al., 2013: Carbon-concentration and carbon-climate feedbacks in CMIP5 earth system models. *Journal of Climate*, **26 (15)**.

Avis, C. A., 2012: Simulating the present-day and future distribution of permafrost in the UVic Earth system climate model. Ph.D. thesis, University of Victoria.

Avis, C. A., A. J. Weaver, and K. J. Meissner, 2011: Reduction in areal extent of high–latitude wetlands in response to permafrost thaw. *Nature Geoscience*, **4**, 444–448, doi:10.1038/ngeo1160.

Azar, C., K. Lindgren, E. Larson, and K. Möllersten, 2006: Carbon capture and storage from fossil fuels and biomass–costs and potential role in stabilizing the atmosphere. *Climatic Change*, **74 (1-3)**, 47–79.

Baldocchi, D. and R. Valentini, 2004: Geographic and temporal variation of carbon exchange by ecosystems and their sensitivity to environmental perturbations. *The global carbon cycle*, C. B. Field and M. R. Raupach, Eds., Island Press.

Barnosky, A. D., et al., 2011: Has the earth's sixth mass extinction already arrived? *Nature*, **471 (7336)**, 51–57.

Boden, T., G. Marland, and B. Andres, 2011: Global $CO_2$ emissions from fossil-fuel burning cement manufacture, and gas flaring: 1751–2008. *Carbon Dioxide Information Analysis Center*.

Boucher, O., et al., 2012: Reversibility in an earth system model in response to $CO_2$ concentration changes. *Environmental Research Letters*, **7 (2)**, 024 013.

Burke, E. J., I. P. Hartley, and C. D. Jones, 2012: Uncertainties in the global temperature change caused by carbon release from permafrost thawing. *The Cryosphere*, **6**, 1063–1076.

Cao, L. and K. Caldeira, 2010: Atmospheric carbon dioxide removal: long-term consequences and commitment. *Environmental Research Letters*, **5 (2)**, 024 011.

Carslaw, H. S. and J. C. Jaeger, 1986: *Conduction of heat in solids*. Oxford University Press, 510 pp.

Ciais, P., et al., 2013: Carbon and other biogeochemical cycles. *Working Group I Contribution to the Intergovernmental Panel on Climate Change Fifth Assessment Report Climate Change 2013: The Physical Science Basis*, T. F. Stocker, D. Qin, G.-K. Plattner, M. Tignor, S. K. Allen, J. Boschung, A. Nauels, Y. Xia, V. Bex, and P. Midgley, Eds., Cambridge University Press.

Collatz, G. J., J. T. Ball, C. Grivet, and J. A. Berry, 1991: Physiological and environmental regulation of stomatal conductance, photosynthesis and transpiration: a model that includes a laminar boundary layer. *Agricultural and Forest Meteorology*, **54 (2)**, 107–136.

Collins, M., et al., 2013: Long-term climate change: Projections, commitments and irreversibility. *Working Group I Contribution to the Intergovernmental Panel on Climate Change Fifth Assessment Report Climate Change 2013: The Physical Science Basis*, Cambridge University Press.

Cox, P., 2001: Description of the "TRIFFID" dynamic global vegetation model.

Cox, P. M., R. A. Betts, C. D. Jones, S. A. Spall, and I. J. Totterdell, 2000: Acceleration of global warming due to carbon–cycle feedbacks in a coupled climate model. *Nature*, **408**, 184–187.

Cox, P. M., R. A. Betts, C. D. Jones, S. A. Spall, and I. J. Totterdell, 2001: Modelling vegetation and the carbon cycle as interactive elements of the climate system. *Proceedings of the RMS millennium conference*.

Cox, P. M., D. Pearson, B. B. Booth, P. Friedlingstein, C. Huntingford, C. D. Jones, and C. M. Luke, 2013: Sensitivity of tropical carbon to climate change constrained by carbon dioxide variability. *Nature*, **494**, 341–344.

Davidson, E. and I. Janssens, 2006: Temperature sensitivity of soil carbon decomposition and feedbacks to climate change. *Nature*, **440 (7081)**, 165–173.

Denman, K., et al., 2007: Couplings between changes in the climate system and biogeochemistry. *Climate Change 2007: The Physical Science Basis. Contribution of Working Group I to the Fourth Assessment Report of the Intergovernmental Panel on Climate Change*, S. Solomon, D. Qin, M. Manning, Z. Chen, M. Marquis, K. Averyt, M. Tignor, and H. Miller, Eds., Cambridge University Press, Cambridge, United Kingdom and New York, NY, USA, chap. 7, 499–587.

Dutta, K., E. A. G. Schuur, J. C. Neff, and S. A. Zimov, 2006: Potential carbon release from permafrost soils of Northeastern Siberia. *Global Change Biology*, **12**, 2336–2351.

Eby, M., K. Zickfeld, A. Montenegro, D. Archer, K. J. Meissner, and A. J. Weaver, 2009: Lifetime of anthropogenic climate change: Millennial time scales of potential $CO_2$ and surface temperature perturbations. *Journal of Climate*, **22**, 2501–2511, doi:10.1175/2008JCLI2554.1.

Falkowski, P., et al., 2000: The global carbon cycle: a test of our knowledge of earth as a system. *Science*, **290 (5490)**, 291–296.

Fischer, R. A., D. Byerlee, and G. O. Edmeades, 2009: Can technology deliver on the yield challenge to 2050? *Expert Meeting on How to feed the World in 2050*.

Forster, P., et al., 2007: Changes in Atmospheric Constituents and in Radiative Forcing. *Climate Change 2007: The Physical Science Basis. Contribution of Working*

*Group I to the Fourth Assessment Report of the Intergovernmental Panel on Climate Change*, S. Solomon, D. Qin, M. Manning, Z. Chen, M. Marquis, K. Averyt, M. Tignor, and H. Miller, Eds., Cambridge University Press, Cambridge, United Kingdom and New York, NY, USA, chap. 2.

Friedlingstein, P., et al., 2006: Climatecarbon cycle feedback analysis: Results from the $C^4$MIP model intercomparison. *Journal of Climate*, **19**, 3337–3353.

Fyke, J. G., 2011: Simulation of the global coupled climate/ice sheet system over millennial timescales. Ph.D. thesis, Victoria University of Wellington.

Fyke, J. G., A. J. Weaver, D. Pollard, M. Eby, L. Carter, and A. Mackintosh, 2011: A new coupled ice sheet/climate model: description and sensitivity to model physics under eemian, last glacial maximum, late holocene and modern climate conditions. *Geoscientific Model Development*, **4**, 117–136.

Gillett, N., V. Arora, K. Zickfeld, S. Marshall, and W. Merryfield, 2011: Ongoing climate change following a complete cessation of carbon dioxide emissions. *Nature Geoscience*, **4 (2)**, 83–87.

Gillett, N. P., V. K. Arora, D. Matthews, and M. R. Allen, 2013: Constraining the ratio of global warming to cumulative $CO_2$ emissions using cmip5 simulations. *Journal of Climate*, **26**, 6844–6858.

Greenblatt, J. B. and J. L. Sarmiento, 2004: Variability and climate feedback mechanisms in ocean uptake of $CO_2$. *The global carbon cycle*, C. B. Field and M. R. Raupach, Eds., Island Press.

Gregory, J. M., C. D. Jones, P. Cadule, and P. Friedlingstein, 2009: Quantifying carbon cycle feedbacks. *Journal of Climate*, **22 (19)**, 5232–5250.

Grosse, G., et al., 2013: Distribution of late pleistocene ice-rich syngenetic permafrost of the yedoma suite in east and central siberia, russia. *US Geological Survey Open File Report*, **2013 (1078)**, 1–37.

Hansen, J., M. Sato, and R. Ruedy, 1997: Radiative forcing and climate response. *Journal of Geophysical Research: Atmospheres (1984–2012)*, **102 (D6)**, 6831–6864.

Hansen, J., et al., 2008: Target atmospheric $CO_2$: Where should humanity aim? *Open Atmospheric Science Journal*, **2**, 217–231.

Hegerl, G. C., et al., 2007: Understanding and attributing climate change. *Climate Change 2007: The Physical Science Basis. Contribution of Working Group I to the Fourth Assessment Report of the Intergovernmental Panel on Climate Change*, S. Solomon, D. Qin, M. Manning, Z. Chen, M. Marquis, K. Averyt, M. Tignor, and H. Miller, Eds., Cambridge University Press.

Held, I. M., M. Winton, K. Takahashi, T. Delworth, F. Zeng, and G. K. Vallis, 2010: Probing the fast and slow components of global warming by returning abruptly to preindustrial forcing. *Journal of Climate*, **23 (9)**, 2418–2427.

Hugelius, G., C. Tarnocai, G. Broll, J. Canadell, P. Kuhry, and D. Swanson, 2013: The northern circumpolar soil carbon database: spatially distributed datasets of soil coverage and soil carbon storage in the northern permafrost regions. *Earth System Science Data*, **5 (1)**, 3–13.

Huntingford, C., P. Cox, L. Mercado, S. Sitch, N. Bellouin, O. Boucher, and N. Gedney, 2011: Highly contrasting effects of different climate forcing agents on terrestrial ecosystem services. *Philosophical Transactions of the Royal Society A: Mathematical, Physical and Engineering Sciences*, **369 (1943)**, 2026–2037.

IPCC, 2013: Summary for policymakers. *Working Group I Contribution to the Intergovernmental Panel on Climate Change Fifth Assessment Report Climate Change 2013: The Physical Science Basis*, L. Alexander, S. Allen, N. L. Bindoff, F.-M. Bron, J. Church, U. Cubasch, S. Emori, P. Forster, P. Friedlingstein, N. Gillett, J. Gregory, D. Hartmann, E. Jansen, B. Kirtman, R. Knutti, K. K. Kanikicharla, P. Lemke, J. Marotzke, V. Masson-Delmotte, G. Meehl, I. Mokhov, S. Piao, G.-K. Plattner, Q. Dahe, V. Ramaswamy, D. Randall, M. Rhein, M. Rojas, C. Sabine, D. Shindell, T. F. Stocker, L. Talley, D. Vaughan, and S.-P. Xie, Eds., Cambridge University Press.

Jeffrey, A. and D. Zwillinger, 2000: *Table of Integrals, Series, and Products*. Elsevier Science.

Jenkinson, D., D. Adams, and A. Wild, 1991: Model estimates of $CO_2$ emissions from soil in response to global warming. *Nature*, **351 (6324)**, 304–306.

Jobbágy, E. G. and R. B. Jackson, 2000: The vertical distribution of soil organic carbon and its relation to climate and vegetation. *Journal of Applied Ecology*, **5**, 423–451.

Keith, D. W., M. Ha-Duong, and J. K. Stolaroff, 2006: Climate strategy with $CO_2$ capture from the air. *Climatic Change*, **74 (1-3)**, 17–45.

Koven, C. D., B. Ringeval, P. Friedlingstein, P. Ciais, P. Cadule, D. Khvorostyanov, G. Krinner, and C. Tarnocai, 2011: Permafrost carbon–climate feedbacks accelerate global warming. *Proceedings of the National Academy of Sciences*, **108**, 14 769–14 774, doi:10.1073/Proceedings of the National Academy of Sciences.1103910108.

Lawrence, D. M. and A. G. Slater, 2008: Incorporating organic soil into a global climate model. *Climate Dynamics*, **30**, 145–160, doi:10.1007/s00382-007-0278-1.

Le Qéré, C. and N. Metzl, 2004: Natural processes regulating the ocean uptake of $co_2$. *The global carbon cycle*, C. B. Field and M. R. Raupach, Eds., Island Press.

Lohmann, U. and J. Feichter, 2005: Global indirect aerosol effects: a review. *Atmospheric Chemistry and Physics*, **5 (3)**, 715–737.

Luke, C. M. and P. M. Cox, 2011: Soil carbon and climate change: from the Jenkinson effect to the compost–bomb instability. *European Journal of Soil Science*, **62**, 5–12.

Luo, Y. and X. Zhou, 2006: *Soil respiration and the environment*. Academic press.

MacDougall, A. H., C. A. Avis, and A. J. Weaver, 2012: Significant existing commitment to warming from the permafrost carbon feedback. *Nature Geoscience*, **5**, 719–721, doi:10.1038/NGEO1573.

Malhi, Y., et al., 2009: Exploring the likelihood and mechanism of a climate-change-induced dieback of the amazon rainforest. *Proceedings of the National Academy of Sciences*, **106 (49)**, 20 610–20 615.

Marcott, S. A., J. D. Shakun, P. U. Clark, and A. C. Mix, 2013: A reconstruction of regional and global temperature for the past 11,300 years. *Science*, **339 (6124)**, 1198–1201.

Marion, G. M. and W. C. Oechel, 1993: Mid-to late-holocene carbon balance in arctic alaska and its implications for future global warming. *The Holocene*, **3 (3)**, 193–200.

Matthews, H. and A. Weaver, 2010: Committed climate warming. *Nature Geoscience*, **3 (3)**, 142–143.

Matthews, H. and K. Zickfeld, 2012: Climate response to zeroed emissions of greenhouse gases and aerosols. *Nature Climate Change*, **2 (5)**, 338–341.

Matthews, H. D., 2010: Can carbon cycle geoengineering be a useful complement to ambitious climate mitigation? *Carbon Management*, **1 (1)**, 135–144.

Matthews, H. D., N. P. Gillett, P. A. Stott, and K. Zickfeld, 2009: The proportionality of global warming to cumulative carbon emissions. *Nature*, **459**, 829–832, doi:10.1038/nature08047.

Matthews, H. D., A. J. Weaver, K. J. Meissner, N. P. Gillett, and M. Eby, 2004: Natural and anthropogenic climate change: incorporating historical land cover change, vegetation dynamics and the global carbon cycle. *Climate Dynamics*, **22**, 461–479, doi:10.1007/s00382-004-0392-2.

Meissner, K. J., A. J. Weaver, H. D. Matthews, and P. M. Cox, 2003: The role of land–surface dynamics in glacial inception: A study with the UVic Earth system model. *Climate Dynamics*, **21**, 515–537.

Moss, R. H., et al., 2010: The next generation of scenarios for climate change research and assessment. *Nature*, **463**, 747–754, doi:10.1038/nature08823.

Murphy, D., S. Solomon, R. Portmann, K. Rosenlof, P. Forster, and T. Wong, 2009: An observationally based energy balance for the earth since 1950. *Journal of Geophysical Research-Atmospheres*, **114**.

Najjar, R. G., 1992: Marine biogeochemistry. *Climate System Modeling*, K. E. Trenberth, Ed., Cambridge University Press.

O'Connor, F. M., et al., 2010: Possible role of wetlands, permafrost, and methane hydrates in the methane cycle under future climate change: a review. *Reviews of Geophysics*, **48**, 2010RG000 326.

Olivier, J. G., J. A. Peters, and G. Janssens-Maenhout, 2012: *Trends in global $CO_2$ emissions 2012 report*. PBL Netherlands Environmental Assessment Agency.

Orr, J., R. Najjar, C. Sabine, and F. Joos, 1999: Abiotic-how-to, internal OCMIP report. *LSCE/CEA Saclay*.

Pacanowski, R., 1995: MOM 2 documentation user's guide and reference manual, GDFL ocean group technical report. *NOAA, GFDL*, 232.

Planton, S., 2013: Annex III: Glossary. *Climate Change 2013: The Physical Science Basis. Contribution of Working Group I to the Fifth Assessment Report of the Intergovernmental Panel on Climate Change*, Cambridge University Press.

Raupach, M., 2013: The exponential eigenmodes of the carbon-climate system, and their implications for ratios of responses to forcings. *Earth System Dynamics*, **4**, 31–49.

Samanta, A., B. T. Anderson, S. Ganguly, Y. Knyazikhin, R. R. Nemani, and R. B. Myneni, 2010: Physical climate response to a reduction of anthropogenic climate forcing. *Earth Interactions*, **14 (7)**, 1–11.

Schädel, C., et al., 2014: Circumpolar assessment of permafrost C quality and its vulnerability over time using long-term incubation data. *Global change biology*, **20 (2)**, 641–652.

Schaefer, K., T. Zhang, L. Bruhwiler, and A. P. Barrett, 2011: Amount and timing of permafrost carbon release in response to climate warming. *Tellus*, **63B**, 165–180, doi:doi:10.1111/j.1600-0889.2011.00527.x.

Schmittner, A., A. Oschlies, H. D. Matthews, , and E. D. Galbraith, 2008: Future changes in climate, ocean circulation, ecosystems, and biogeochemical cycling simulated for a business-as-usual $CO_2$ emission scenario until year 4000 AD. *Global biogeochemical cycles*, **22**, GB1013, doi:10.1029/2007GB002953.

Schneider von Deimling, T., M. Meinshausen, A. Levermann, V. Huber, K. Frieler, D. M. Lawrence, and V. Brovkin, 2012: Estimating the near-surface permafrost-carbon feedback on global warming. *Biogeosciences*, **9**, 649–665, doi:10.5194/bg-9-649-2012.

Scholes, R. and E. B. de Colstoun, 2012: ISLSCP II global gridded soil characteristics. ORNL distributed active archive center, Oak Ridge, Tennessee, USA, URL `http://www.daac.ornl.gov`.

Schuur, E. A. and B. Abbott, 2011: High risk of permafrost thaw. *Nature*, **480**.

Schuur, E. A. G., et al., 2008: Vulnerability of permafrost carbon to climate change: Implications for the global carbon cycle. *BioScience*, **58**, 701–714.

Shepherd, J., 2009: *Geoengineering the climate: science, governance and uncertainty*. Royal Society.

Sigman, D. M., M. P. Hain, and G. H. Haug, 2010: The polar ocean and glacial cycles in atmospheric $CO_2$ concentration. *Nature*, **466**, 47–55, doi:10.1038/nature09149.

Tarnocai, C., J. G. Canadell, E. A. G. Schuur, P. Kuhry, G. Mazhitova, , and S. Zimov, 2009: Soil organic carbon pools in the northern circumpolar permafrost region. *Global biogeochemical cycles*, **23**, GB2023, doi:10.1029/2008GB003327.

Taylor, K. E., R. J. Stouffer, and G. A. Meehl, 2012: An overview of CMIP5 and the experiment design. *Bulletin of the American Meteorological Society*, **93 (4)**, 485–498.

Thomas, C. D., et al., 2004: Extinction risk from climate change. *Nature*, **427 (6970)**, 145–148.

Thompsom, A. and S. G. Warren, 1982: Parameterization of outgoing infrared radiation derived from detailed radiative calculations. *Journal of the Atmospheric Sciences*, **39**, 2667–2680.

Weaver, A. J., et al., 2001: The UVic Earth system climate model: Model description, climatology, and applications to past, present and future climates. *Atmosphere–Ocean*, **39**, 1–67.

Weaver, A. J., et al., 2012: Stability of the atlantic meridional overturning circulation: A model intercomparison. *Geophysical Research Letters*, **39 (20)**.

Wigley, T. M. and M. E. Schlesinger, 1985: Analytical solution for the effect of increasing $CO_2$ on global mean temperature. *Nature*, **315**, 649–652.

Wigley, T. M. L., 1987: Relative contributions of different trace gases to the greenhouse effect. *Climate Monitor*, **16 (1)**, 14–28.

Zhuang, Q., et al., 2006: $CO_2$ and $CH_4$ exchanges between land ecosystems and the atmosphere in northern high latitudes over the 21st century. *Geophysical Research Letters*, **33**, L17 403, doi:10.1029/2006GL026972.

Zickfeld, K., V. Arora, and N. Gillett, 2012: Is the climate response to $CO_2$ emissions path dependent? *Geophysical Research Letters*, **39 (5)**, L05 703.

Zickfeld, K., M. Eby, H. D. Matthews, and A. J. Weaver, 2008: Setting cumulative emissions targets to reduce the risk of dangerous climate change. *Proceedings of the National Academy of Sciences*, **106**, 16 129–16 134, doi:10.1073/Proceedings of the National Academy of Sciences.0805800106.

Zickfeld, K., et al., 2013: Long-term climate change commitment and reversibility: An EMIC intercomparison. *Journal of Climate*, **26 (16)**.

Zimov, S., S. Davydov, G. Zimova, A. Davydova, E. Schuur, K. Dutta, and F. Chapin, 2006: Permafrost carbon: Stock and decomposability of a globally significant carbon pool. *Geophysical Research Letters*, **33 (20)**.